INVESTIGATION OF STRUCTURAL RESPONSE OF MAGNETO RHEOLOGICAL ELASTOMER (MRE) BASED MULTI DEGREE OF FREEDOM (MDOF) ISOLATED STRUCTURE UNDER SINUSOIDAL AND EARTHQUAKE EXCITATIONS

By

MUHAMMAD AHSAN TARIQ

(00000172380)

This thesis is submitted in partial fulfillment of

the requirements for the degree of

Master of Science

in

Structural Engineering

National Institute of Civil Engineering (NICE)

School of Civil & Environmental Engineering (SCEE)

National University of Sciences and Technology (NUST)

Islamabad, Pakistan

Sep, 2020

This is to certify

that Thesis entitled

INVESTIGATION OF STRUCTURAL RESPONSE OF MAGNETO RHEOLOGICAL ELASTOMER (MRE) BASED MULTI DEGREE OF FREEDOM (MDOF) ISOLATED STRUCTURE UNDER SINUSOIDAL AND EARTHQUAKE EXCITATIONS

Submitted by

MUHAMMAD AHSAN TARIQ

has been accepted towards the partial fulfillment

of

the requirements

for award of degree of

Master of Science in Structural Engineering

Thesis Supervisor

_____

Dr. Muhammad Usman
Assistant Professor
NUST Institute of Civil Engineering (NICE)
School of Civil and Environmental Engineering (SCEE)
National University of Sciences and Technology (NUST)
Sep 2020, Islamabad Pakistan

THESIS ACCEPTANCE CERTIFICATE

Certified that final copy of MS thesis written by Mr. Muhammad Ahsan Tariq, Registration No. 00000172380, student of MS Structural Engineering 2016 Batch NICE has been vetted by undersigned, found complete in all respects as per NUST Statutes / Regulations, is free of plagiarism, errors, and mistakes and is accepted as partial fulfillment for award of MS/MPhil degree. It is further certified that necessary amendments as pointed out by GEC members of the scholar have also been incorporated in the said thesis.

Signature: _____

Name of Supervisor: Dr. Muhammad Usman_____

Date: _____

Signature (HOD): _____

Date: _____

Signature (Dean/Principal): _____

Date: _____

ACKNOWLEDGMENTS

I owe the successful completion of my MS Programme to ALLAH ALMIGHTY, without the help and enlightenment of WHOM it was never possible.

I am highly obliged and indebted to my supervisor, Dr. Muhammad Usman, for his unmatched guidance, perpetual motivation and support throughout the research activities. To take up this interdisciplinary research topic in the start, which was worked on for the first time in Pakistan, was not possible without his guidance and support. He helped me at all the stages of my research and provided me the thorough insight into the subject.

I would like to express my gratitude to my GEC members Dr. Syed Hassan Farooq, Dr. Fawad Ahmed Najam and Dr. Ather Ali for their guidance, useful suggestions and assistance in carrying out research activities as well as improving my research work. Moreover, I would like to thank the entire administration of NUST Institute of Civil Engineering (NICE) for their support.

My words are incomplete without appraising my employers/directors Engr. Munawwar Ghani (Director, ABS), Engr. Karamet Ali (Director, AN Associates), Engr. Hasan Waqas Ghauri (HoD, Civil Works, AWC) and Engr. Zaheer Abbas (Project Director, Civil Works, AWC) for their support and cooperation throughout different phases of my MS Programme.

Last but not the least, I would like to thank my parents for their prayers, untiring support and encouragement throughout the journey of my life. I could not have been achieved anything without their backing and prayers.

ABSTRACT

Fixed base structures subjected to earthquake forces are prone to problems like attraction of greater forces to structure, amplified accelerations to non-structural components, expensive design for better seismic performance etc. Base isolation applied at foundation of the vulnerable structures is a radical bypass from the conventional approaches utilized by structural engineers. But practical implementation of Passive Base Isolation is constrained by factors like large displacements at isolation level, uplifting forces at isolators and vulnerability to unpredictable and versatile earthquakes.

This study is focused on the development of MRE based adaptive seismic isolator and evaluation of smart base isolation system under various harmonic and earthquake loadings. The proposed system employs a magneto-rheological elastomer (MRE) based adaptive isolation layer under the building structure. The building is idealized as 5 degree-of-freedom (DOF) structure with the mass lumped at each storey. The stiffness of MRE isolation layer is adjusted using Linear Quadratic Regulator (LQR) optimal feedback control algorithm.

A total of 36 simulations have been performed for fixed base, passively isolated and MRE based isolated structures under various harmonic and earthquake loadings for analyzing a total of 612 responses of the structures. The simulation results show that MRE based isolation has significantly reduced all the responses compared to passively isolated structure for most of the earthquake loadings. For harmonic loading however, the passively isolated structure outperformed the MRE isolated structure in terms of storey drift and acceleration responses.

Table of Contents

List of Figures

List of Tables

Chapter 1: Introduction

1.1 Base Isolation in Structures

Earthquakes around the world have caused much of a damage to human lives, infrastructure and economy apart from wars and pandemics over the years. For buildings located in moderate to high seismic zones, a territory host to a substantial portion of world population, earthquake loading becomes prime factor to be considered for structural design of buildings. For the case of fixed base RCC buildings whose fundamental period of vibration falls in the range of predominant time period of earthquakes, the governing earthquake forces demand a very stiff structural system, the design of which becomes impractical and inefficient for functional use of structure. Moreover a stiff fixed base system tend to attracts more forces to the structure and amplify ground motion. An effort to minimize this amplification require higher rigidity or a superior damping. High rigidity implies bulky structural members and amplified accelerations to non-structural members that may include sensitive equipment and delicate facilities while a superior damping implies damage to the system and expensive design.

With a view to strike a balance between construction cost and efficient performance of structure and constructed facilities against the destructive environmental forces, efforts have been made in the field of structural engineering to come up with a new and better systems. Base isolation using elastomeric or sliding bearing system applied at foundation of the vulnerable structures is a radical bypass from the conventional approaches utilized by structural engineers. This technique allows the engineers to control damage for both the structural and non-structural elements in events of moderate and large earthquakes at a significantly lessened cost. Base isolation is carried out by introducing a soft layer at the base of the building. The horizontal stiffness of the layer is much lower compared to the structure above it due to which the structure gets decoupled from the ground vibrations. This modified system attains a time period much higher than the original fixed base structure and consequently higher than the predominant earthquake time period. Thus, the fundamental mode of vibration of the building involves the deformation only at the isolation layer, leaving the structure above remaining almost rigid. Higher modes responsible of producing deformation in the structure are orthogonal to 1^{st} mode and consequently to the ground motion. As a result, these higher modes, typically possess low modal participation factors so that in case of high energy in the ground motion at the higher modal frequencies, a minimum energy is transmitted to the structure.

Despite significant success in improving the seismic performance of structures, practical implementation of base isolation technique is still constrained by factors like large relative displacements in isolation layers, possibility of uplift of isolators under severe earthquakes and vulnerability to unpredicTable and versatile earthquakes because once implemented, the parameters of passively isolated structures may never be changed. Studies have been carried out on Hybrid Base isolation Systems to address the short comings of passive isolation. They eliminate excessive base drift by providing additional damping through an active or semi-active actuator. But this complementary damping does not change stiffness of passively isolated structure and thus its fundamental time period of vibration. Moreover, this extra damping brings problems such as transmitting energy at high modes in superstructure, instability, high cost, periodic maintenance and high power consumption. Thus a base isolation system, whose lateral stiffness and consequently the fundamental period of the structure can be controlled at any time instant with relative ease, becomes highly desirable that enables the structure to instantly decouple from earthquake excitations.

1.2 Magneto Rheological Elastomers (MREs)

Magneto-rheological Elastomer (MRE) is a smart material with magnetic sensitive particles dispersed in an elastomer matrix. It possesses a controllable shear modulus under application of magnetic field and upon removal of the magnetic field original state of properties can be reclaimed. Thus the physical state of the material adjusted from a soft elastomer to semi-solid depending upon the extent of applied magnetic flux. Owing to its key features mentioned above, MRE has found its applications in devices like vibration absorbers (suspension bushings, engineering mounts), vibration isolators (seat vibration isolator, adaptive seismic isolators), controllable valves, and adaptive beam structures with a potential to contribute to smart braking systems and haptic devices etc. The application of MR elastomers civil engineering structures, especially for a base isolation system has drawn a lot of interest of the researchers especially in addressing the shortcomings of passive and hybrid isolation systems.

1.3 Problem Statement

There is a need to develop large scale smart base isolator which can support larger vertical loads and respond to a wider range of earthquake excitations so that the performance range of conventional base isolation systems can be increased. Comprehensive testing on MRE based seismic isolated structures needs to be conducted using standardized parameters for a

convincing demonstration of the effectiveness and versatility of the seismic protection strategy under various seismic activities.

1.4 Research Objectives

This research is conducted with the view to achieve following objectives:

- Development and experimental testing of highly adaptive magneto-rheological elastomer (MRE) based seismic isolator for its performance evaluation.
- Investigation of the response of magneto-rheological elastomer (MRE) based 5 degree-of-freedom (DOF) isolated structure with vibration control under sinusoidal excitation using MATLAB simulations.
- Investigation of the response of magneto-rheological elastomer (MRE) based 5 degree-of-freedom (DOF) isolated structure with vibration control under the available strong motion earthquake excitations using MATLAB simulations.
- Comparison of the response between fixed base, passive and MRE controlled base isolation systems.

1.5 Scope of Research

This research is aimed at the study and development of large scale MRE based seismic isolator and investigation of MRE based isolated structure under harmonic excitations as well as under the historic near fault and far fault earthquakes.

1.6 Thesis Organization

The first chapter provides a brief introduction of the base isolation and MR elastomers. The second chapter provides an insight into the available literature. The third chapter deals with the materials and equipment. The fourth chapter discusses the methodology of simulation. The fifth chapter presents the results and discussions. The sixth chapter deals with conclusions and recommendations.

Chapter 2: Literature Review

Base isolation is an effective technique to protect civil engineering structures like buildings and bridges against harmful ground excitations, as in the case of an earthquake. Different base isolation systems have been developed and used in the recent past. Base isolation systems are generally installed in the base of a structure to decouple the structure from horizontal components of ground excitations in the frequency range most vulnerable to the structure. In addition, this is a cost-effective technique to reduce inter-story drifts and floor accelerations.

2.1 Base Isolation Systems

Base isolation system, or simply base isolator, primarily consists of rubber pads sandwiched between lamination sheets, with metallic plates at both ends to connect with the structure to be isolated as shown in Figure 1.

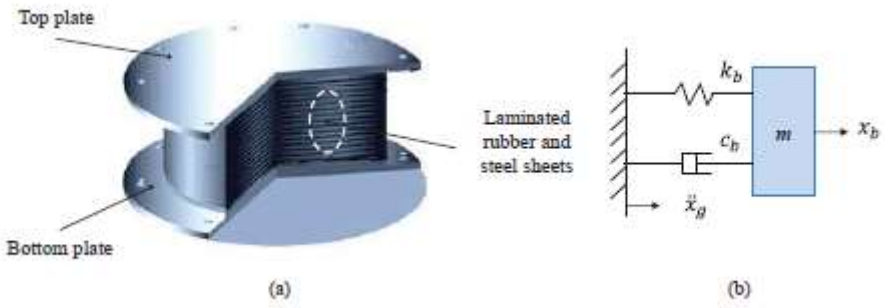

Figure 1: Laminated Rubber Bearing [10]

Following are the main types of base isolation systems.

2.1.1 Passive Base Isolation Systems

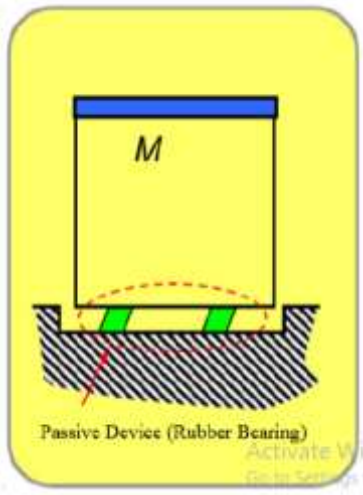

Figure 2: Passive Base Isolation [9]

Passive base isolation is the most widely used base isolation technique. It consists of a conventional base isolator installed at the base of a structure. Passive base isolation is simple and economical. Though the technique is quite effective, but there are some limitations. It tends to increase the natural period as well as the base displacement of the structure. This results in increased cost problem as the isolation system requires considerable seismic gaps between the structure and the ground. Moreover, the non-adaptability of passive base isolation systems to different ground excitations is another drawback.

2.1.2 Hybrid or Active Base Isolation Systems

To improve the performance of passive base isolation systems, hybrid or active base isolation systems were developed. Hybrid base isolation systems are similar to passive base isolation systems with the addition of actuator.

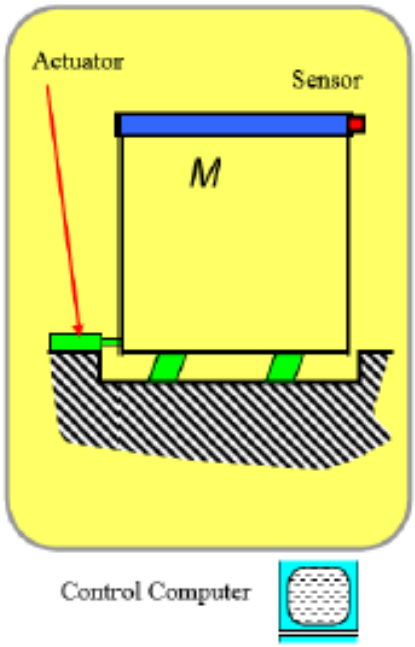

Figure 3: Hybrid Base Isolation System [9]

Hybrid base isolation systems eliminate the excessive base displacement of the structures by providing additional damping. Hybrid base isolation systems have high performance for mitigating vibrations and they are highly adaptable to various ground excitations. However, there are few drawbacks of hybrid base isolation systems, which include reliability, instability, high cost, periodic maintenance and high power consumption.

2.1.3 Smart or Semi-Active Base Isolation Systems

In smart or semi-active base isolation, some semi-active device is used instead of the actuator. Smart base isolation has the quality of robustness or adaptability and stability. Thus, it possesses qualities of both passive and hybrid base isolation systems. Moreover, they have relatively small power requirements as compared to hybrid systems. MR fluid damper based base isolation system is an example of smart or semi-active base isolation system. This type of base isolation has limitations like unidirectional properties of MR damper and environmental pollution by liquid leakage.

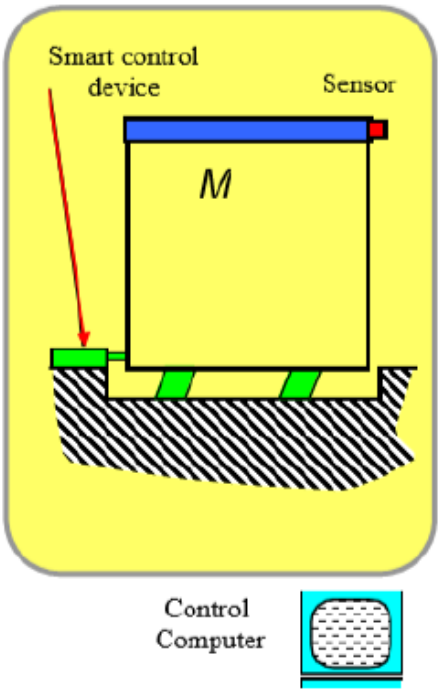

Figure 4: Smart or Semi Active Base Isolation System [9]

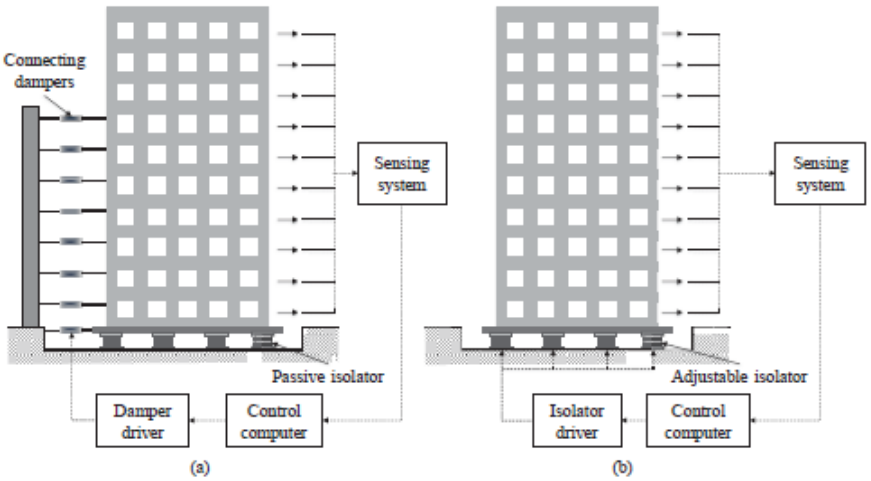

Figure 5: Schematic diagram of (a) hybrid isolation system combining passive base isolation with supplementary dampers; (b) "smart" base isolation system with controllable isolators [10]

2.2 Development of Magneto Rheological Materials

MR materials fall in the category of innovative or smart materials whose rheological properties can be controlled by changing the applied external magnetic field [15]. MR materials comprise of micro-sized iron particles dispersed in elastic matrix, which is non-magnetic in nature. When a magnetic field is applied, the rheological properties of these materials can be rapidly and reversibly changed [16]. This phenomenon is due to alignment of magnetic particles present within the elastic matrix as shown in Figure 6.

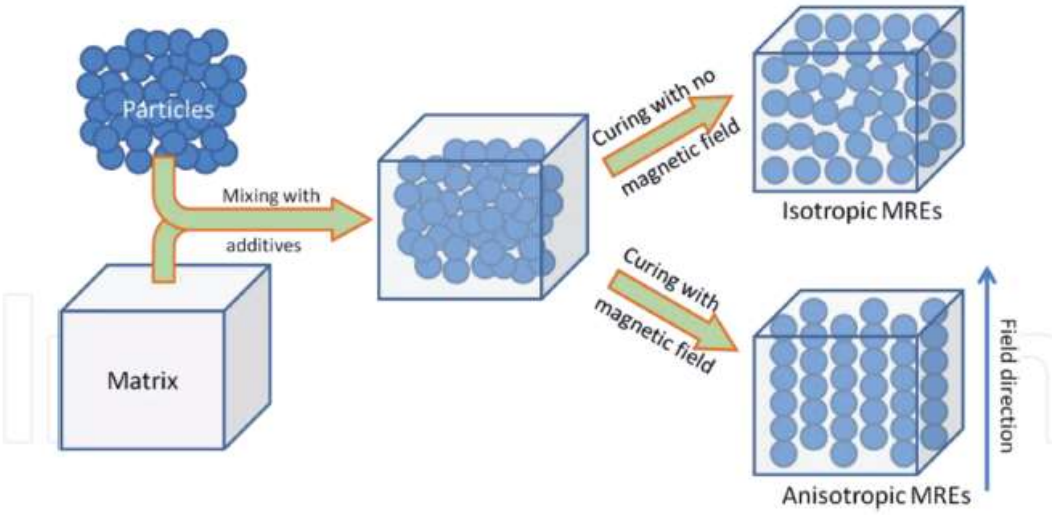

Figure 6: Composition of Magneto Rheological Materials [32]

The development of MR materials can be traced to mid-twentieth century. In 1948, MRFs were discovered at the US National Bureau of Standards by Rabinow [17]. MRFs are suspensions which can alter their phase between liquid and solid in the presence of a magnetic field. MRFs have qualities like quick response to magnetic field, rapid reversibility and controllable performance. This makes MRFs excellent for use in applications in which controlled energy dissipation is needed. Examples of these applications are brakes and clutches for exercise equipment [18, 19, 20] and controllable dampers for vehicle suspensions [9, 10, 11].

MREs are solid analogues of MRFs. In comparison to MRFs, MREs exhibit sTable MR performance because the particles do not undergo sedimentation with the passage of time, as it happens in MRFs. Moreover, the thermal stability of MREs is also higher. Also their resistance to degradation is greater. It has been observed [24] that the response time of an MRE is less than milliseconds. In addition, MRFs have a magnetic field dependent yield stress whereas MREs have magnetic field-dependent elastic modulus. Comparing their use, MREs being solid

in nature, are used in stiffness controllable devices, whereas MRFs are used in viscosity controllable devices.

2.3 Microstructure of MREs

MREs can be prepared with or without presence of magnetic field during the process of curing. The former technique results in anisotropic or structured MREs [25] whereas the latter results in isotropic or homogenous MREs [26-29] as shown in Figure 7 and Figure 8. When a magnetic field is applied, the magnetic particles get magnetized and magnetic dipoles are formed. The dipoles tend to move along magnetic field lines to form chain like structure in the matrix. Various factors influence the distribution of magnetic particles in MREs including orientation and strength of magnetic field, volume fraction of magnetic particles, temperature and magnetic interaction forces between particles.

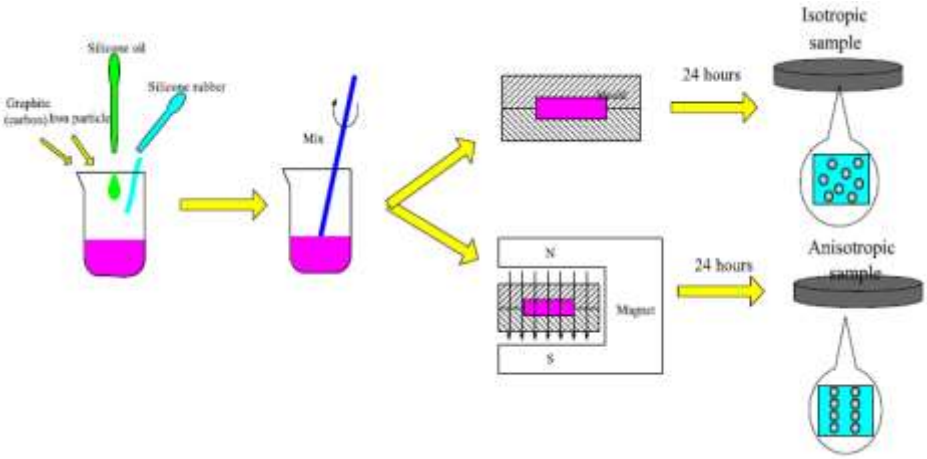

Figure 7: Fabrication of isotropic and anisotropic MR elastomers [31]

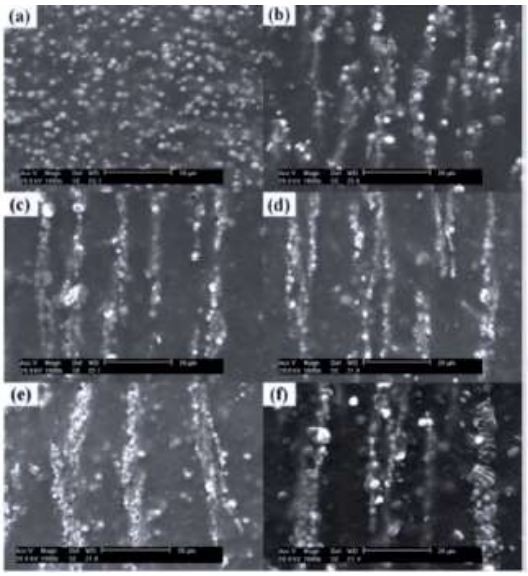

Figure 8: SEM Images of MREs cured at a) 0T, b) 0.2T, c) 0.4T, d) 0.6T, e) 0.8T, f) 1.0T [33]

2.4 MR Effect

MREs can be categorized as viscoelastic materials. Their properties are described by equations typical for viscoelastic materials, with some additional parameters to account for the influence of external magnetic field on the rheological properties. The MR effect can be defined as the change in the viscoelastic properties of an MR material when subjected to magnetic field. This is one of the most important properties of MR materials. It was observed that MR effect is related to the tendency of magnetic particles to change their position when subjected to a magnetic field [34]. The magnetic field introduces dipole movements in the magnetic particles. This movement of particles causes deformations in the elastomer, which results in increase in shear modulus and stiffness of the material.

2.5 Factors affecting Properties of MREs

It has been observed that the shear strength of isotropic and anisotropic MREs increases in the presence of an external magnetic field. Moreover, maximum increase in shear modulus is obtained when iron particles are fully magnetized [35]. The increase in the shear modulus is shown to be proportional to the magnetic field strength, at low or moderate magnetic flux densities [36, 37]. It was noticed that the increase in magnetic field results in increase in the stiffness of MREs [38], as shown in Figure 9.

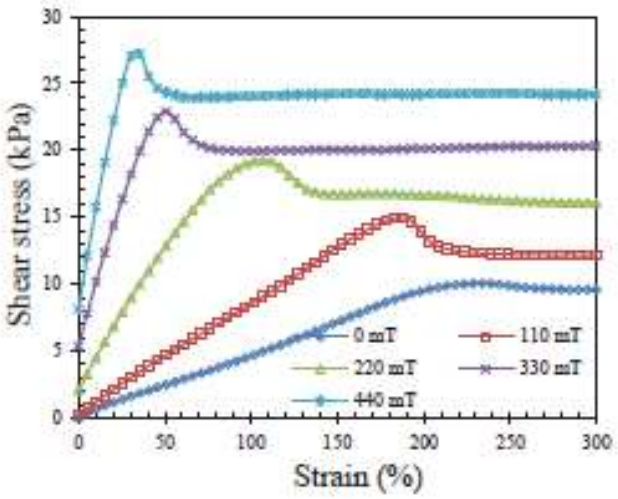

Figure 9: Variation in stiffness of MRE with magnetic field [41]

Magnetic particles are significant component of MREs. The size, shape and type of magnetic particles greatly influence the properties of MREs. The effect of size of magnetic particles on shear storage and loss modulus of isotropic and anisotropic MREs was studied [39]. It was observed that, without magnetic field, the larger sized magnetic particles had modulus less than smaller sized magnetic particles. Whereas, in the presence of a magnetic field, the field induced

modulus was higher in MREs with larger particles and it exceeded significantly compared to MREs with smaller particles.

It has also been observed that the composition or type of magnetic particles has an effect on mechanical properties of MREs. The magnetic particles with low carbon content show high field induced shear modulus than high carbon content magnetic particles [40].

The behavior of MREs has generally been studied in low frequency range of 1-50 Hz. [42] found significant MR effect at higher frequencies, with frequency range over 1 kHz and 27% iron particles by volume. Similarly, it was observed [38] that increase in frequency of loading results in an increase in strain rate effect of MREs.

Strain amplitude is also an important factor which influences mechanical properties of MREs. Generally, the shear modulus of anisotropic MREs decreases by increasing the strain amplitude [43, 44]. This happens because the molecules of elastic matrix begin to slide when the strain is increased. As the distance between ends of two molecule chains increased, the chains were easily separated upon application of shear stress [43].

Additives also effect properties of MREs. It has been observed [44] that the additives like paraffin oil can reduce stiffness of the composite and produce a stronger MR effect. It was found [45] that the addition of silicon oil resulted in increase in MR effect. The addition of silicon oil results in increased wetting of iron particles due to which adhesion between iron particles and the elastic matrix increases and thus preventing agglomeration of iron particles [46].

2.6 Engineering Application

Due to magnetic field dependent properties of MREs, they have various applications in different fields of engineering. These applications include adaptive tuned vibration absorbers (suspension bushings, engineering mounts) [47-53, 73], stiffness tunable mounts [54], vibration isolators (seat vibration isolator, adaptive seismic isolators) [14, 55-63], controllable valves [68], adaptive beam structures [69-72] and dampers [64].

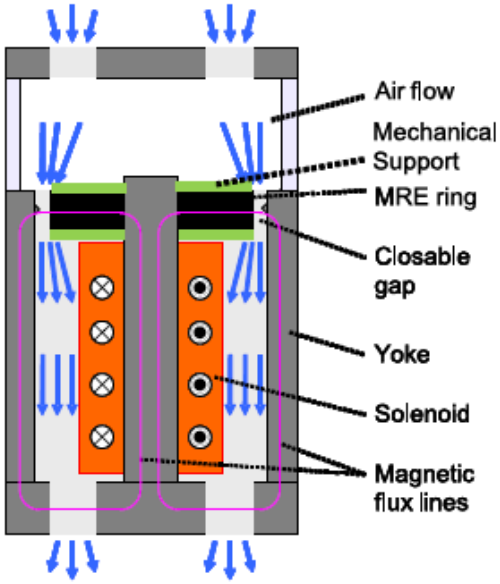

Figure 10: MRE based Controllable valve [68]

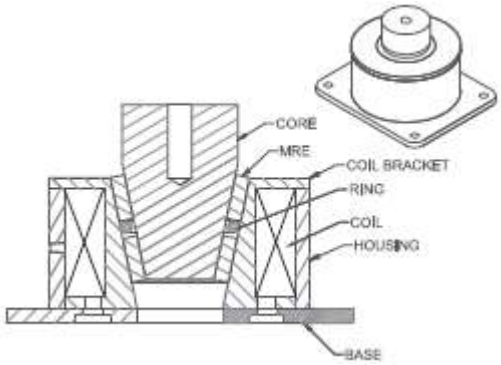

Figure 11: Schematics of MRE seat isolator [73]

In civil engineering field, MREs have found their applications in the development of adaptive seismic isolators [1, 13, 65-66]. The results suggest that the MRE based seismic isolators have the potential to overcome the limitations of traditional seismic isolators particularly in reducing the responses of structures during seismic excitations [13].

2.7 MRE in Base Isolation

Studies [1, 65] have been conducted to investigate the suitability of MRE based isolation using numerical simulations. The results validated that MR elastomer base isolation outperforms the traditional passive system in terms of response improvement during earthquake excitations. Jung et al [13] developed a single degree-of-freedom scaled model above an MR elastomer and performed experimental testing on the system under harmonic excitation and earthquake time histories.

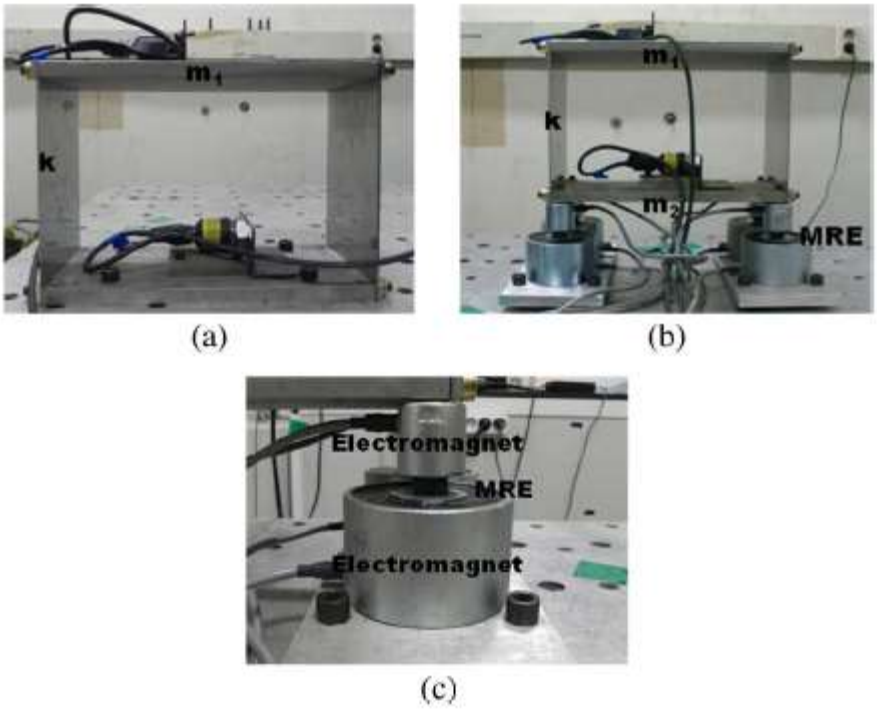

Figure 12: Experimental setup. (a) Fixed structure (b) smart isolated system (c) MR elastomer and electromagnets [13]

Behrooz et al [14, 74] developed a variable stiffness and damping isolator (VSDI) for base isolation of a civil structure; see Figure 13. Four MRE samples, each 12 mm thick and trapezoidal in shape were proposed in the design with a shim dividing them. Four electromagnetic coils were provided on the top and bottom of MRE samples to generate the magnetic flux. The coils were covered with two steel caps along with steel cores. The overall dimensions of VSDI is 128 mm× 64 mm× 110 mm. The number of turns in a single coil is 800, and the power required for each device is 234.2W at 4 A current. A maximum increase of 57% was reported in shear mode. However, a main drawback for this design of the isolator for civil structures is the limited loading capacity in vertical direction.

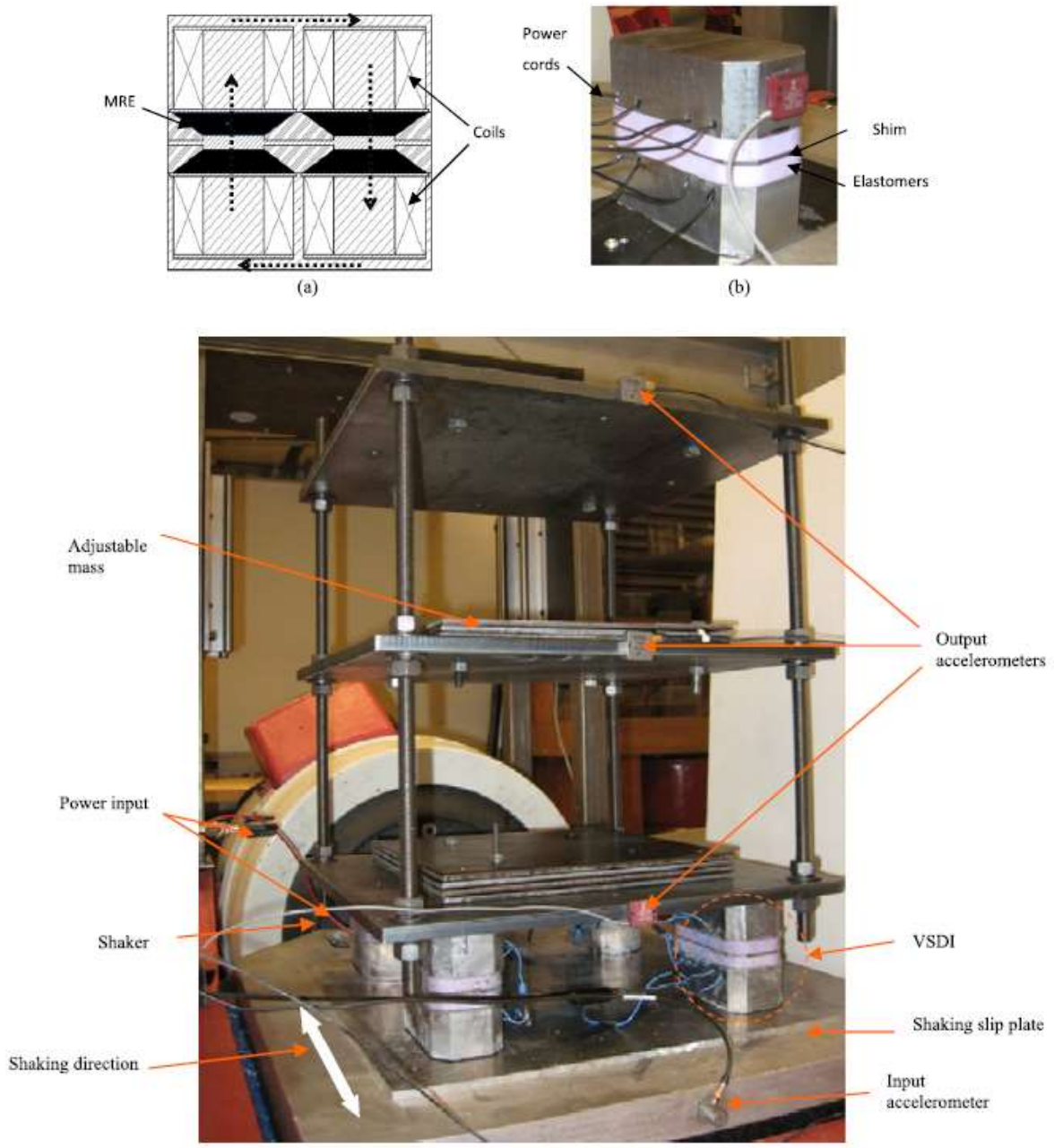

Figure 13: VSDI proposed by Behrooz and Experimental Setup [14, 74]

Li et al [66, 75] put forward, for the first time, a laminated MRE base isolator containing 47 sheets of MR elastomer each 2 mm thick with the diameter of 140 mm; see Figure 14. Every MRE layer is accompanied with a 1mm thick steel sheet of same diameter with a total of 46 steel sheets. This configuration makes the laminated structure 140 mm high. An electromagnetic coil was positioned outside the laminations. An enclosed magnetic path is formed with the steel plates at top and bottom, the hollow steel yoke, the cylindrical steel block and the laminated structure also forming the core of the electromagnetic coil. The benefits of

the laminated design are: greater vertical loading capacity of the isolator and an improved magnetic conductivity of the structure and the widely practiced design of base isolator. This device can take a maximum load of 370 kg in compression for its weakest state, i.e. 0 magnetic flux and at a maximum design displacement of 26 mm. An even greater vertical loading capacity is expected under the application of magnetic field. This loading capacity furnishes the minimum requirements for its use in the seismic isolation of civil structures. Experimental tests on a shake Table demonstrated an effective stiffness increase of 37% and a 45% that of force under a designed maximum current of 5A. The uniformed magnetic field of 0.3 T is estimated to energize all of the MR elastomer layers in the device.

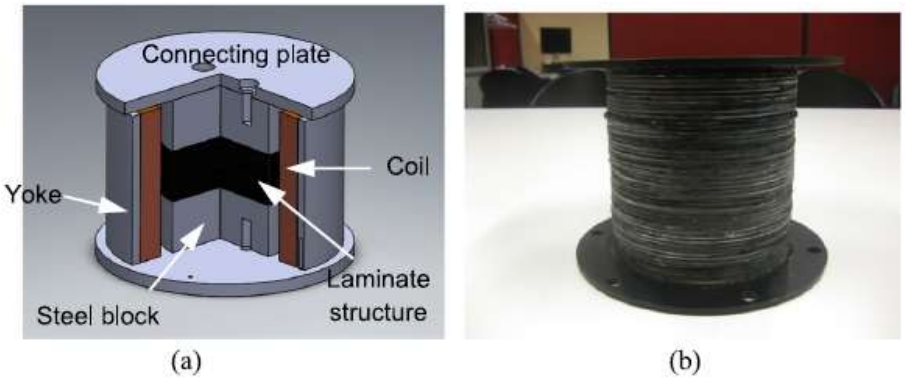

Figure 14: Laminated MRE base isolator [66, 75]

Furthermore, an MR elastomer of highly adjusTable nature with laminated structure was developed and experimentally tested by Li et al [63] using a soft MRE. The device contains 25 sheets of MR elastomer, each 1 mm thick with diameters of 120 mm. The MR elastomer used in the new device can produce force increase of 1479% and stiffness increase of 1630%, when the magnetic field varied from 0T to 0.44T.

Yang et al [60] conducted a study on design and experimental testing of a novel MRE based isolator with hybrid magnetic system. This hybrid magnetic system is capable of generating a magnetic field that is the superposition of a permanent magnetic field and an electromagnetic field as shown in Figure 15, 16. A negative stiffness change in the isolator has been reported due to the incorporated hybrid magnetic system. Stiffness of the isolator can be increased or decreased based on the direction of current in proposed isolator design as shown in Figure 15, 16.

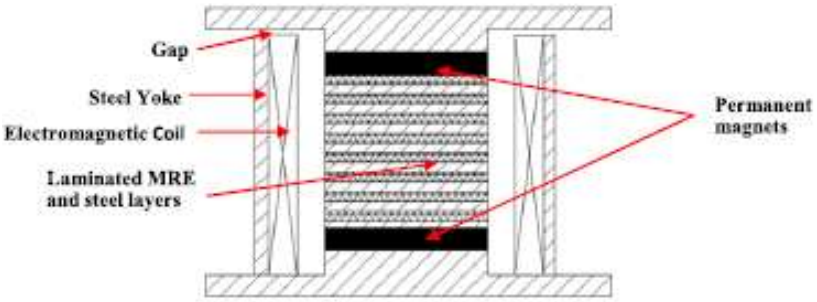

Figure 15: MRE isolator with hybrid magnetic system [60]

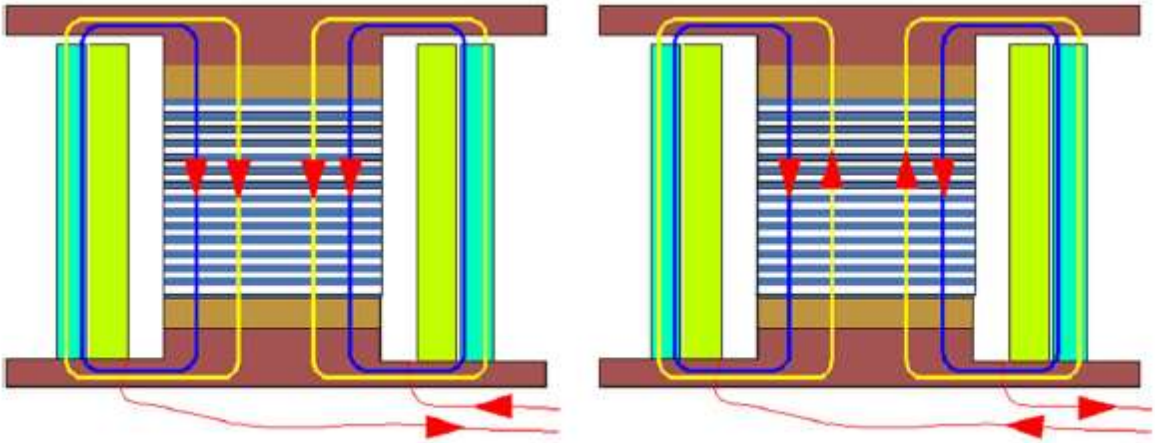

Figure 16: Working modes of hybrid magnetic system [60]

Chapter 3: Materials and Equipments

This chapter gives details about different materials, processes and equipment used to fabricate, assemble and experimentally test the base isolator. The base isolator can be categorized into four major components i.e. steel plates, steel laminations, elastomer, and magnetic coil. A schematic diagram of the isolator is presented in Figure 17. The details of components are discussed in proceeding sections.

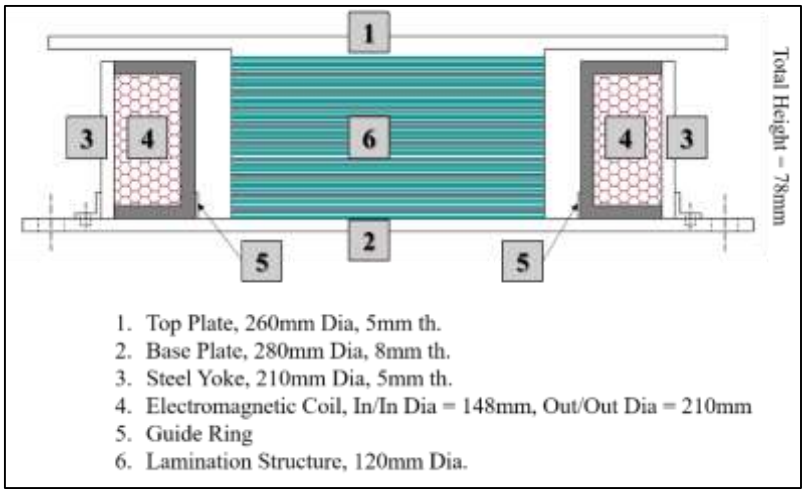

Figure 17: Schematics of base isolator

3.1 Steel Plates

The top plate is provided at top of the laminated structure to support vertical loads from and transmit horizontal loads from shake table to the super structure. It provides the platform for the models to get connected to the isolator. It is 260mm diameter with 5mm thickness, made up of mild steel grade A-36 which also contribute to an enclosed path of magnetic flux to laminated structure.

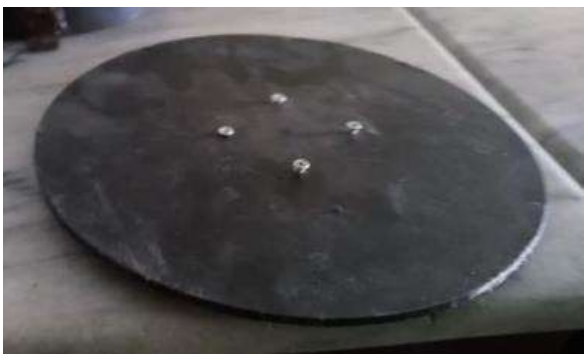

Figure 18: Steel Top Plate

Similarly, the bottom plate is also a mild steel grade A-36 plate with 5mm total thickness provided at the base of the laminated assembly. It supports all the assembly of the isolator, provides a fixture to connect to shake Table and facilitate the magnetic flux towards MRE laminations.

Figure 19: Steel Bottom Plate

A steel yoke, extending to full height of electromagnetic coil, has also been designed which is placed firmly outside the coil with the purpose to complete the magnetic flux path.

Figure 20: Steel Yoke

The configuration of these steel plates have been selected to provide an optimized magnetic flux within the laminated structure for a given electric current to the coil after a thorough analysis and numerous trials using FEMM software.

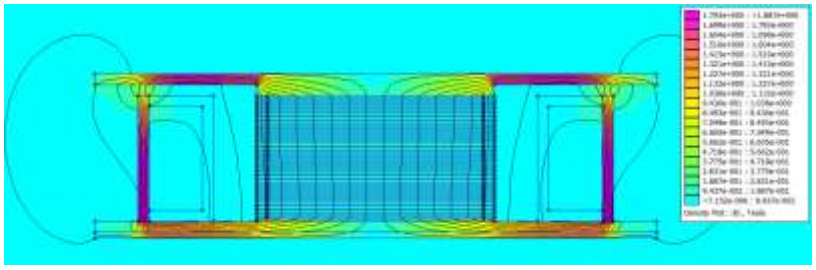

Figure 21: FEMM Output for Optimized Parameters

3.2 Steel Lamination Sheets

The isolator make use of the laminated design of traditional rubber bearing isolators. There are 17 x MRE sheets 1-2mm thick bonded onto 17 x steel plates of 1mm thickness. This laminated structure provides advantages like heavy load carrying capacity in vertical direction, prevention of lateral bulging of the rubber and attraction of magnetic flux towards themselves and thus to the non-magnetic elastomer sheets thus ensure high magnetic conductivity of the laminated structure.

Figure 22: Steel Lamination Sheets and Laminated Structure

3.3 Elastomer

MR elastomer sheets were fabricated using silicon rubber, silicon oil and iron particles mixed in an optimum proportions. The mix composition used for MRE sample is presented in Table 1.

Table 1: Mix Composition of MR Elastomer

Silicon Rubber	160ml
Silicon Oil	160ml
Iron Particles (3-4um)	440g
Iron Particles (10um)	189g
Iron % by Volume	20%

3.3.1 Silicon Rubber

Silicon rubber has been used as an elastic matrix for the fabrication of elastomer. The main reason for using the silicon rubber was that the MR phenomenon can be significantly observed in silicon rubber based elastomer.

Table 2: Technical Parameters of Silicon Rubber

Model	HY-E605
Colour	Translucent
Hardness	5 ± 2 Shore A
Curing Time	4-5 hrs.
Tensile Strength	3.5 ± 1 MPa
Viscosity	12 ± 5 kN/m
Shrinkage Rate	3000 ± 1000 mPa.s
Elongation	400%

Figure 23: Silicon Rubber

A two part silicon rubber has been used which gets hardened within 24 hours once both the parts get mixed in equal proportions. Silicon Rubber was procured from ShenZhen Hong Ye Jie Technology Co. Ltd. China. It is mainly used in mold making. The technical parameters of silicon rubber are listed in Table 2.

3.3.2 Iron Particles

Iron powder was obtained from Chengdu Best New Materials Co., Ltd. China. Literature indicates that micron sized iron particles depicts enhanced MR phenomenon in comparison to larger sized iron particles. Therefore, the micron sized iron particles were selected for fabrication of elastomer. Other technical parameters of iron powder are listed in Table 3.

Table 3: Technical Parameters of Iron Particles

Bulk Density	1.32 g/cc
Fe	98.49%
Carbon	0.87%
Oxygen	0.54%
Nitrogen	0.1%

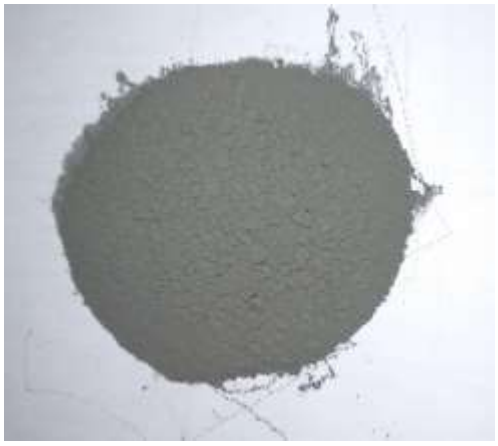

Figure 24: Iron Particles

3.4 Electromagnetic Coil

An electromagnetic coil is placed around the laminated assembly. The coil consists of a non-magnetic reel 148mm to 210mm diameter and 5mm thick made up of POM plastic around which the magnetic wire is wound. The non-magnetic reel is shown in Figure 25.

Figure 25: Non-magnetic Reel (148mm to 210mm dia, 5mm th.)

The magnetic wire is 1mm in diameter with an ampacity of 2.4-4 Amp. A total of 1000 turns have been accommodated within the reel. The wire is made up of copper with total length of magnetic wire is 827m and the total resistance of the electromagnetic coil is 17.7 Ω. The coil is shown in Figure 26.

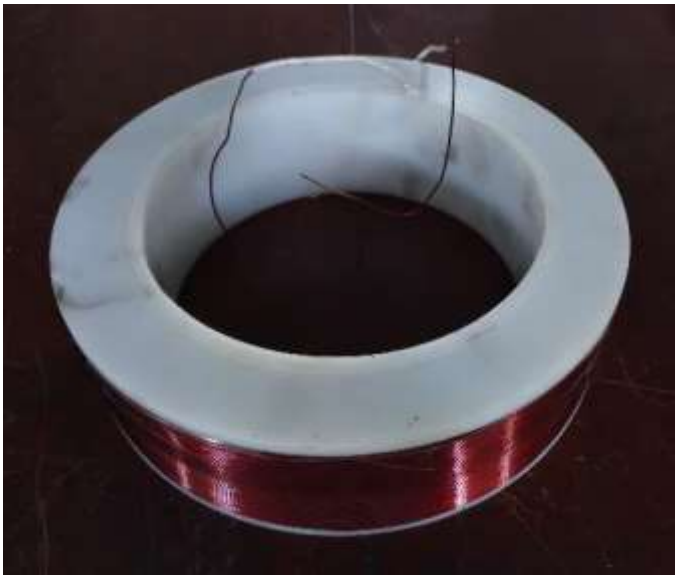

Figure 26: Electromagnetic Coil

This electromagnetic coil upon the input of current forms the magnetic core and the laminated structure together with top plate, bottom plate and steel yoke forms a complete path for the magnetic flux.

3.5 Casting of Magneto Rheological Elastomer and Laminated Structure

The fabrication of magneto-rheological elastomers requires an elastic matrix and magnetic particles. The elastic matrix used in this study was combination of silicon rubber and silicon oil whereas iron particles were used as magnetic particles. First of all silicon oil with the required volume as mentioned in Table 1 was poured in a beaker. Then the iron particles were weighed according to the requirement and mixed with the silicon oil with the help of stirring rod.

Figure 27: Iron Particles, Silicon Oil and Mixture

The part A of silicon rubber was then measured in required proportion and poured in the blend of silicon oil and iron particles. The mixture is then placed into an ultrasonic cleaner bath sonicator (Model: DSA150-SK2, size: 5.7L) for uniform mixing, dispersing and de-agglomerating and of iron particles in a mixture of silicon rubber part A and silicon oil. Sonication was done for 30 minutes.

Figure 28: Sonication of the Mix

After sonication, part B of silicon rubber was added and mixed thoroughly with the help of stirring rod. Then a mixture is poured into an exclusive casting mold that is a container with cylindrical wall bonded to a base plate made up of hardened acrylic with the help of water proof super glue (Figure 29). The diameter of container is kept as 210mm equal to that of laminated structure.

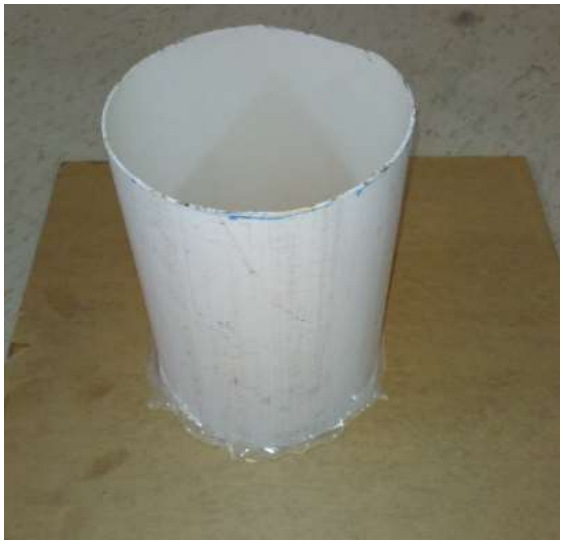

Figure 29: Casting Mold

After the pouring of mixture into casting mold, the steel plates and aluminum rings were placed one by one into the casting mold that is now partially filled with liquid elastomer. This placement of plates and rings ensured the MR elastomer sheets with required thickness once the mixture is hardened after 24 hrs.

Figure 30: Steel Sheets and Aluminum Rings

After the lapse of hardening time of silicon rubber, the laminated structure was removed from the mold and laminations were separated from each other. Aluminum rings were extracted out from hardened MR elastomer sheets after which the steel plates and MRE sheets were attached permanently to each other with the help of high strength epoxy. The final laminated structure is shown in Figure 31.

Figure 31: Laminated Structure

3.6 Experimental Testing

So far, the details regarding fabrication and arrangement of the components of adaptive base isolator have been discussed. These components can easily be arranged as per the schematics presented in Figure. For experimental testing of the isolator, the MRE base isolator is firmly fixed above the shake Table and the movement of its base will be along the shake Table vibration as shown in Figure 32. During testing, the load cell and the top plate of the isolator remain still thus eliminating any undesirable forces that may develop by the movement of top plate.

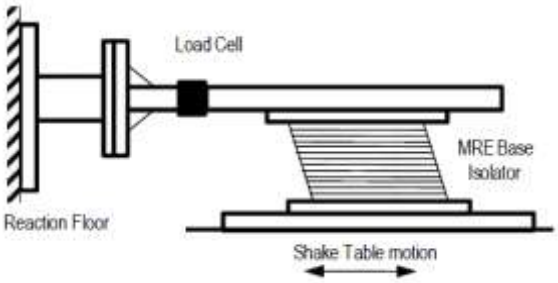

Figure 32: Sketch Map of Experimental Setup

Load cell would be installed to link the MRE base isolator and a fixed reaction rig outside of the Table to measure the lateral load applied to the isolators. Load cell has been developed exclusively for the experimental testing. It consists of a force sensor, data acquisition controller and controller modules linked together with exclusive circuit design and computer programming. Force sensor has a maximum sensing capacity of 200N with a sensitivity of 0.001N. One end of the load cell will be connected to top plate and the other would be connected to the reaction rig through a bench-fitting job. In this way, the force induced at plate end (connected to top plate) relative to the fixed end (connected to reaction rig) would be measured. The data of the load cell is stored in memory card that can be transferred to computer

once the experiment is finished for post processing. The components of load cell are shown in Figure 33.

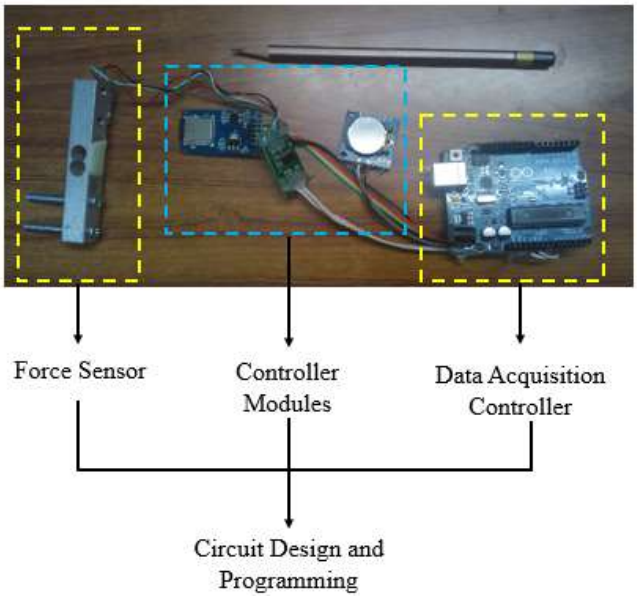

Figure 33: Load Cell

A power supply, preferably DC, with the rated capacity of 6A provides current to the magnetic coil. During testing under dynamic loading, a series of harmonic excitations at various frequencies ranging from 0.5Hz to 3.0Hz, the amplitudes of the input motion and values of input current to electromagnetic coil can be varied for a comprehensive evaluation of isolator under different kinds of vibrations.

Due to the pandemic situation in the country and subsequent decisions regarding educational/research institutes, the experimental work could not be performed and thus the objectives of this research related to experimental evaluation of MRE base isolator could not be achieved.

Chapter 4: Methodology

This chapter discusses the methodology employed for carrying out the simulation. A process flow chart showing the complete process of simulation adopted during this study is shown in Figure 35.

4.1 Structure Parameters and Characteristics

A benchmark 5 storey building structure [1,2] has been used for evaluating the structural response. The building structure can be idealized as 5 degree-of-freedom (DOF) model with mass lumped at each storey. The simple representation of the idealized model is shown in Figure 34.

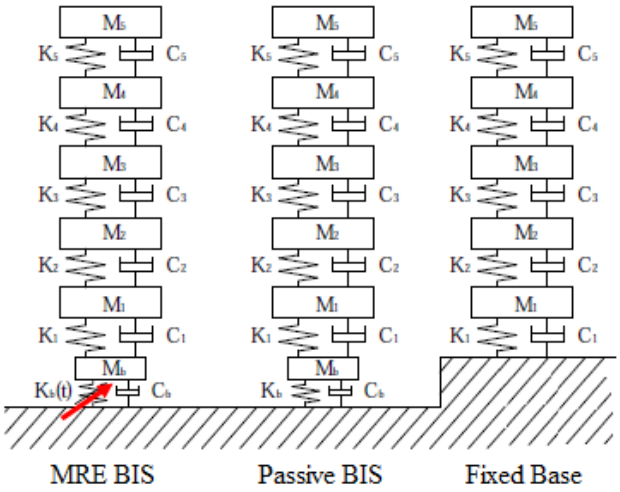

Figure 34: Building structure idealized representation [1]

With addition of isolation layer, the model can be treated as 6 degree-of-freedom system for both passive and MRE controlled isolated structural models. In Figure 34, M, K and C represent mass, stiffness and damping while their subscripts represent the level at which the given values are applicable. For example M_b is mass at isolation layer. Similarly, K_b is stiffness and C_b is damping coefficient at isolation level. Since MRE controlled isolation has the tendency to change its stiffness at any time instance, the stiffness is denoted as K(t).

The parameters of building model used in simulation are adopted from [1,2] and presented in Table 4.

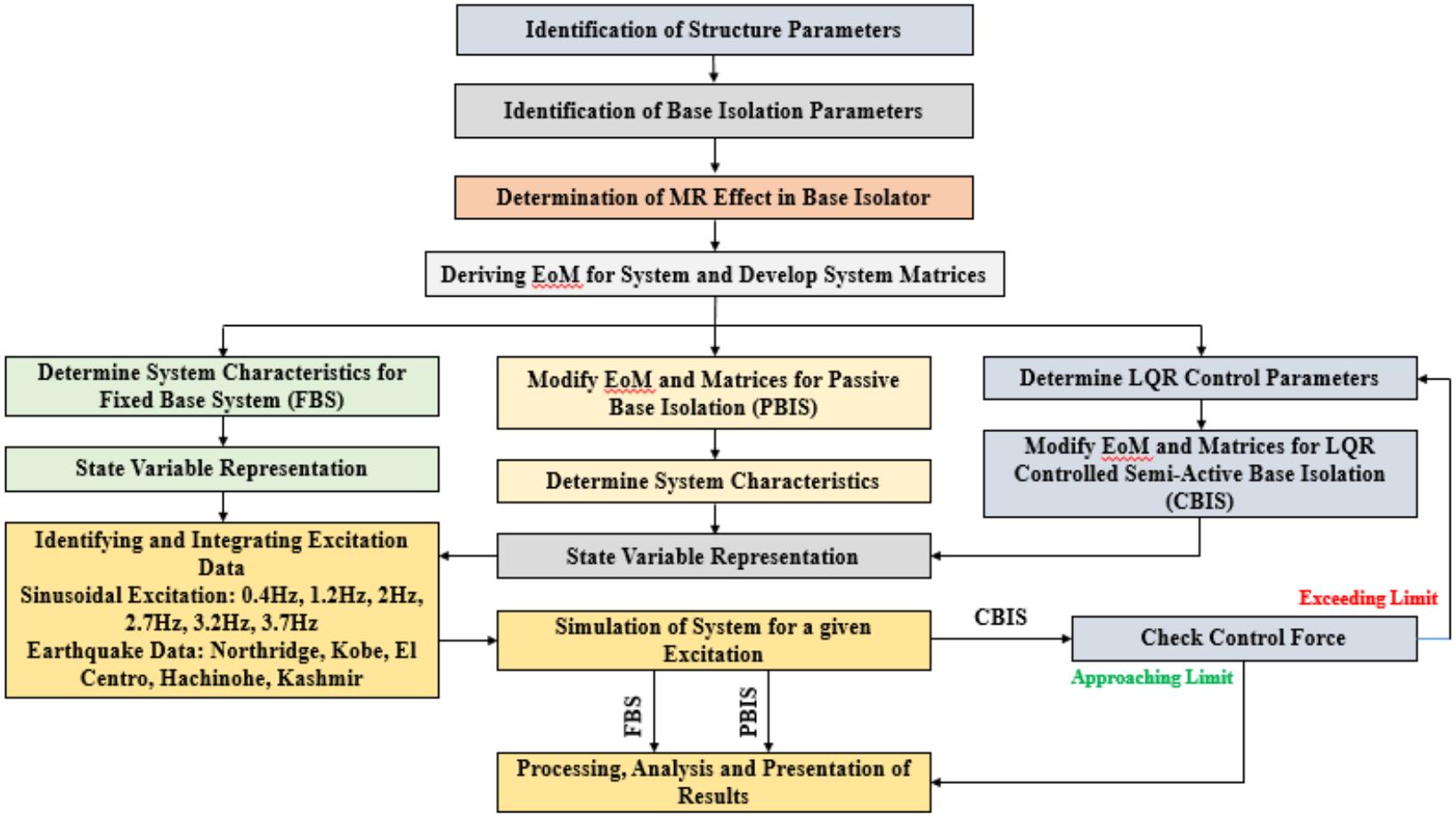

Figure 35: Simulation Process Flowchart

Table 4: Structure Parameters

Storey	Mass (kg)	Stiffness (kN/m)	Damping (kN.s/m)
1	5897	33732	67
2	5897	29093	58
3	5897	28621	57
4	5897	24954	50
5	5897	19059	38

The parameters of isolation layer used for simulation are adopted from [3] and presented in Table 5.

Table 5: Base Isolation Parameters

Stiffness	232 kN/m
Damping	3.74 kN.s/m
MR Effect	137%

Using above parameters, the corresponding structure characteristics like time periods, natural frequencies can be worked out as they are the Eigen values depending on the mass and stiffness of the structure. These as are tabulated in Table 6.

Table 6: Structure vibration characteristics

	Fixed Base		Passive BIS	
Mode	Frequency (Hz)	Time Period (s)	Frequency (Hz)	Time Period (s)
1	3.20	0.31	0.40	2.5
2	8.72	0.11	5.47	0.2
3	13.62	0.07	10.30	0.1
4	17.61	0.06	14.73	0.07
5	20.92	0.05	18.41	0.05
6	-	-	21.32	0.04

Similarly, mode shapes can be plotted from the Eigen vectors of the system matrices depending on the mass and stiffness values of the structure. Mode shapes of fixed base structure and isolated structures are shown in Figure 36 and 37 respectively.

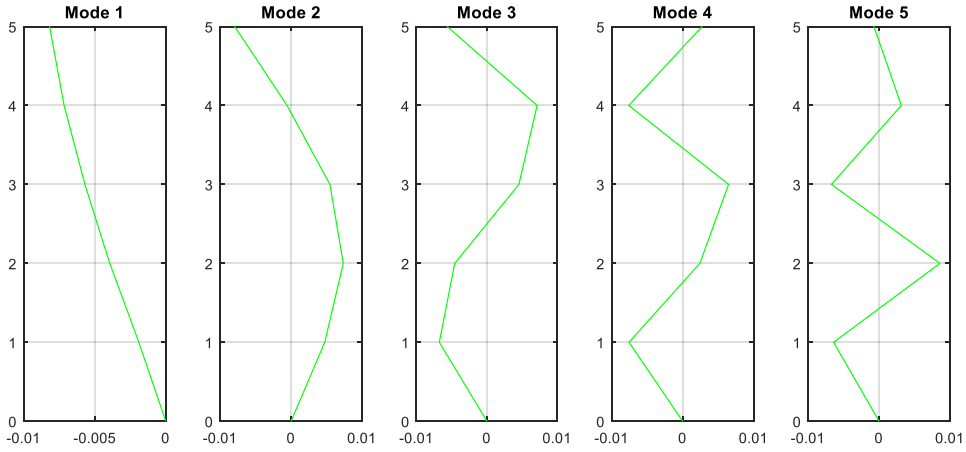

Figure 36: Mode Shapes of Fixed Base Structure

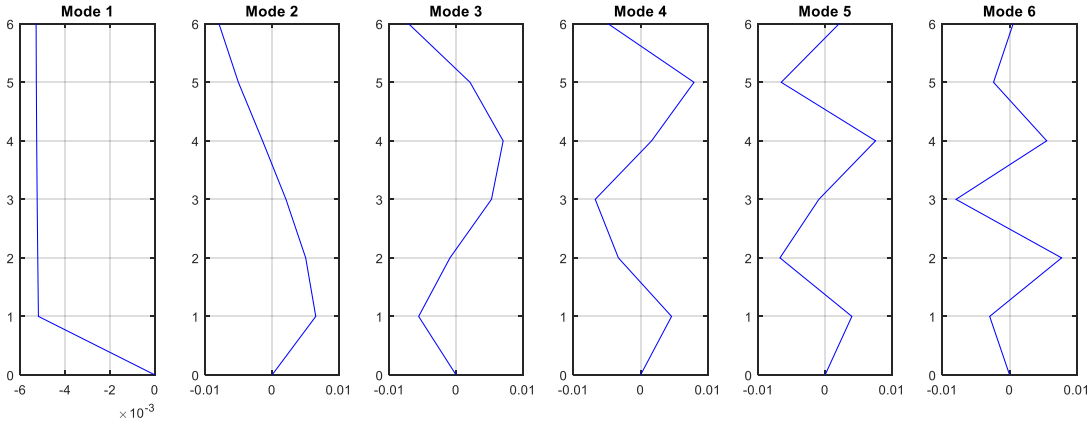

Figure 37: Mode Shapes of Base Isolated Structure

4.2 Equation of Motion and System Matrices

Assuming linear structure properties and representing the displacements relative to the ground as

$$x = \begin{bmatrix} x_b & x_1 & x_2 & x_3 & x_4 & x_5 \end{bmatrix}^T$$

the equation of motion for structure reduced into matrix form can be expressed as

$$[M]\{\ddot{x}(t)\} + [C]\{\dot{x}(t)\} + [K]\{x(t)\} = [\gamma]\{u(t)\} + [\delta]\ddot{x}_g \quad \text{..... (1)}$$

The mass, stiffness and damping matrices for fixed base system are 5x5 matrices and can be given as

$$M = Mass\ matrix = \begin{bmatrix} m_1 & 0 & 0 & 0 & 0 \\ 0 & m_2 & 0 & 0 & 0 \\ 0 & 0 & m_3 & 0 & 0 \\ 0 & 0 & 0 & m_4 & 0 \\ 0 & 0 & 0 & 0 & m_5 \end{bmatrix}$$

$$C = Damping\ matrix = \begin{bmatrix} c_1 + c_2 & -c_2 & 0 & 0 & 0 \\ -c_2 & c_2 + c_3 & -c_3 & 0 & 0 \\ 0 & -c_3 & c_3 + c_4 & -c_4 & 0 \\ 0 & 0 & -c_4 & c_4 + c_5 & -c_5 \\ 0 & 0 & 0 & -c_5 & c_5 \end{bmatrix}$$

$$K = Stiffness\ matrix = \begin{bmatrix} k_1 + k_2 & -k_2 & 0 & 0 & 0 \\ -k_2 & k_2 + k_3 & -k_3 & 0 & 0 \\ 0 & -k_3 & k_3 + k_4 & -k_4 & 0 \\ 0 & 0 & -k_4 & k_4 + k_5 & -k_5 \\ 0 & 0 & 0 & -k_5 & k_5 \end{bmatrix}$$

The mass, stiffness and damping matrices for base isolated structure are 6x6 matrices and can be given as

$$M = Mass\ matrix = \begin{bmatrix} m_b & 0 & 0 & 0 & 0 & 0 \\ 0 & m_1 & 0 & 0 & 0 & 0 \\ 0 & 0 & m_2 & 0 & 0 & 0 \\ 0 & 0 & 0 & m_3 & 0 & 0 \\ 0 & 0 & 0 & 0 & m_4 & 0 \\ 0 & 0 & 0 & 0 & 0 & m_5 \end{bmatrix}$$

$$C = Damping\ matrix = \begin{bmatrix} c_b + c_1 & -c_1 & 0 & 0 & 0 & 0 \\ -c_1 & c_1 + c_2 & -c_2 & 0 & 0 & 0 \\ 0 & -c_2 & c_2 + c_3 & -c_3 & 0 & 0 \\ 0 & 0 & -c_3 & c_3 + c_4 & -c_4 & 0 \\ 0 & 0 & 0 & -c_4 & c_4 + c_5 & -c_5 \\ 0 & 0 & 0 & 0 & -c_5 & c_5 \end{bmatrix}$$

$$K = Stiffness\ matrix = \begin{bmatrix} k_b + k_1 & -k_1 & 0 & 0 & 0 & 0 \\ -k_1 & k_1 + k_2 & -k_2 & 0 & 0 & 0 \\ 0 & -k_2 & k_2 + k_3 & -k_3 & 0 & 0 \\ 0 & 0 & -k_3 & k_3 + k_4 & -k_4 & 0 \\ 0 & 0 & 0 & -k_4 & k_4 + k_5 & -k_5 \\ 0 & 0 & 0 & 0 & -k_5 & k_5 \end{bmatrix}$$

γ is the force location matrix to be used only for MRE based isolated structure model. For fixed base and passive isolated models, γ would be a null matrix. Similarly u(t) is the applied force and applicable only to MRE isolated structure model.

$$\gamma = \text{n x r force location matrix} = [-1\ \ 0\ \ 0\ \ 0\ \ 0\ \ 0]^T$$

$$u(t) = [u(t)_b\ u(t)_1\ u(t)_2\ u(t)_3\ u(t)_4\ u(t)_5]^T$$

δ is the coefficient vector for earthquake ground acceleration, $\ddot{x}_g$. δ will be 5x1 for fixed base structure model and 6x1 for isolated structure models.

$\delta = [m_1\ m_2\ m_3\ m_4\ m_5]^T$ - For fixed base structure.

$\delta = [m_b\ m_1\ m_2\ m_3\ m_4\ m_5]^T$ - For isolated structures.

4.3 State-space Representation

Equation (1) can be re-arranged in terms of structural acceleration as

$$\{\ddot{x}(t)\} = -[M]^{-1}[C]\{\dot{x}(t)\} - [M]^{-1}[K]\{x(t)\} + [M]^{-1}[\gamma]\{u(t)\} + [M]^{-1}\{\delta\}\ddot{x}_g(t)$$

The equations can now be re-written in the form

$$\begin{Bmatrix}\{\dot{x}(t)\}\\ \{\ddot{x}(t)\}\end{Bmatrix} = \begin{bmatrix}[0] & [I]\\ -[M]^{-1}[K] & -[M]^{-1}[C]\end{bmatrix}\begin{Bmatrix}x(t)\\ \dot{x}(t)\end{Bmatrix} + \begin{bmatrix}[0]\\ [M]^{-1}[\gamma]\end{bmatrix}\{u(t)\} + \begin{Bmatrix}[0]\\ [M]^{-1}\{\delta\}\end{Bmatrix}\ddot{x}_g(t) \quad \ldots\ldots \quad (2)$$

The second-order equation of motion (1) can be cast to its first-order state-variable representation by defining the following state-vector in an effort to apply linear control theory developed for first order dynamic systems [4,5,6,7].

$$\{Z(t)\} = \begin{Bmatrix}x(t)\\ \dot{x}(t)\end{Bmatrix}$$

Then equation (2) can be expressed as

$$\{\dot{Z}(t)\} = [A]\{Z(t)\} + [B_u]\{u(t)\} + \{B_r\}\ddot{x}_g(t) \quad \ldots\ldots \quad (3)$$

where

$$\{\dot{Z}(t)\} = \begin{Bmatrix}\{\dot{x}(t)\}\\ \{\ddot{x}(t)\}\end{Bmatrix}$$

Matrix [A] in equation (3), also known as plant matrix would be 10x10 matrix for fixed base structure and 12x12 matrix for isolated structure models and will be expressed as:

$$[A] = \begin{bmatrix}[0] & [I]\\ -[M]^{-1}[K] & -[M]^{-1}[C]\end{bmatrix}$$

$[B_u]$ would be null matrix for fixed base and passive base isolated structure model and 12x1 matrix for MRE isolated structure model and will be expressed as:

$$[B_u] = \begin{bmatrix} [0] \\ [M]^{-1}[\gamma] \end{bmatrix}$$

$[B_r]$ would be 10x1 vector for fixed base structure and 12x1 vector for both passive base isolated structure and MRE isolated structure models. It can be expressed as:

$$\{B_r\} = \begin{Bmatrix} \{0\} \\ [M]^{-1}\{\delta\} \end{Bmatrix}$$

4.4 LQR Feedback Control

Equarion (3) cannot be solved directly because the number of equations, 12 is less than the number of unknown variables, 13 in case of base isolation i.e. 12 x response outputs Z(t) and 1 x control force u(t). So, one more equation in this case is needed in an effort to solve the control problem. This 1 equation is referred as the feedback control law. There are 3 control outlines through which the feedback control law can be implemented [4,5,7] to the smart structure model i.e.

- Open-loop feedback control
- Closed-loop feedback control
- Open-closed loop feedback control

For open loop feedback control the control force is determined by a feedback of excitation at the base, such as sinusoidal motion or earthquake ground motion. The input information for its control law is only the base excitation data acquired with the help of accelerometers etc. The obtained information is then used to calculate the required control force. The schematics of open loop control is shown in Figure 38.

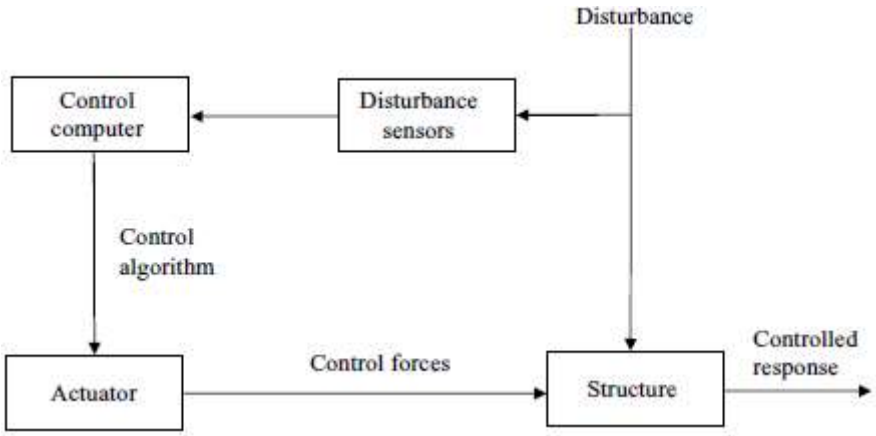

Figure 38: Schematics of open loop feedback control [8]

For closed loop feedback control, the control force is determined by a feedback of structure responses at each or some degree-of-freedom. The input information for its control law consists of the structure responses such as velocities or relative displacements with the help of sensors. The acquired information is then used to calculate the required control force. The schematics of closed loop control is shown in Figure 39.

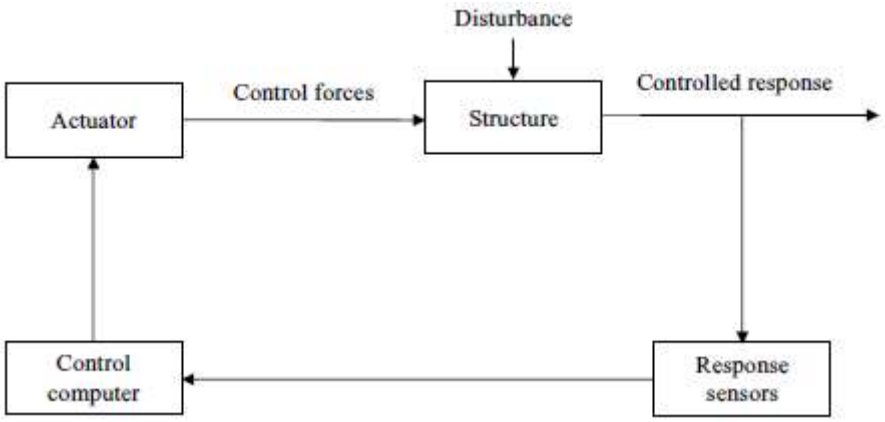

Figure 39: Schematics of closed loop feedback control [8]

The open-closed-loop scheme is a combination of both the closed loop and open-loop control schemes. It can obtain information of both the ground motions and the structure responses. Schematics of open-closed loop control are shown in Figure 40. The control force is dependent on ground motion, displacement and velocity responses.

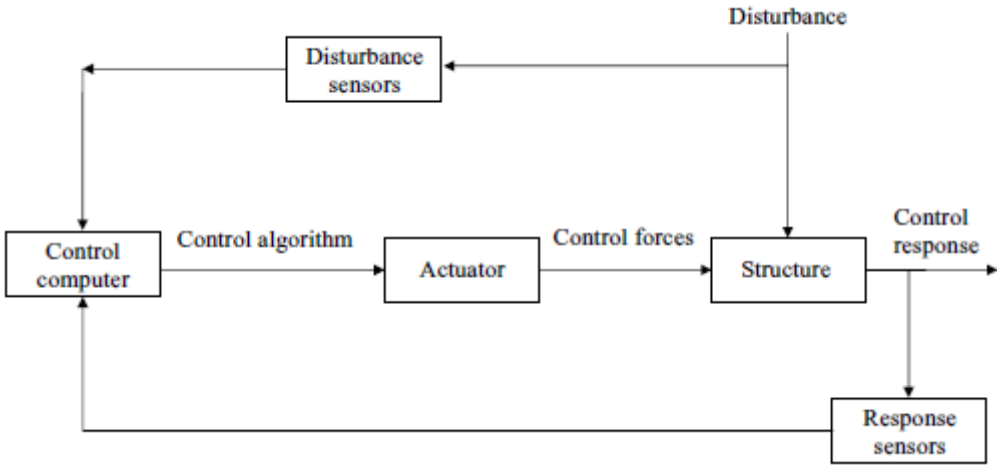

Figure 40: Schematics of open-closed-loop feedback control [8]

Utilizing one of the above discussed control schemes, equation (3) can be solved mathematically. For structure with closed-loop feedback control, the control force matrix is determined by using the measurements of response values and feeding them back to the equation. In this way, the feedback law will be given as

$$\{u(t)\} = -[G]\ \{Z(t)\} \quad \ldots\ldots \quad (4)$$

In case of MRE base isolated model, u will be a single value of force applied at isolation level. G is 1x12 matrix of feedback gain. Hence, the key parameter to make equation (3) mathematically solvable is gain matrix G. In current study, the gain matrix is obtained by using Linear Quadratic Regulator (LQR) algorithm and discussed ahead.

Once G is obtained, the closed-loop system takes the form as expressed below

$$\{\dot{Z}(t)\} = [A_c]\{Z(t)\} + \{B_r\}\ddot{x}_g(t)$$

Where A_c is the closed loop plant matrix obtained through substitution operation of equation (4) into equation (3) and expressed as

$$[A_c] = [A] - [B_u][G]$$

Linear Quadratic Regulator (LQR) algorithm for structural control is an optimal control algorithm. The key objective of LQR is to minimize the following quadratic cost function J with respect to the control force input u(t).

$$J = \int_0^t [z^T(t)Qz(t) + u^T(t)Ru(t)]dt$$

In regulator type algorithm problems, the system is idealized to be in equilibrium, and LQR control algorithm serves the purpose of maintaining that equilibrium regardless of the fact that the system is subjected to turbulences or of minimizing the response of the system under consideration from any sorts of disturbances [9].

The parameters Q and R in the quadratic cost function J are used as design parameters to penalize the state variables and the control signals respectively. The larger these values are, the more will be penalizing of these signals. Choosing a large value for R means system is intended to get stabilized with less (weighted) force. This is usually known as expensive control strategy. On the other hand, choosing a small value for R means the control force will not be penalized.

Similarly, a large value for Q means the system is intended to get stabilize with the least possible changes in the states and small Q implies less concern about the changes in the states.

So Q and R are basically the tuning knobs requiring the adjustments to strike a balance between state response and control force.

There is an exclusive function of 'lqr()' in MATLAB [91] to calculate the gain matrix from the input of closed loop plant matrix A_c and B_u along with Q and R values. The syntax is shown below.

```
[G,S,E]=lqr(cA,Bu,Q,R);
```

4.5 Control Force

In this study, the MR elastomer is idealized as a linear stiffness element. Though the assumption of linear behavior does not represent the actual characteristics of MR elastomers but it does denotes the general dynamics of the material in a small strain range and permits a rather simple approach to investigate the controllable isolation system [1].

The stiffness of the MR elastomer is expressed as K(t), which is the sum of actual (zero field) stiffness and the varying stiffness that is dependent on the external magnetic field or the current value through electromagnetic coil. The MRE stiffness can be written as

$$K(t) = K_o + K_1(u(t))$$

where K_0 is the actual (baseline) stiffness of MREs and $K_1(u(t))$ denotes the variation in stiffness with time due to the command input u(t) at any time instant. In current study, an MR elastomer material with MR effect of 137% has been adopted as reported in [3]. Hence, the maximum values of the stiffness that can be physically achieved is

$$K_{1,max} = 1.37K_o$$

Thus, K(t) will vary from 0 to $2.37K_o$. This maximum achievable stiffness value provides an upper limit to the control force that is

$$u(t)_{max} \leq K(t)_{max} * x_b$$

For ensuring the optimal performance of the system, the control force u(t) has to be approaching the limit. If the control force is considerably lower than its upper limit, then the isolator would be underperforming and if it is higher than the limit, then isolator will not be able to generate the required force. So some trials have to be performed, for every excitation loading, by varying Q and R parameters of LQR algorithm until a control force equal to its limit is obtained.

4.6 Excitation Data

The fixed base, passively isolated and MRE controlled isolated structures are subjected to sinusoidal and earthquake excitations in form of acceleration for analyzing their responses.

4.6.1 Sinusoidal Excitation

The harmonic loadings selected for the loading are tabulated below, Table 7. Fundamental frequencies of fixed base and isolated structures are selected to analyze the response of all 3 structures. Intermediate frequencies have also been selected to gauge the response over the range of frequencies. The peak acceleration has been selected as 0.18g for all the cases.

Table 7: Harmonic Excitation Data

Frequency of Vibration	Comments
0.4 Hz.	Fundamental frequency of passively isolated structure.
1.2 Hz.	
2.0 Hz.	
2.7 Hz.	
3.2 Hz.	Fundamental frequency of fixed base structure.
3.7 Hz.	

The selected sinusoidal excitation time histories are shown in Figures 41-46 below:

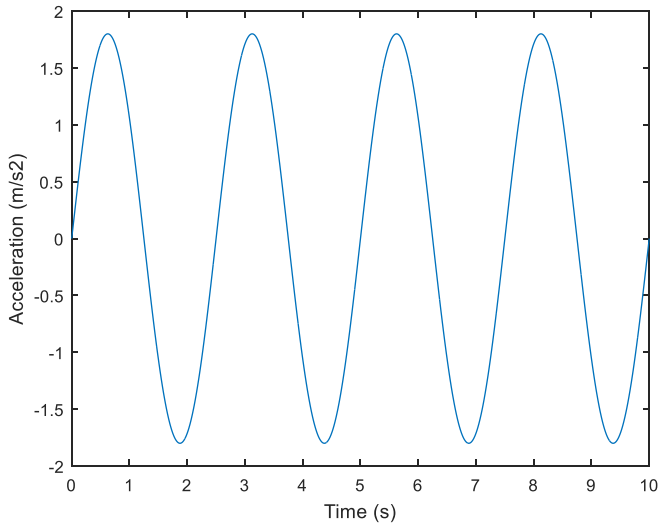

Figure 41: Excitation at 0.4Hz.

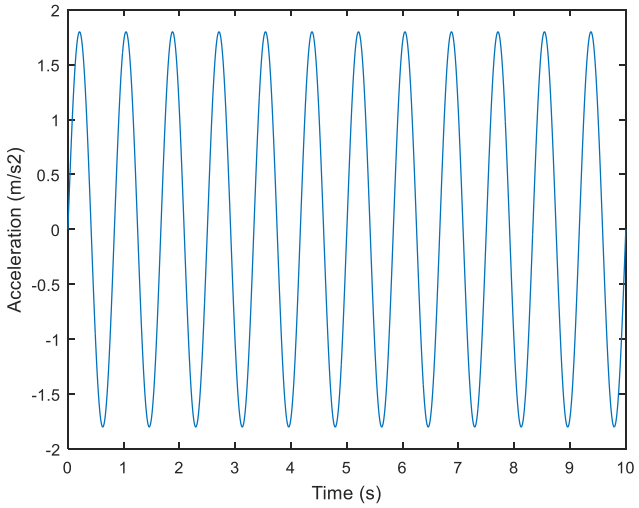

Figure 42: Excitation at 1.2Hz.

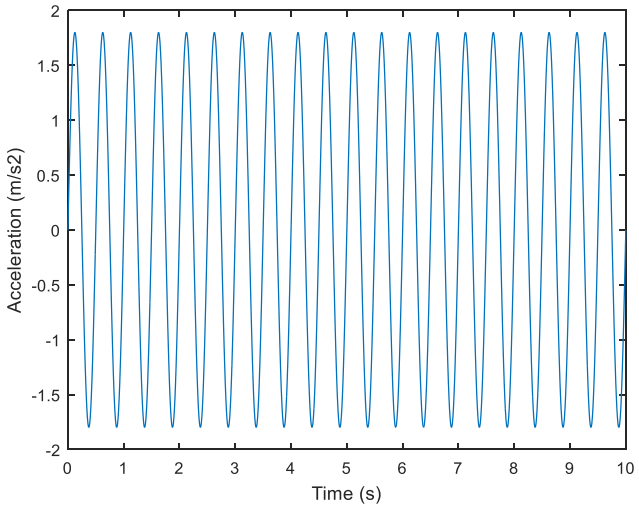

Figure 43: Excitation at 2.0Hz.

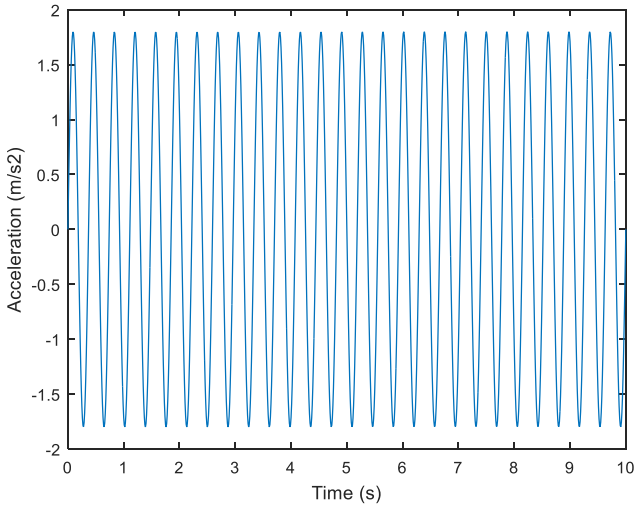

Figure 44: Excitation at 2.7Hz.

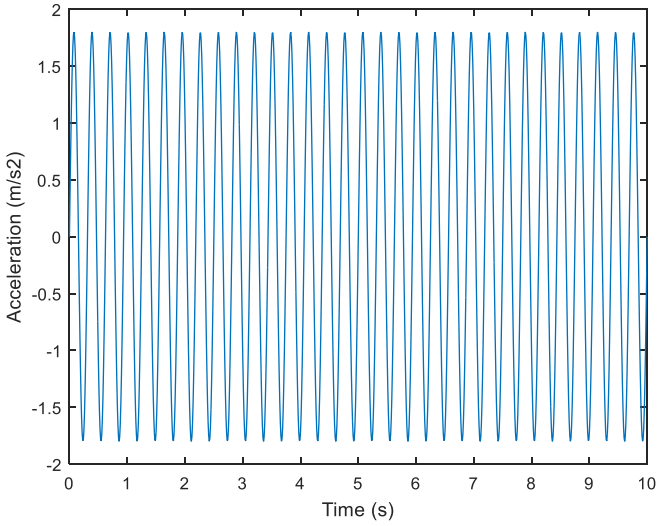

Figure 45: Excitation at 3.2Hz.

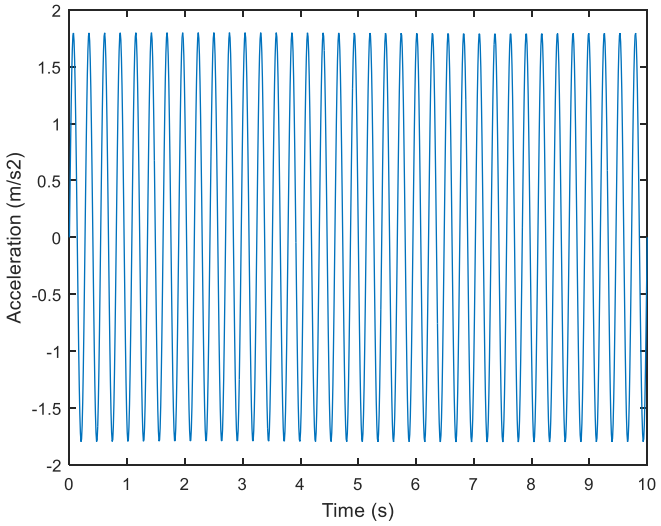

Figure 46: Excitation at 3.7Hz.

4.6.2 Earthquake Time Histories

In current study, near-fault earthquake ground motion [76-90] time histories have been selected from 1999 Chi-Chi, 1979 Imperial Valley and 1999 Kocaeli earthquakes. These records are taken from stations Taichung, Brawley Airport and Izmit respectively [78]. Furthermore, another set of earthquake time histories, which are recorded from the same earthquakes events, at the same site geological conditions with fault located at a distance far away from the site, is selected to demonstrate far field ground motion characteristics [76-90]. The properties and description of all the adopted time histories are presented in Table 8.

		Near Fault				Far Fault			
Event	**M_w**	**Station**	**PGA**	**PGV (cm/s)**	**Distance to fault (km)**	**Station**	**PGA**	**PGV (cm/s)**	**Distance to fault (km)**
Chi-Chi (1999)	7.6	Taichung	0.2g	36.3	9.50	Ilan	0.2g	11.8	49
Imperial Valley (1979)	6.9	Brawley Airport	0.16g	36.6	8.50	Compuertas	0.15g	9.5	35
Kocaeli (1999)	7.8	Izmit	0.17g	22.6	4.8	Fatih	0.16g	12	64.5

Table 8: Earthquake Parameters

The ground motion time histories are adopted from the PEER Strong Motion Database [78].

It has been aimed to acquire two time history records with same peak ground acceleration of each earthquake (Chi-Chi 1999, Imperial Valley 1979 and Kocaeli 1999) for a more accurate and a fair comparison of the results [76]. So, the selection of records have been made with more diligence. If the ground motion time histories of each earthquake were selected randomly (different peak acceleration values and/or site conditions), the meaningful comparison of the responses could not have been established with confidence. So, it is aimed to eliminate this contradiction by selected ground motion records with same peak acceleration values at same site conditions [76, 78].

The acceleration, velocity, and response spectra records of the adopted earthquake time histories are shown in Figures 47, 48 and 49. Same vertical scale in the plots have been adopted for near fault and far fault records to demonstrate the difference between the earthquakes. These figures show the significant velocity pulses for the near-fault ground motions compared to far-field records [77] despite have same peak ground acceleration, that are one of the main characteristics of destructive near field earthquake records [76-90].

In this way, a total of 12 simulations have been performed for each of the fixed base, passively isolated and MR elastomer based isolated structures using MATLAB [91]. The cumulative number to simulations for all the 3 structures and 12 load cases sums up to 36. A total of 612 responses were compiled and analyzed after which the results are processed, compared and presented.

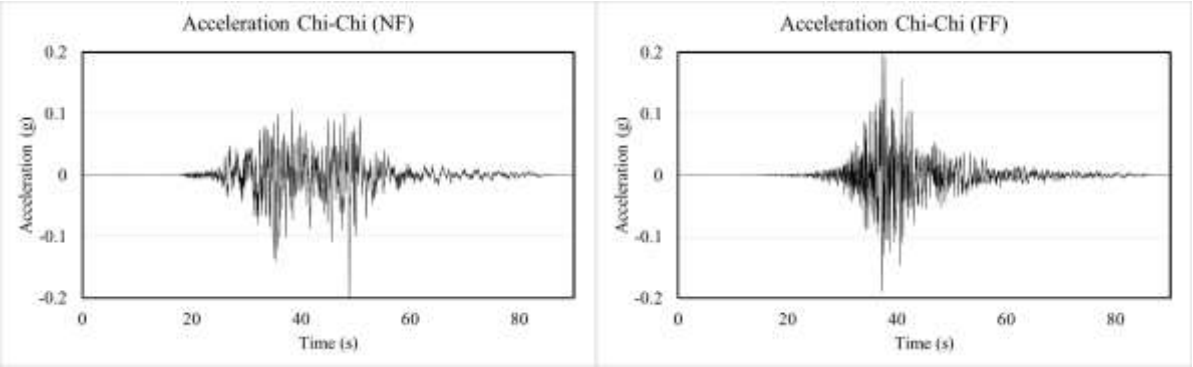

(a)

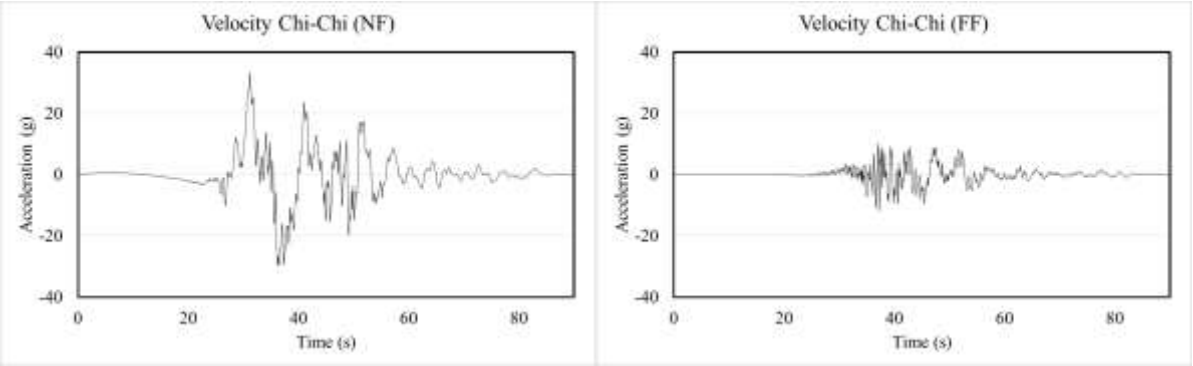

(b)

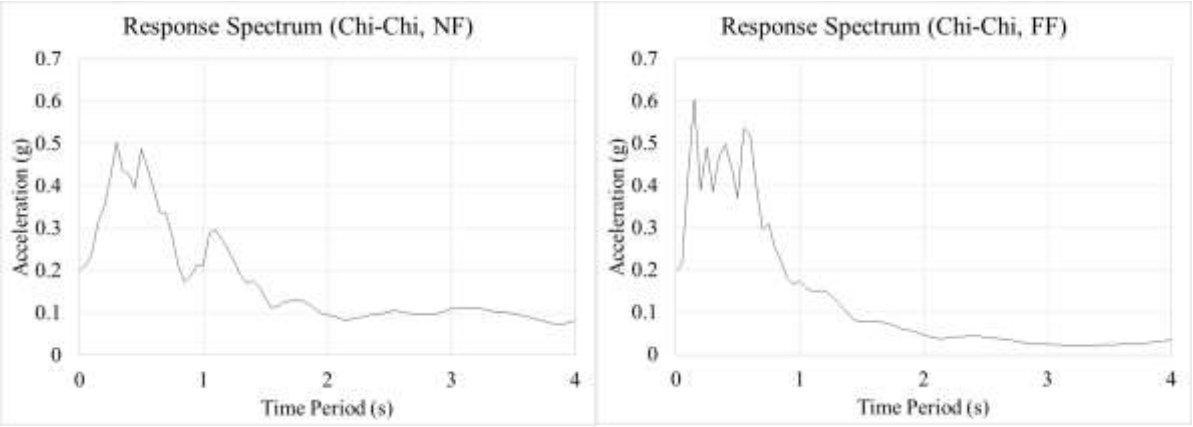

(c)

Figure 47: Near-fault and far-fault ground motions recorded at Chi-Chi earthquake 1999. a Acceleration time histories for near-fault and far-fault earthquake record. b Velocity time-histories for near-fault and far-fault earthquake record. c Response spectra for near-fault and far-fault earthquake record [78].

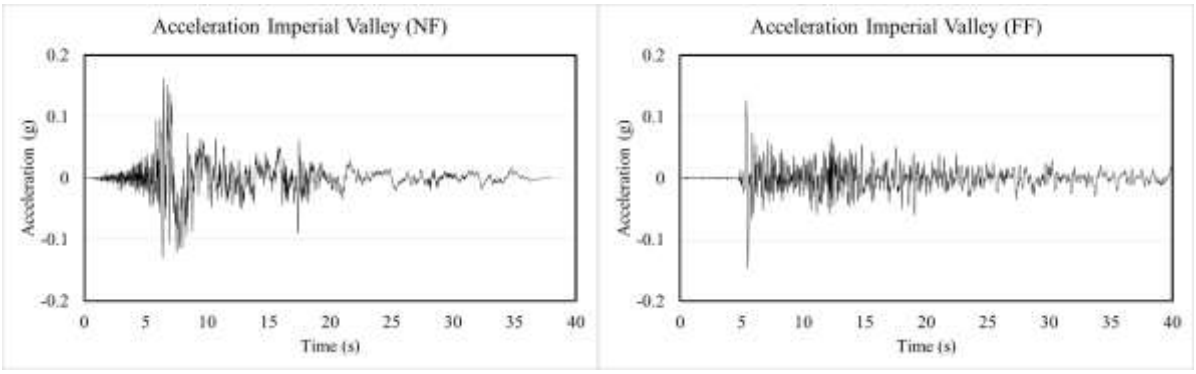

(a)

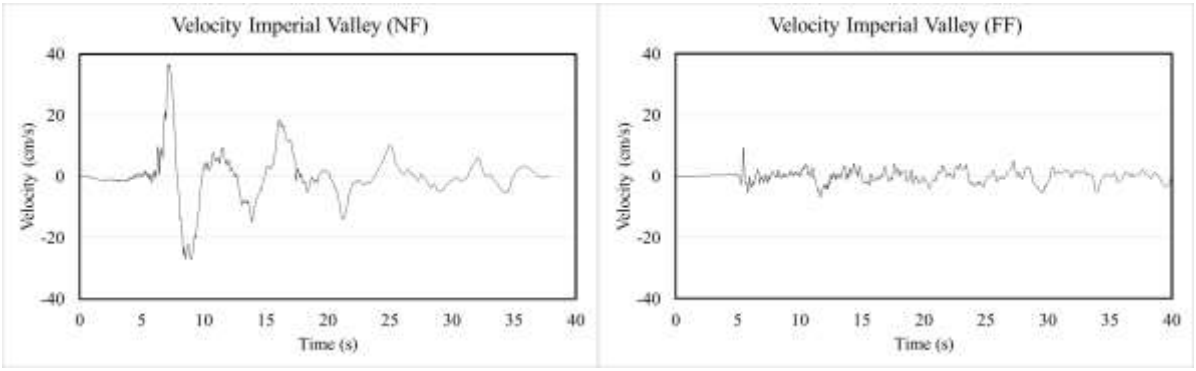

(b)

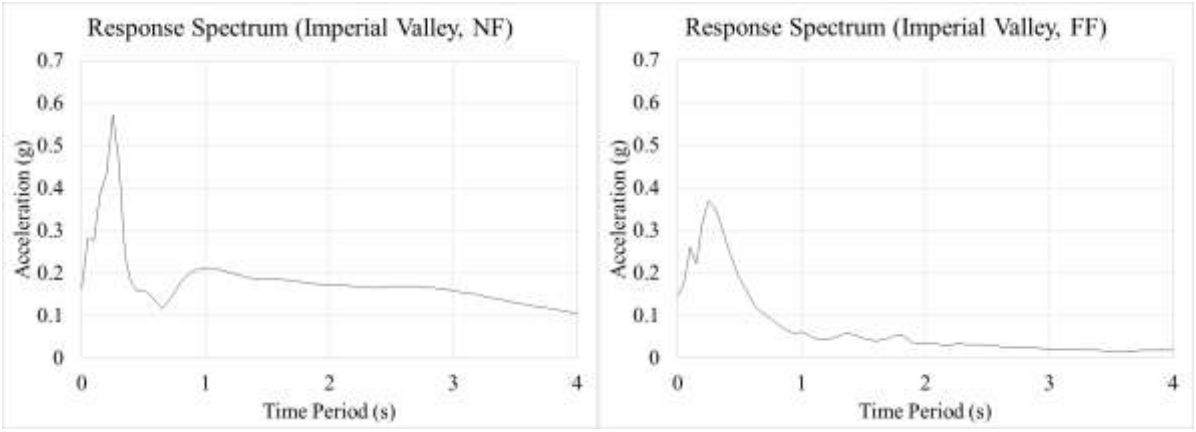

(c)

Figure 48: Near-fault and far-fault ground motions recorded at Imperial Valley earthquake 1979. a Acceleration time history for near-fault and far-fault earthquake records. b Velocity time-history for near-fault and far-fault earthquake records. c Response spectra for near-fault and far-fault earthquake records [78].

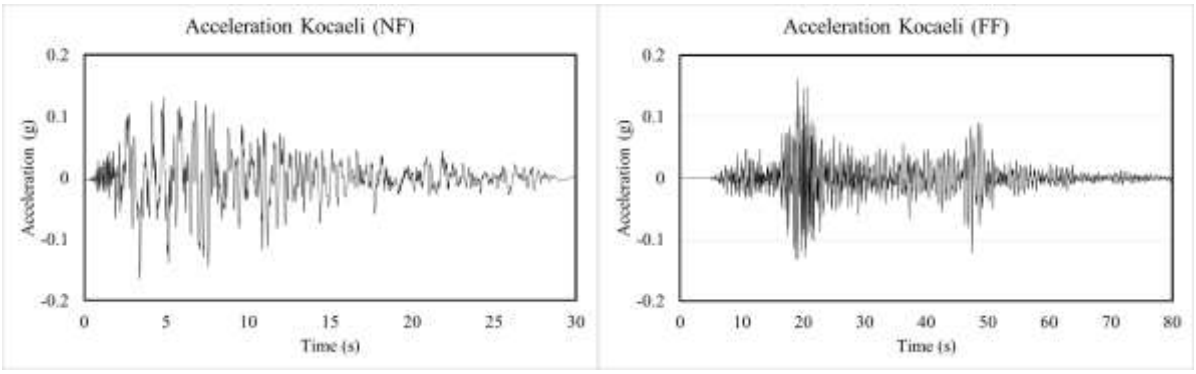

(a)

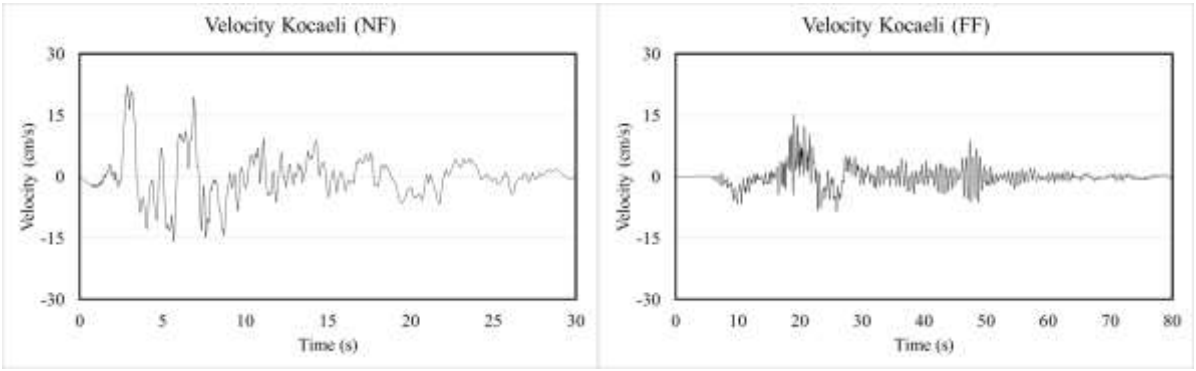

(b)

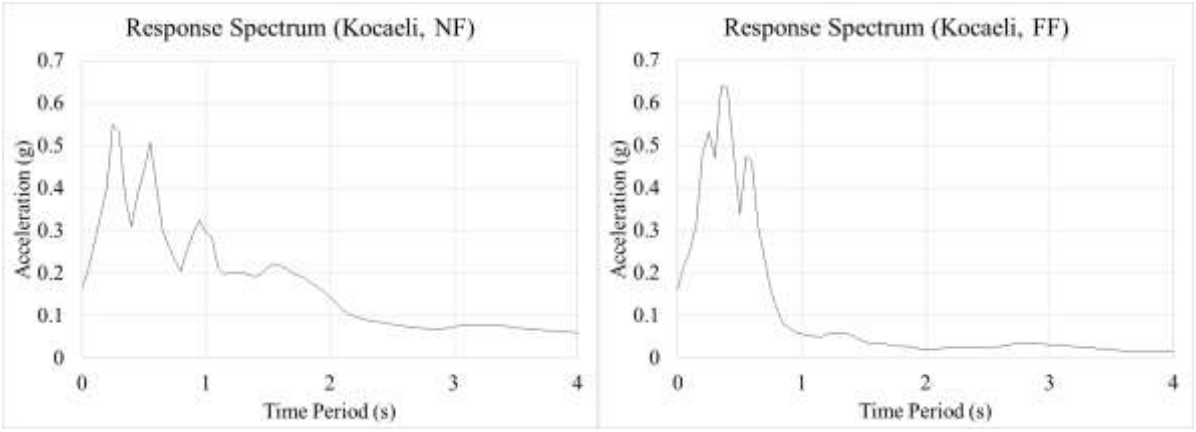

(c)

Figure 49: Near-fault and far-fault ground motions recorded at Kocaeli earthquake 1999. a Acceleration time histories for near-fault and far-fault earthquake record. b Velocity time-histories for near-fault and far-fault earthquake record. c Response spectra for near-fault and far-fault earthquake record [78].

Chapter 5: Results and Discussions

This chapter presents the results of simulations performed and discussions regarding those results. First off, the displacement, storey drifts and acceleration responses along with the representative time histories of sinusoidal excitations are presented and compared. Then the responses for the case of earthquake excitation time histories are analyzed and discussed.

5.1 Sinusoidal Excitation

As discussed in chapter 4, six loading frequencies have been selected for evaluating the response of structures. The responses against those frequencies are discussed below.

5.1.1 Displacement Responses

Displacement response is the total displacement of the storey at the corresponding degree-of-freedom. The peak and RMS values of displacement responses against loading frequencies for fixed base, passively isolated and MR elastomer based isolated structures are tabulated in Table 9.

Table 9: Displacement Peak and RMS Values (Harmonic loading)

		Fixed Base		Passive BIS		MRE BIS	
	Storey	Peak (cm)	RMS (cm)	Peak (cm)	RMS (cm)	Peak (cm)	RMS (cm)
0.4 Hz	Base	-	-	645.14	339.37	19.99	13.98
	1	0.17	0.11	648.76	341.28	20.12	14.07
	2	0.33	0.22	652.12	343.05	20.24	14.15
	3	0.45	0.30	654.68	344.40	20.33	14.21
	4	0.55	0.36	656.65	345.43	20.40	14.26
	5	0.61	0.40	657.93	346.11	20.44	14.29
1.2 Hz	Base	-	-	13.75	4.14	8.84	2.45
	1	0.23	0.13	13.83	4.17	8.89	2.47
	2	0.46	0.25	13.90	4.19	8.94	2.48
	3	0.63	0.34	13.96	4.20	8.98	2.49
	4	0.77	0.41	14.00	4.22	9.01	2.50
	5	0.87	0.46	14.03	4.23	9.04	2.51
2.0 Hz	Base	-	-	5.98	2.02	4.59	0.92
	1	0.36	0.17	6.02	2.03	4.62	0.93
	2	0.72	0.34	6.05	2.04	4.65	0.93
	3	1.02	0.48	6.08	2.05	4.67	0.94
	4	1.25	0.58	6.09	2.05	4.69	0.94

	5	1.41	0.66	6.11	2.06	4.70	0.95
2.7 Hz	Base	-	-	4.74	1.41	3.27	0.55
	1	0.74	0.35	4.77	1.42	3.29	0.56
	2	1.52	0.70	4.79	1.42	3.31	0.56
	3	2.17	1.00	4.81	1.43	3.32	0.56
	4	2.70	1.24	4.83	1.43	3.33	0.57
	5	3.07	1.40	4.84	1.44	3.34	0.57
3.2 Hz	Base	-	-	3.85	1.16	2.75	0.42
	1	3.33	2.27	3.87	1.17	2.77	0.42
	2	6.92	4.71	3.89	1.17	2.79	0.42
	3	9.99	6.80	3.91	1.18	2.81	0.43
	4	12.56	8.55	3.92	1.18	2.82	0.43
	5	14.36	9.77	3.93	1.19	2.83	0.43
3.7 Hz	Base	-	-	3.17	0.99	2.32	0.33
	1	0.67	0.26	3.19	1.00	2.33	0.33
	2	1.41	0.56	3.20	1.00	2.34	0.34
	3	2.06	0.83	3.22	1.01	2.35	0.34
	4	2.62	1.06	3.23	1.01	2.36	0.34
	5	3.01	1.23	3.24	1.01	2.37	0.35

Representative displacement time histories are shown in Figures 49, 50 and 51 below. It is clear from the Figures that isolated structures vibrate at much lower frequencies and higher amplitudes compared to fixed base structure. Lower frequencies of vibration is due to higher value of fundamental time period for passively isolated structure. Higher amplitudes are due to larger displacements at base level. Since 0.4 Hz and 3.2 Hz are the fundamental frequencies of passively isolated and fixed base structure respectively, the displacements values of these structures at corresponding fundamental frequencies are much larger compared to other structures and is reflected in time histories.

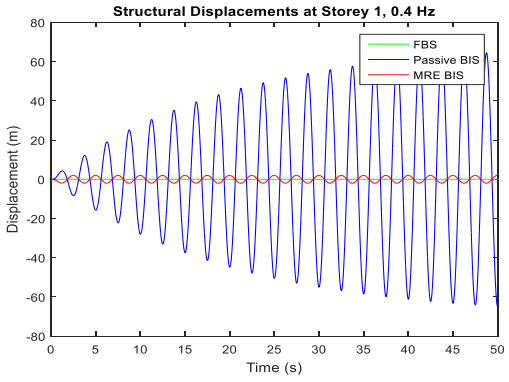

Figure 49: Displacement time history at storey 1 for 0.4 Hz

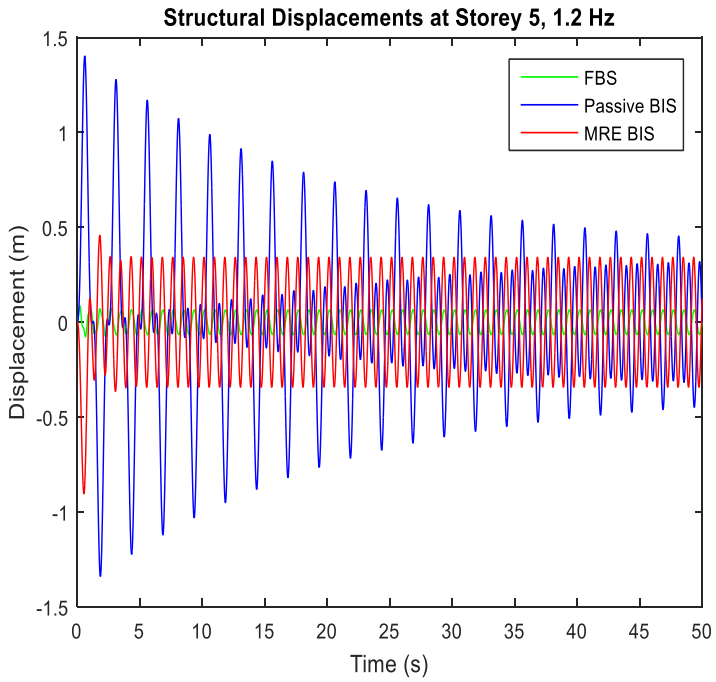

Figure 50: Displacement time history at storey 5 for 1.2 Hz.

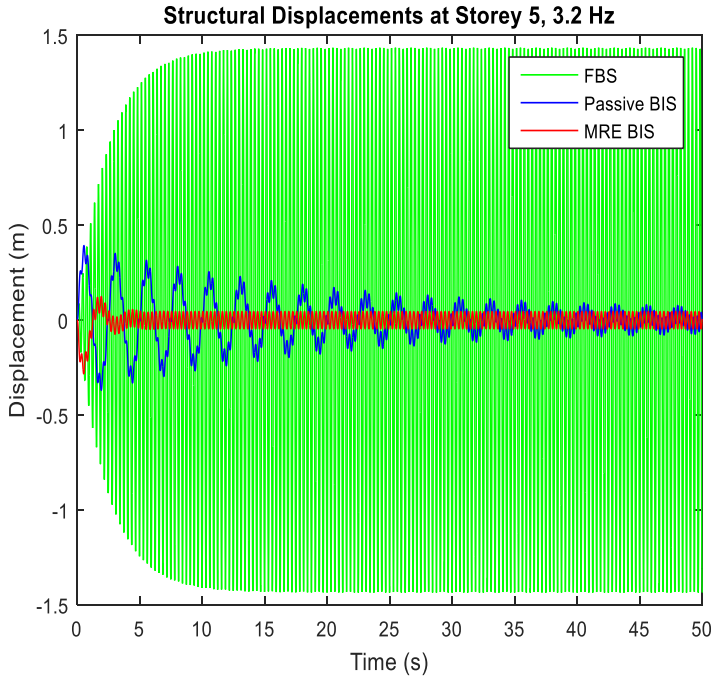

Figure 51: Displacement time history at storey 5 for 3.2 Hz.

The bar charts shown in Figures 43 to 48 below compares the displacement responses of passively isolated structure and MRE based isolated structures.

Figure 52: Peak Displacements at 0.4 Hz

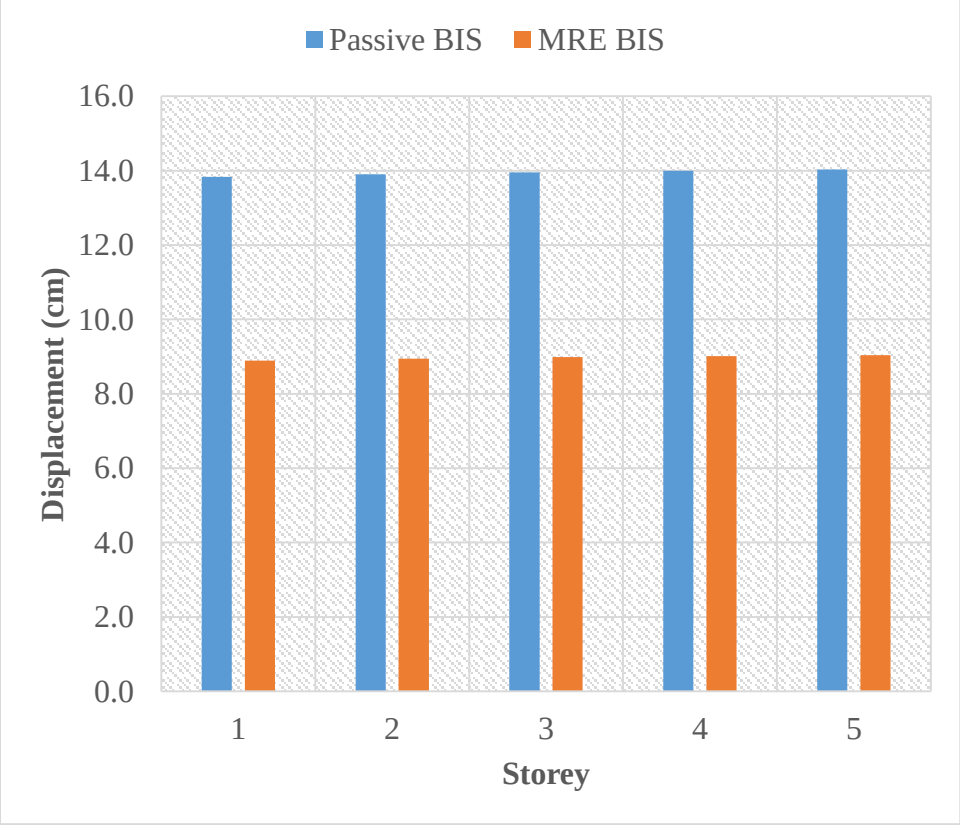

Figure 53: Peak Displacements at 1.2 Hz

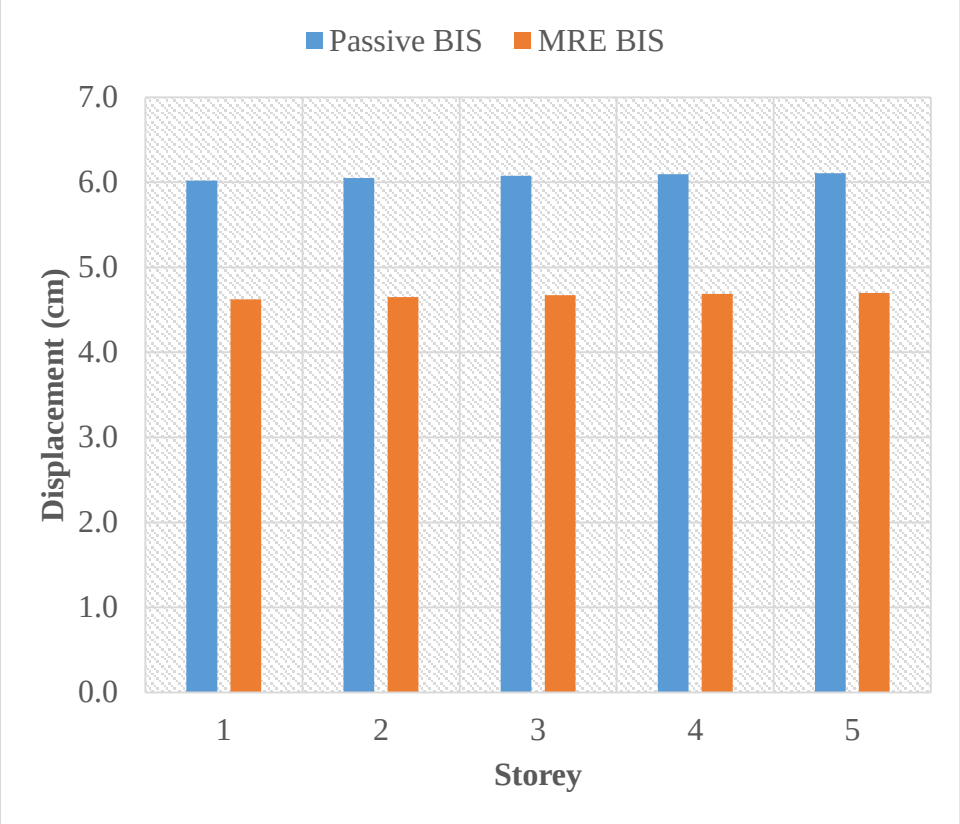

Figure 54: Peak Displacements at 2.0 Hz

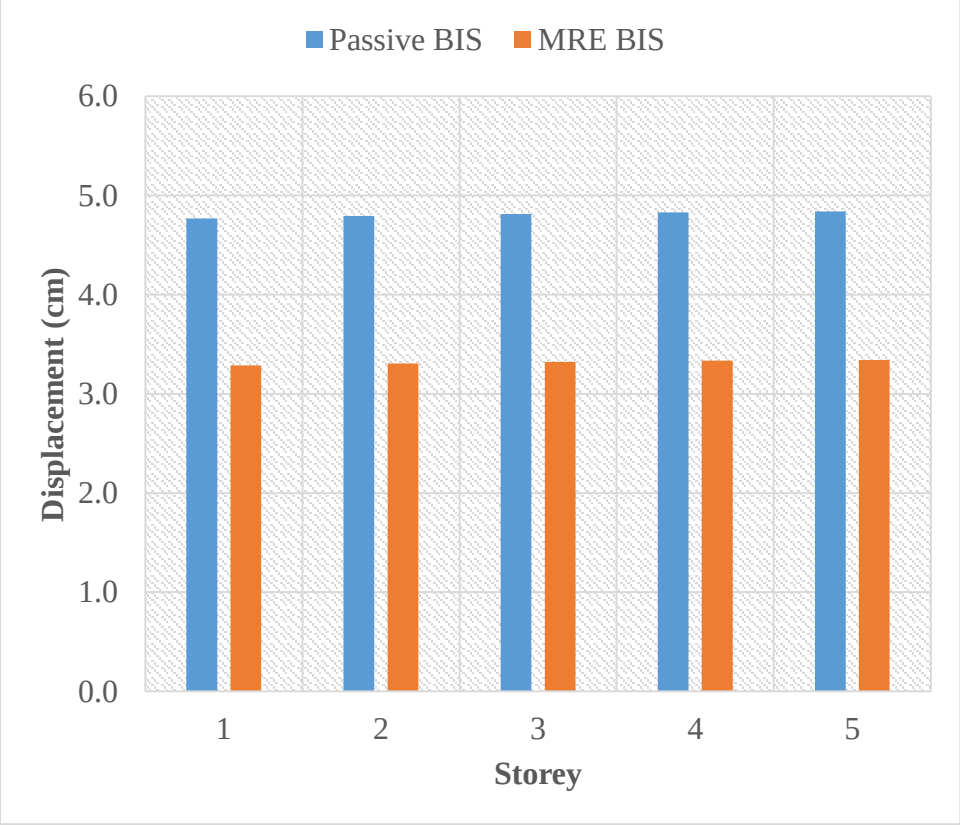

Figure 55: Peak Displacements at 2.7 Hz

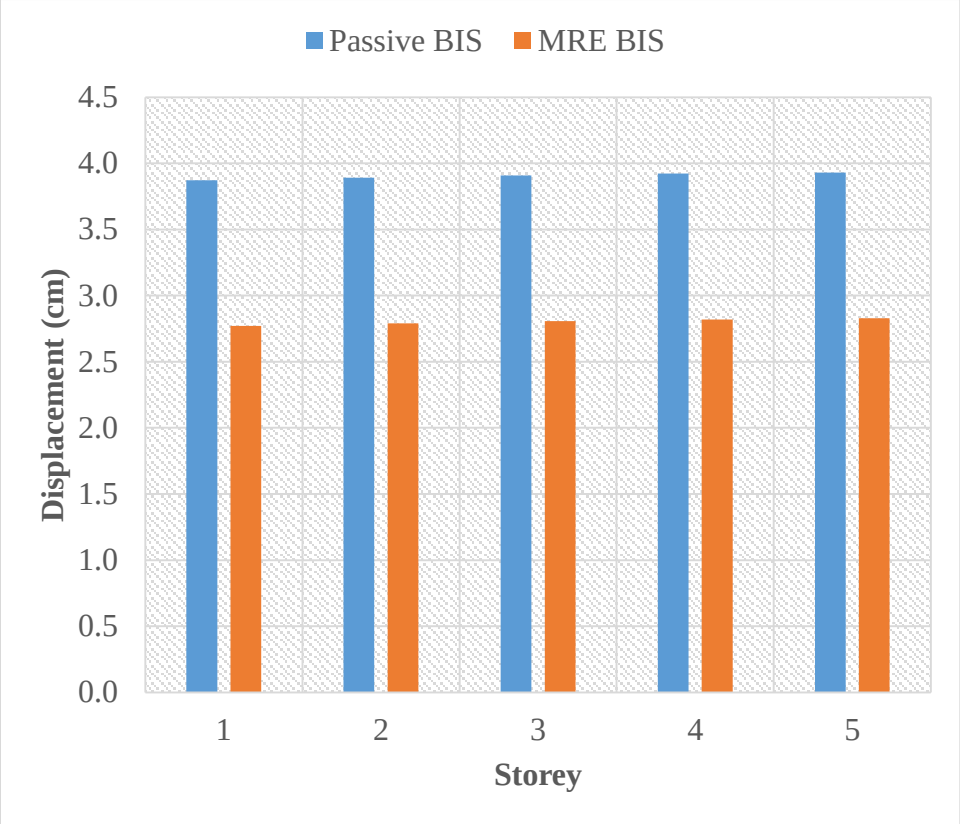

Figure 56: Peak Displacements at 3.2 Hz

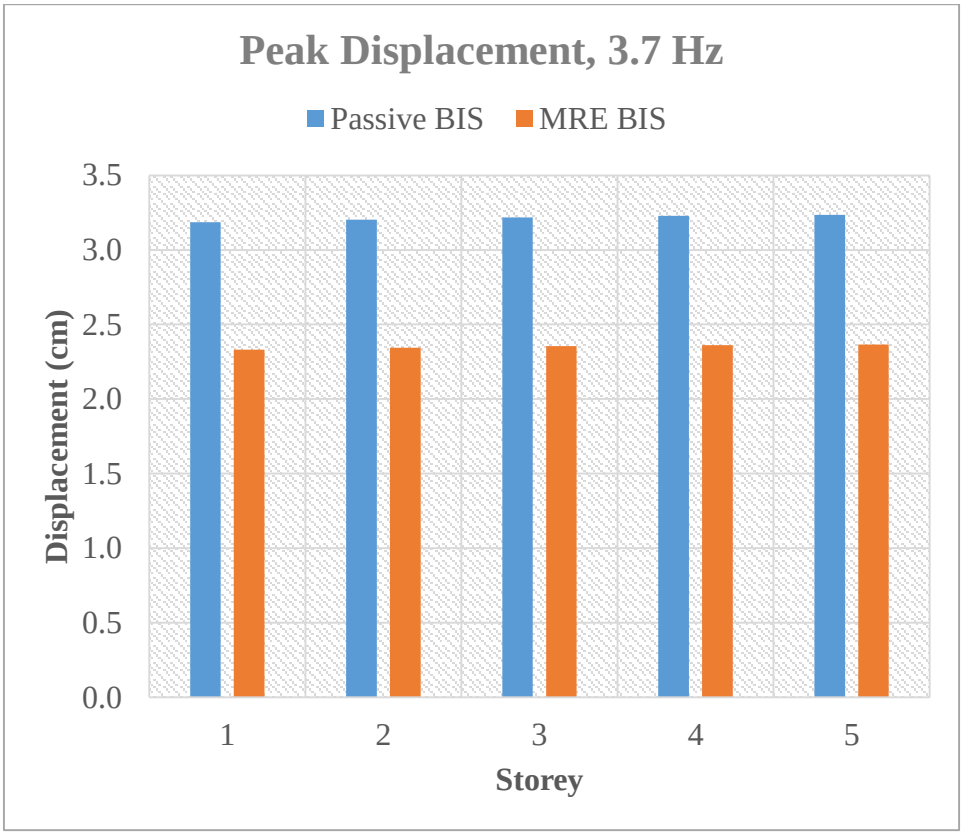

Figure 57: Peak Displacements at 3.7 Hz

It is evident from the charts that MRE based isolated structure has significantly reduced the total displacement response of the structure for all the excitation frequencies. The maximum reduction can be seen for the case of 0.4 Hz which is the fundamental frequency of vibration of isolated structure. Moreover, the displacement values show that the MRE based isolated structure does not possess any fundamental frequency rather it adjusts its stiffness depending on loading frequency and thus the fundamental frequency of the structure.

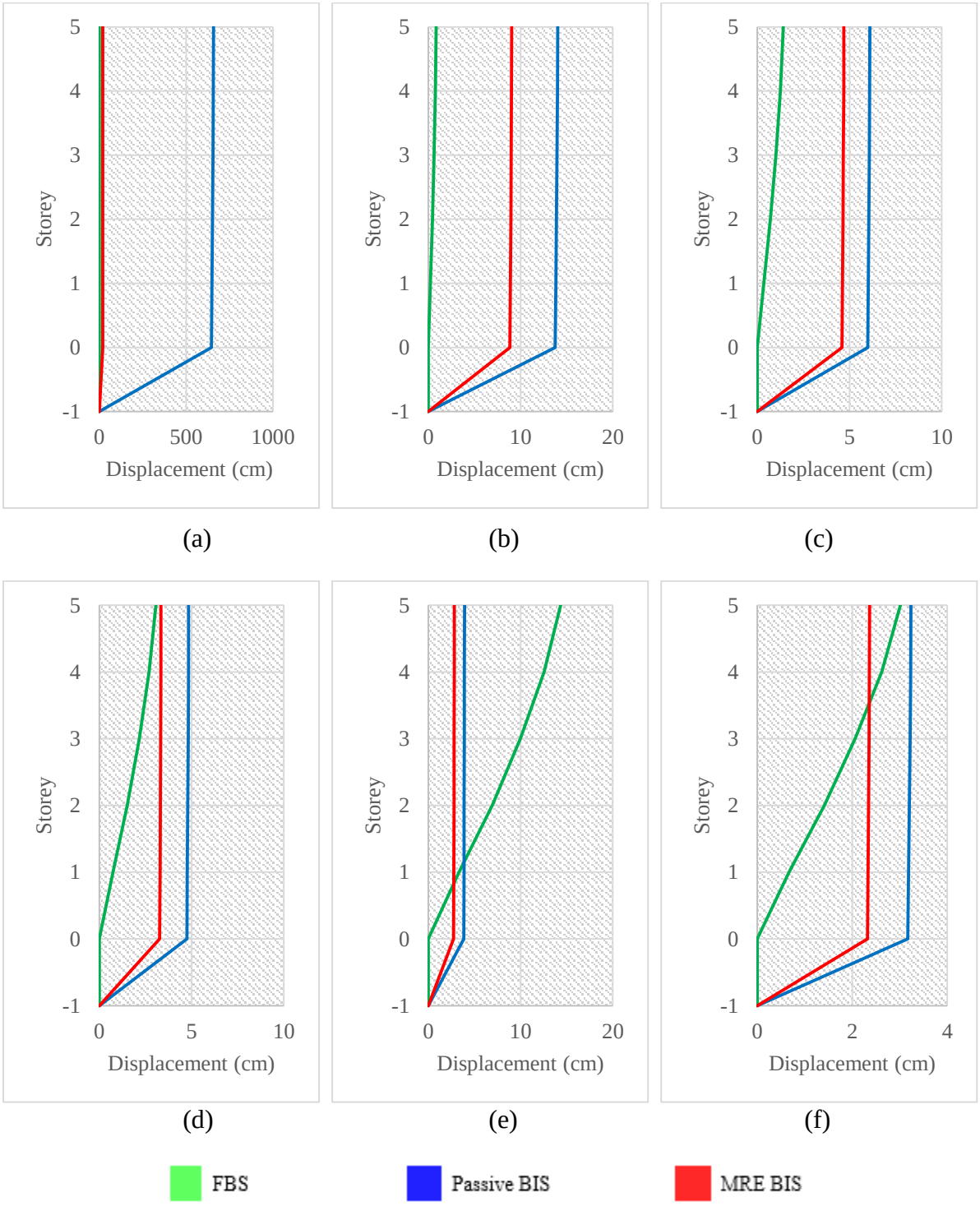

Figure 58: Storey-wise total displacement (a) 0.4 Hz, (b) 1.2 Hz, (c) 2.0 Hz, (d) 2.7 Hz, (e) 3.2 Hz, (f) 3.7 Hz

Storey wise line plots for total displacement response are presented in Figure 58. It can be seen from the Figures that for the isolated structures, a major portion of total displacement (96-98%) is absorbed at the isolation level due to relatively soft isolation layer and very minimal displacement is being transferred to the superstructure. Whereas for the fixed base model, all the displacement is transferred rather uniformly to the superstructure.

It can also be observed in Figure 58(a) that passive base isolated structure is showing unrealistically large displacement. This is because 0.4 Hz is the fundamental frequency of vibration of passively isolated structure and this large response can be attributed to resonance phenomena. But when the adjustable layer of MR elastomer is introduced as isolator to the same isolated structure, the system has successfully avoided the resonance. This validates the adaptable nature of MR elastomer based isolator under severe loading cases. Similarly, MRE based isolated structure has also shown nominal response at all other loading frequencies including that of 3.2 Hz which is the fundamental frequency of fixed base structure.

Storey wise line plots for displacements relative to base are presented in Figure 59. It can be observed that isolated structures are successful in significantly reducing the transmission of displacements to superstructure compared to fixed base for all loading frequencies.

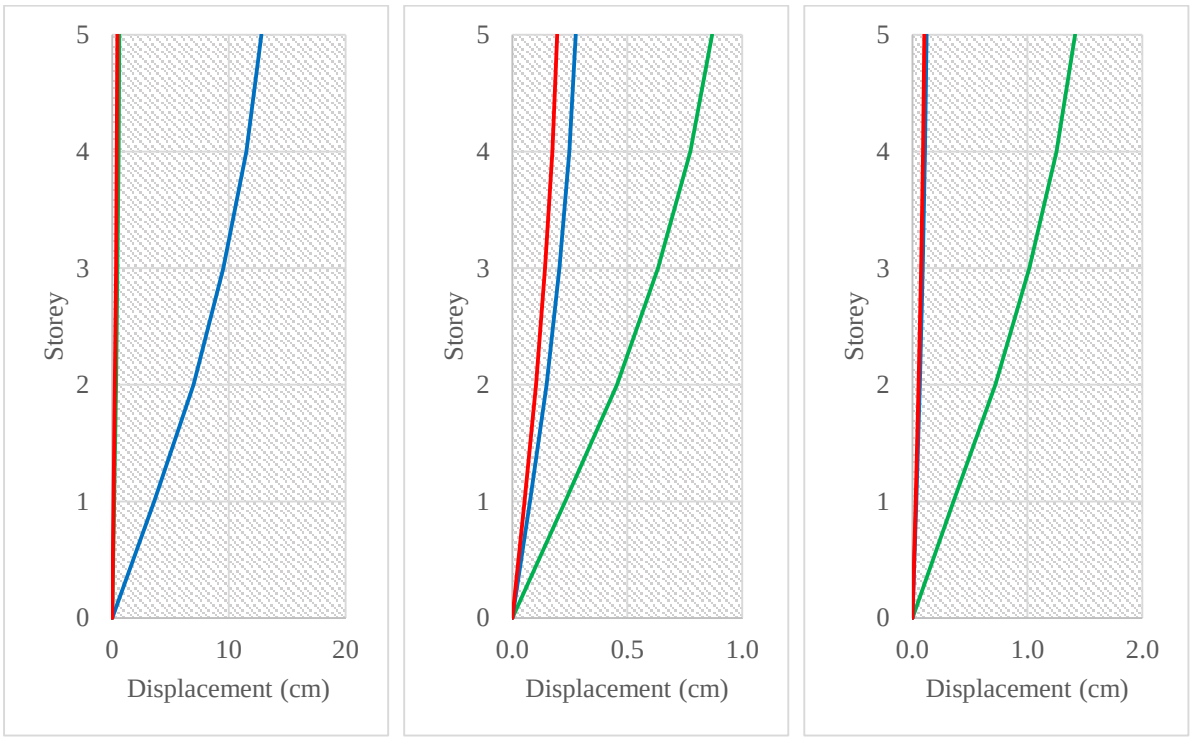

(a) (b) (c)

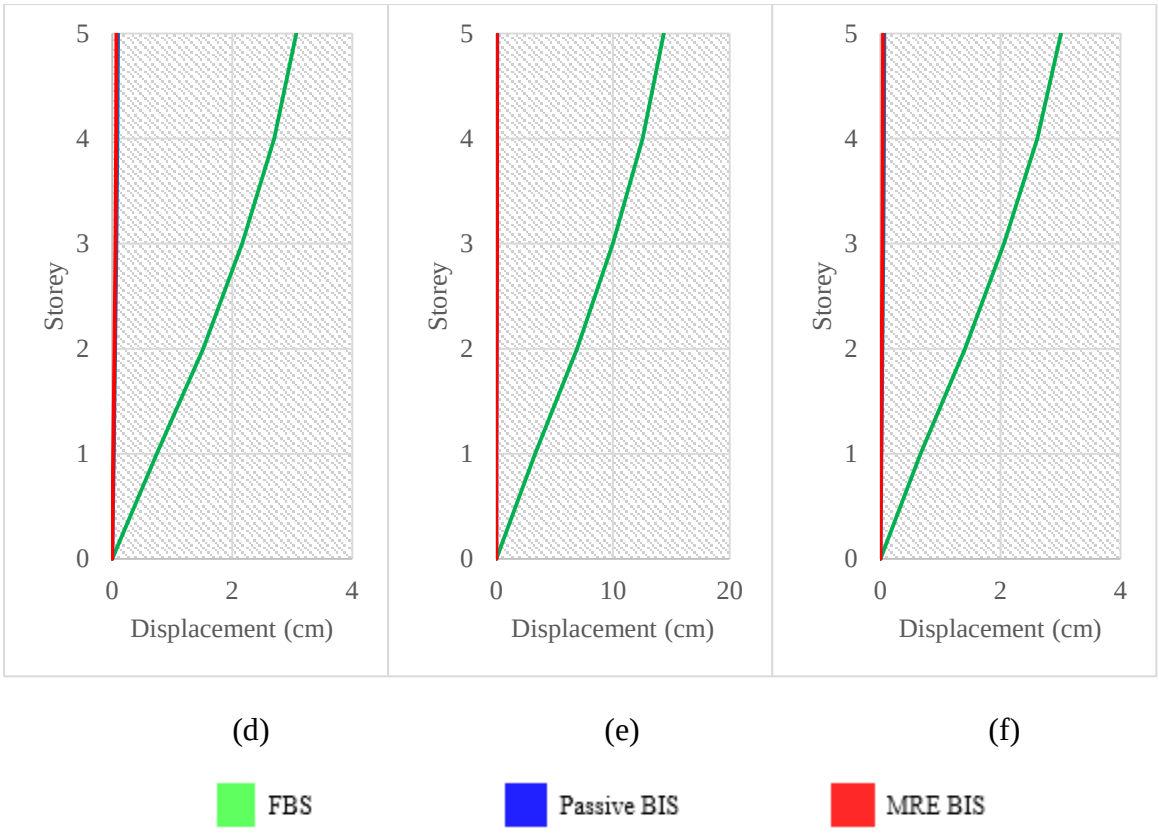

Figure 59: Storey-wise displacement rel to base (a) 0.4 Hz, (b) 1.2 Hz, (c) 2.0 Hz, (d) 2.7 Hz, (e) 3.2 Hz, (f) 3.7 Hz

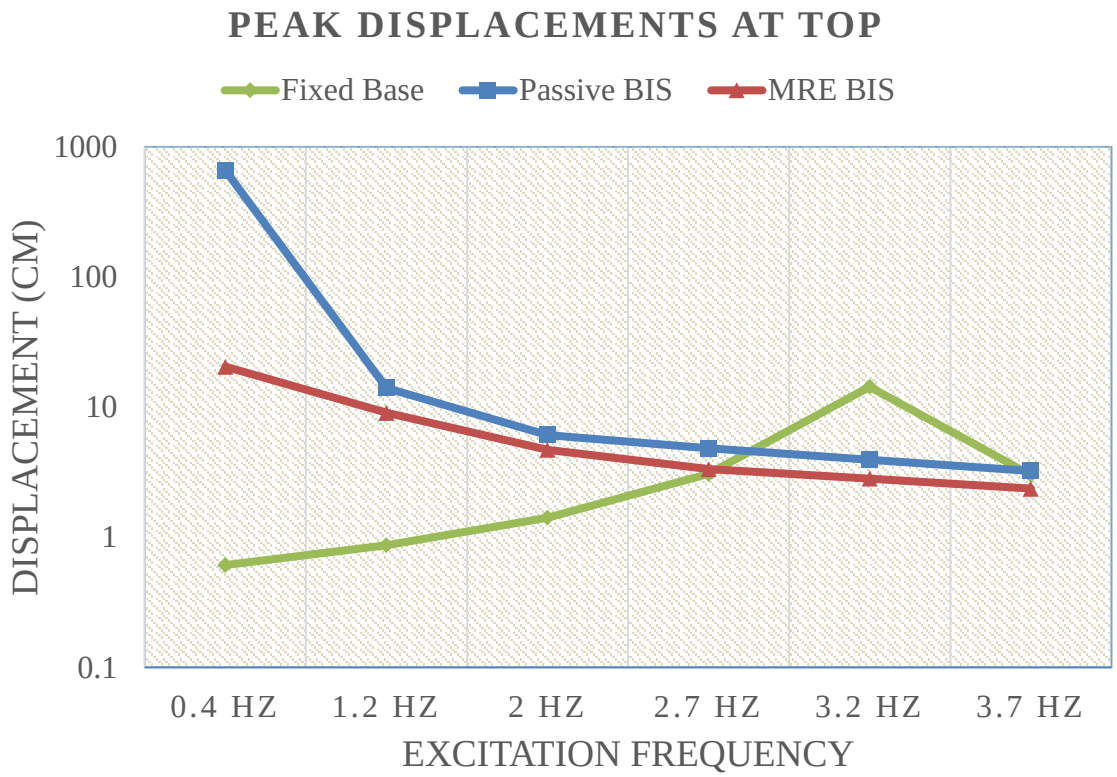

Figure 60: Loading vs. peak displacement plot

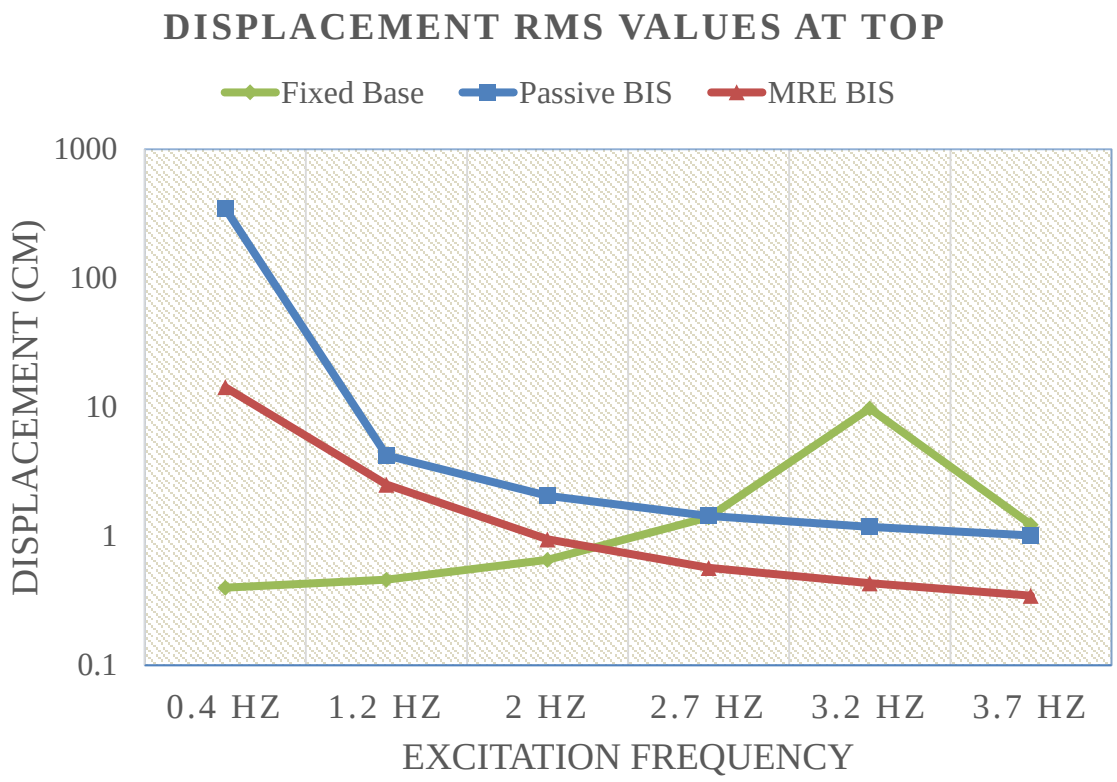

Figure 61: Loading vs. RMS displacement plot

Loading frequency wise peak and RMS displacement plots for the top stories of all the structures are shown in Figures 60 and 61 respectively. It can be observed that for isolated structures the displacements decreases as the loading frequency value increases. For fixed base structure, the displacement increases with the increasing loading frequency up to 3.2Hz and then the drop occurs in displacements. Furthermore, the MRE based isolated structure does not show any resonance in displacement response over the frequency ranges encompassing the fundamental frequencies of fixed base and passively isolated structures which validates the adaptable nature of MR elastomers based seismic isolation.

5.1.2 Storey Drift Responses

Storey drifts refer to difference of displacement of two consecutive stories. The peak and RMS values of storey drift responses against loading frequencies for fixed base, passively isolated and MR elastomer based isolated structures are tabulated in Table 10.

Table 10: Storey Drift Peak and RMS Values (Harmonic loading)

		Fixed Base		Passive BIS		MRE BIS	
	Storey	Peak (mm)	RMS (mm)	Peak (mm)	RMS (mm)	Peak (mm)	RMS (mm)
0.4 Hz	1	1.71	1.13	36.18	19.04	2.01	1.42
	2	1.60	1.05	33.62	17.70	1.87	1.32
	3	1.24	0.80	25.68	13.51	1.43	1.01
	4	0.96	0.61	19.66	10.35	1.09	0.77
	5	0.63	0.40	12.88	6.78	0.72	0.50
1.2 Hz	1	2.30	1.27	0.78	0.23	0.95	0.42
	2	2.25	1.20	0.73	0.22	0.90	0.39
	3	1.79	0.93	0.56	0.17	0.69	0.30
	4	1.41	0.72	0.43	0.13	0.53	0.23
	5	0.95	0.48	0.28	0.09	0.35	0.15
2.0 Hz	1	3.59	1.73	0.34	0.11	0.54	0.19
	2	3.62	1.69	0.32	0.11	0.51	0.19
	3	2.95	1.35	0.25	0.08	0.39	0.15
	4	2.37	1.07	0.19	0.06	0.31	0.12
	5	1.61	0.72	0.13	0.04	0.20	0.08
2.7 Hz	1	7.42	3.46	0.27	0.08	0.39	0.13
	2	7.75	3.56	0.26	0.08	0.39	0.13
	3	6.48	2.94	0.20	0.06	0.32	0.11
	4	5.33	2.40	0.15	0.05	0.26	0.09
	5	3.68	1.64	0.10	0.03	0.18	0.06
3.2 Hz	1	33.31	22.67	0.22	0.07	0.33	0.11
	2	35.89	24.42	0.21	0.06	0.35	0.12
	3	30.72	20.90	0.17	0.05	0.29	0.10
	4	25.69	17.48	0.13	0.04	0.25	0.09
	5	17.94	12.20	0.09	0.03	0.17	0.06
3.7 Hz	1	6.68	2.62	0.19	0.06	0.29	0.11
	2	7.43	3.00	0.18	0.05	0.31	0.12
	3	6.52	2.69	0.14	0.04	0.27	0.11
	4	5.56	2.32	0.11	0.03	0.23	0.09
	5	3.94	1.65	0.07	0.02	0.17	0.07

The bar charts shown in Figures 62-67 below compares the storey drift responses of passively isolated structure and MRE based isolated structures. It can be observed that the storey drifts decreases as we move from bottom storey to top storey for both passively isolated and MRE isolated structures. It can also be observed, like from the displacement responses, that passive base isolated structure is showing unrealistically large storey drifts at excitation frequency of

0.4 Hz which is the fundamental frequency of vibration of passively isolated structure. This large response can be attributed to resonance phenomena. Similar to displacement response, when the adjustable layer of MR elastomer is introduced as isolator to the same isolated structure, the system has successfully avoided the resonance. This validates the adaptable nature of MR elastomer based isolator under severe loading cases.

From Figures 62-67, it is clear, unlike displacement responses, that passive BIS has outperformed MRE BIS for excitation frequencies other than 0.4 Hz. This behavior is typical for hybrid base isolation systems where the supplementary force may forcefully confine the base displacement of the passive base isolation system [10, 11], larger accelerations as well as increase of inter-storey drifts may be introduced to the superstructure [10, 12].

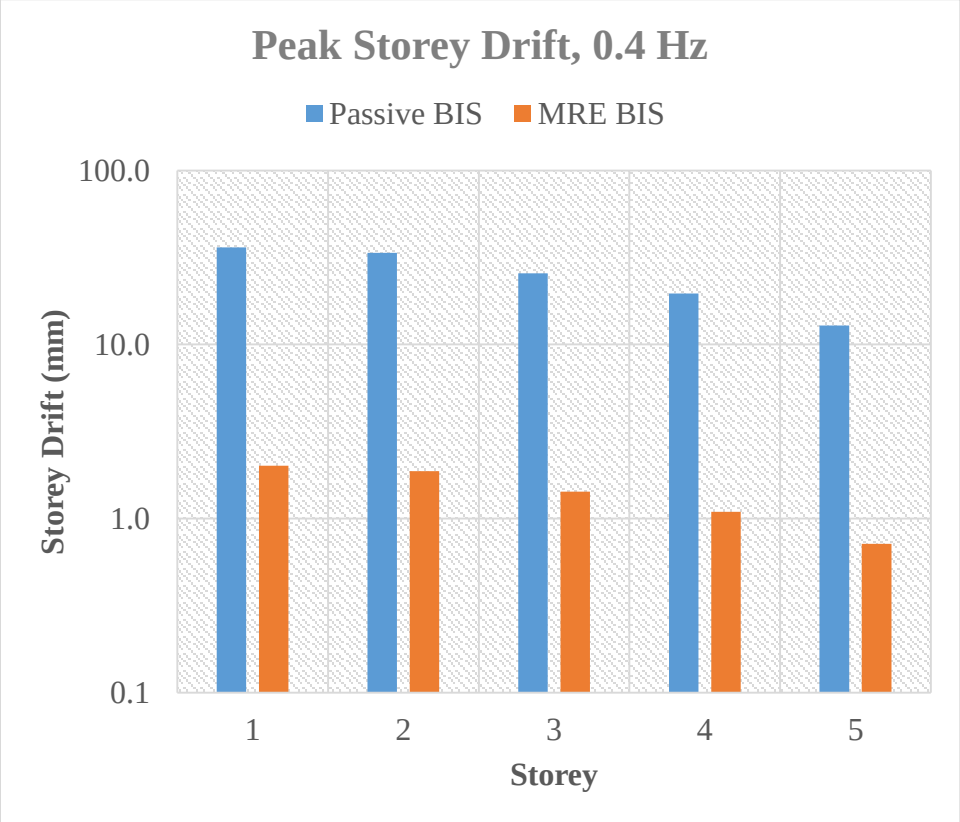

Figure 62: Peak storey drifts at 0.4 Hz

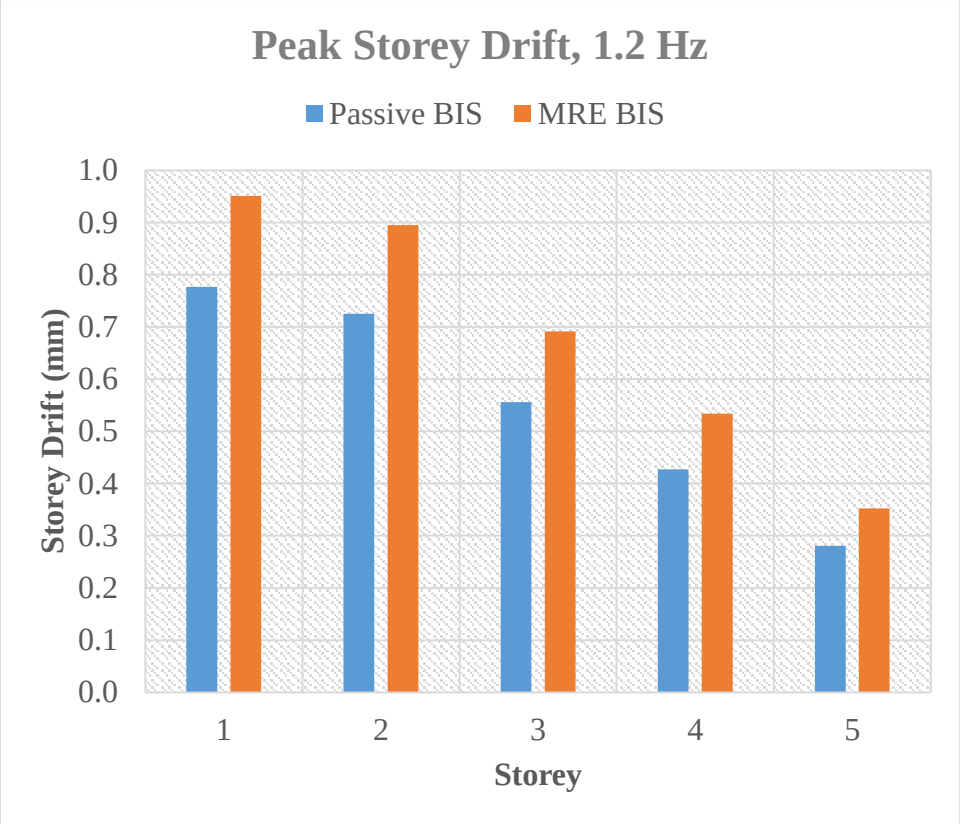

Figure 63: Peak storey drifts at 1.2 Hz

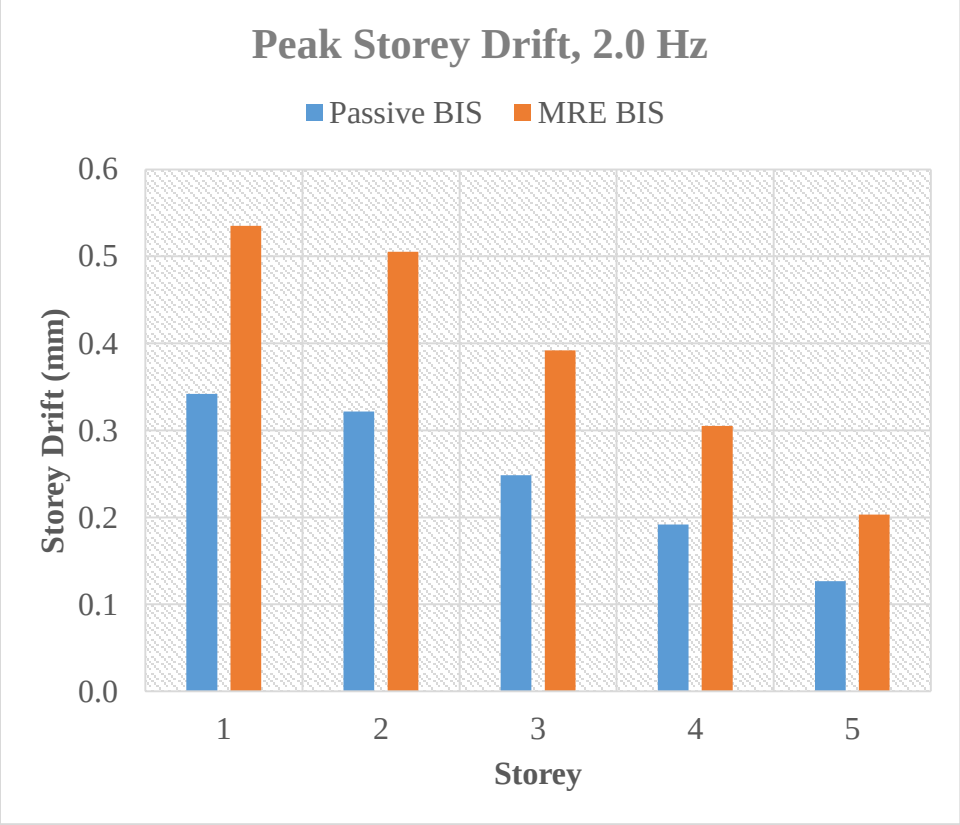

Figure 64: Peak storey drifts at 2.0 Hz

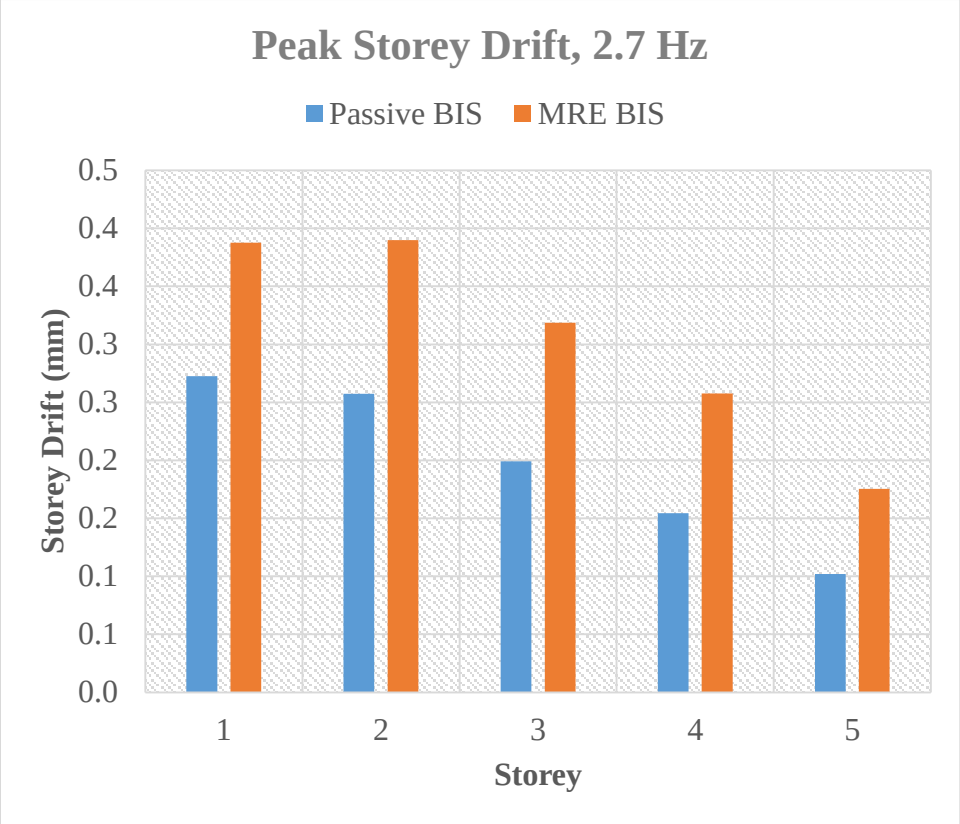

Figure 65: Peak storey drifts at 2.7 Hz

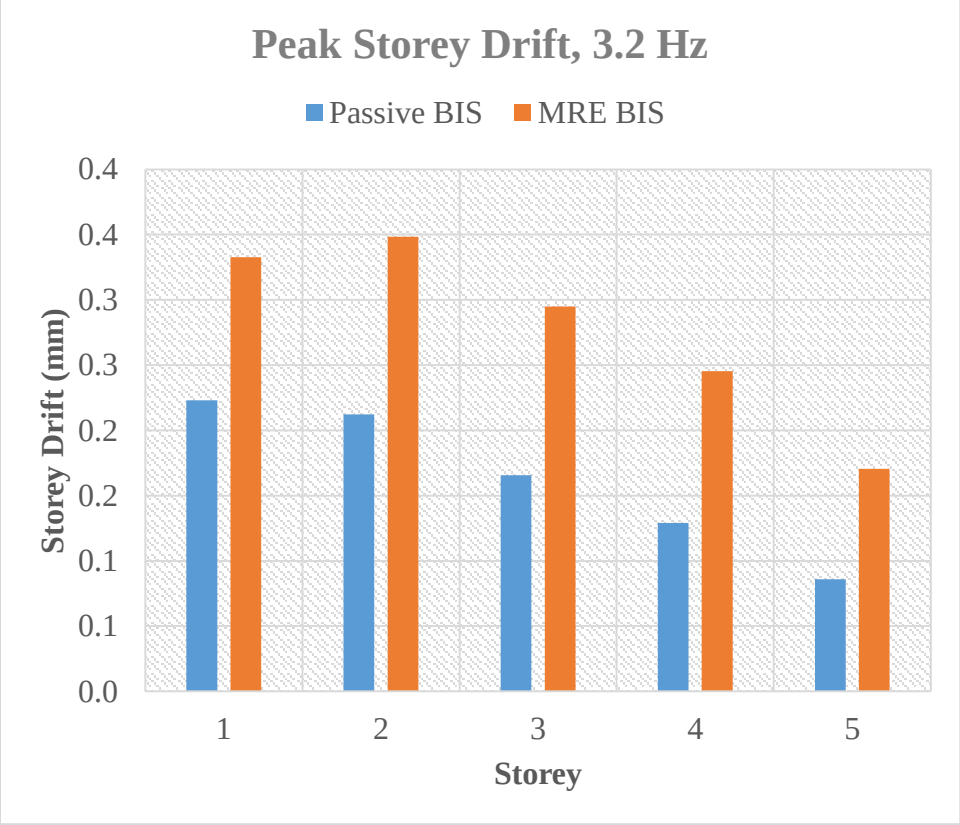

Figure 66: Peak storey drifts at 3.2 Hz

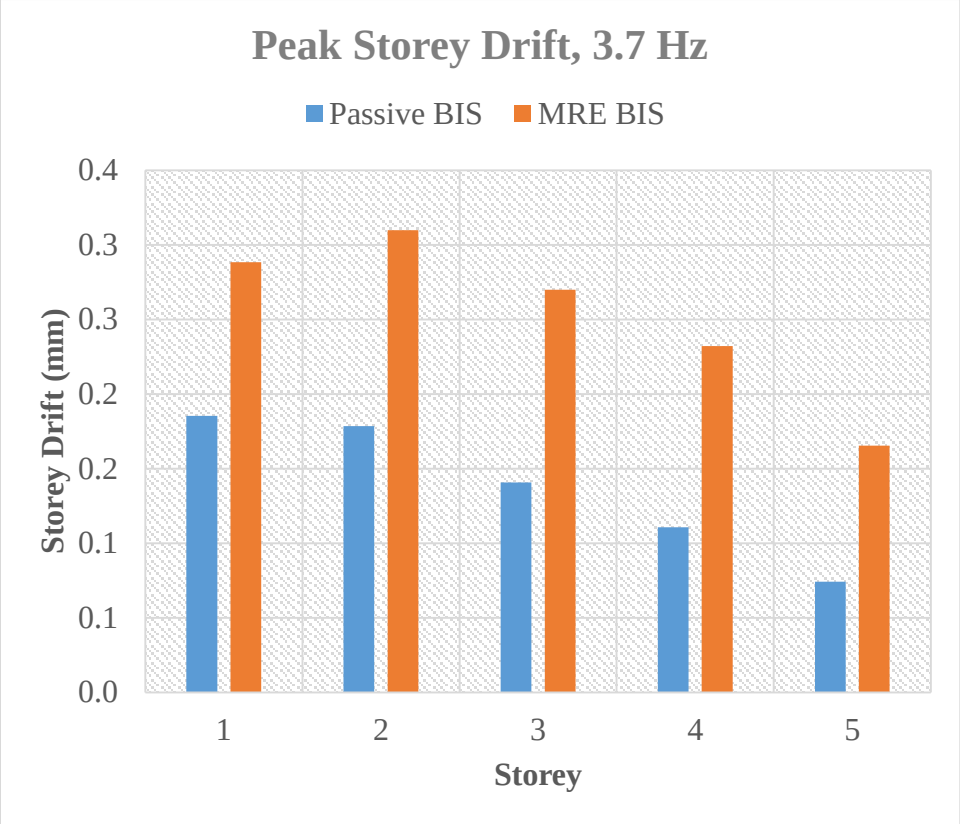

Figure 67: Peak storey drifts at 3.7 Hz

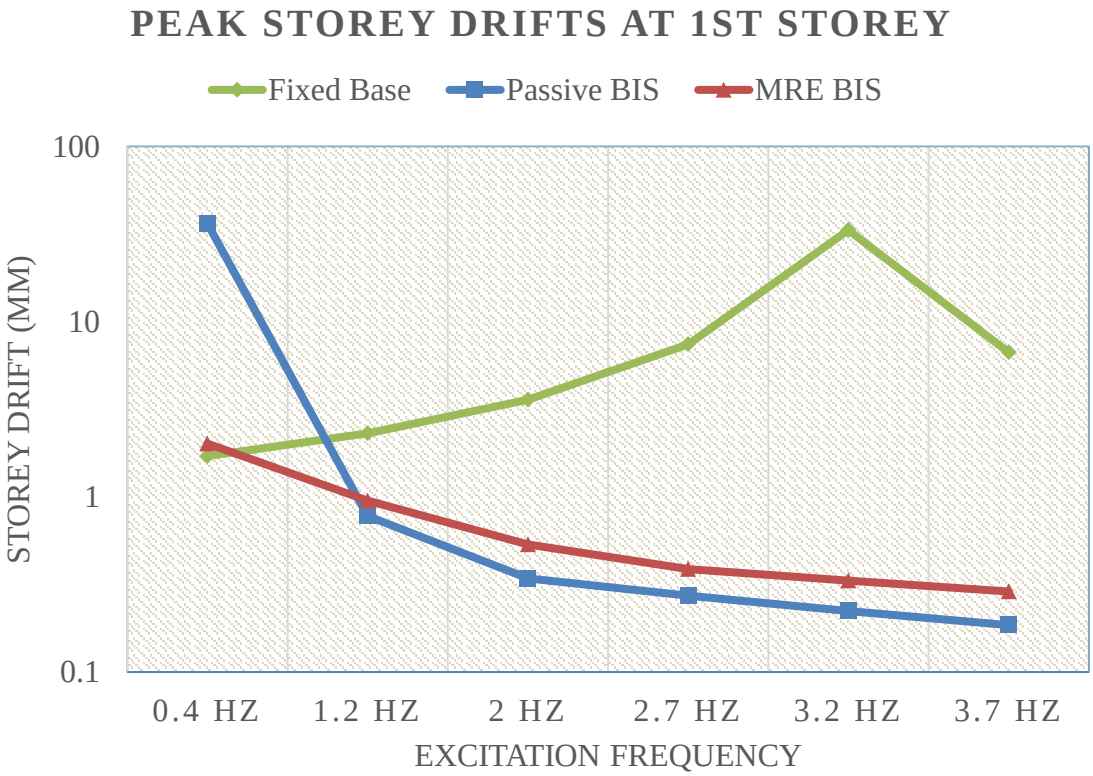

Figure 68: Loading vs. peak storey drift plot

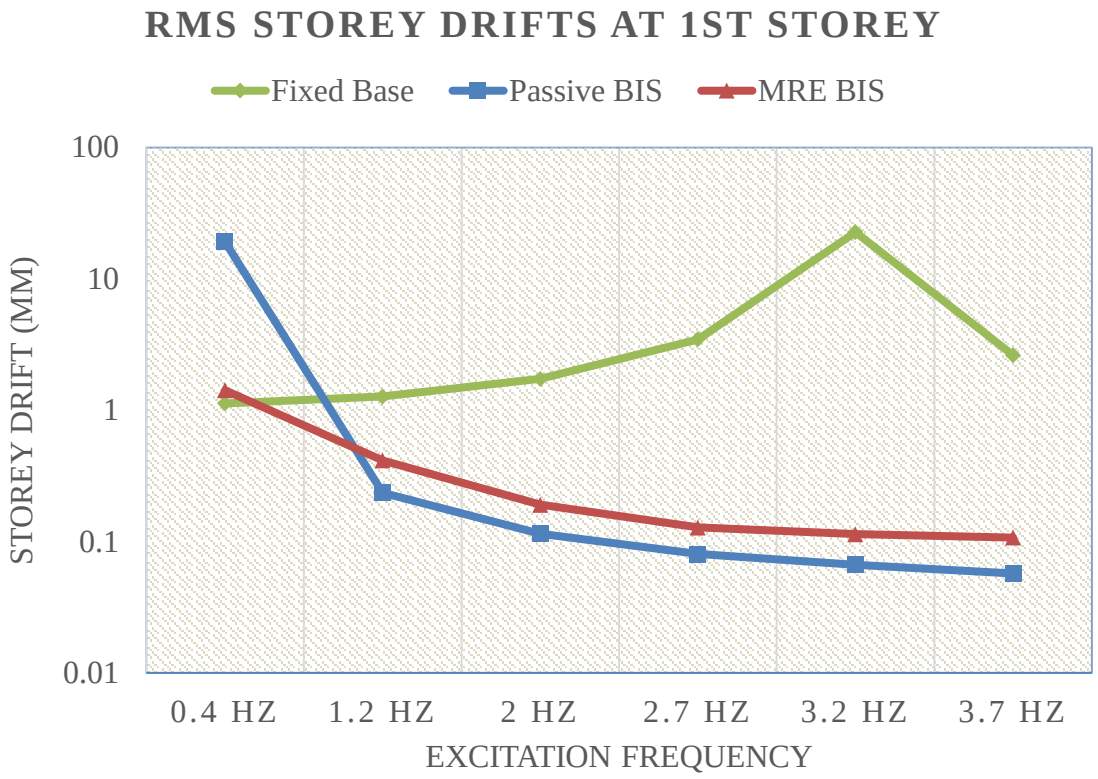

Figure 69: Loading vs. RMS storey drift plot

Loading frequency vs. peak and RMS storey drift plots for the 1st stories of all the structures are compared in Figures 68 and 69 respectively. It can be observed, that for isolated structures the storey drift response decreases as the loading frequency increases. For fixed base structure, the storey drift increases with the increasing loading frequency up to 3.2Hz and then the drop in response occurs as also observed in displacement responses. Furthermore, the MRE based isolated structure does not show any resonance in peak and RMS storey drift responses over the frequency ranges encompassing the fundamental frequencies of fixed base and passively isolated structures which validates the adaptable nature of MR elastomers based seismic isolation.

5.1.3 Acceleration Responses

Acceleration response refer to the total acceleration occurring at corresponding degree-of-freedom/storey. The peak and RMS values of acceleration responses against loading frequencies for fixed base, passively isolated and MR elastomer based isolated structures are tabulated below (Table 11).

Table 11: Acceleration Peak and RMS Values (Harmonic loading)

		Fixed Base		Passive BIS		MRE BIS	
	Storey	Peak (cm/s^2)	RMS (cm/s^2)	Peak (cm/s^2)	RMS (cm/s^2)	Peak (cm/s^2)	RMS (cm/s^2)
0.4 Hz	1	184.28	127.97	4105.21	2160.95	228.47	160.87
	2	190.97	128.64	4126.45	2172.13	229.65	161.70
	3	196.44	129.16	4142.67	2180.66	230.55	162.33
	4	200.72	129.56	4155.08	2187.19	231.24	162.82
	5	203.52	129.82	4163.22	2191.47	231.69	163.14
1.2 Hz	1	212.87	134.44	86.50	25.98	102.74	44.02
	2	244.55	141.34	87.98	26.53	106.38	46.21
	3	270.24	146.72	89.14	26.95	109.56	47.91
	4	291.45	150.92	90.07	27.29	112.17	49.23
	5	306.02	153.70	90.69	27.51	113.94	50.10
2.0 Hz	1	267.62	154.41	36.85	12.54	57.85	17.22
	2	356.75	181.34	38.19	12.90	60.34	20.08
	3	427.55	202.89	39.33	13.21	61.76	22.36
	4	482.78	220.01	40.29	13.47	63.63	24.17
	5	521.33	231.54	40.96	13.65	65.67	25.39
2.7 Hz	1	422.77	226.15	28.98	8.71	31.75	8.66
	2	678.02	328.86	30.29	8.99	38.15	12.26
	3	892.61	413.95	31.39	9.27	45.84	15.27
	4	1069.94	483.34	32.33	9.53	52.39	17.75
	5	1192.82	530.94	33.00	9.73	56.78	19.45
3.2 Hz	1	1357.15	924.00	23.17	7.18	27.70	5.08
	2	2801.28	1906.01	24.50	7.40	31.35	9.69
	3	4040.85	2749.13	25.76	7.69	39.29	13.79
	4	5078.19	3454.78	26.89	7.99	48.64	17.26
	5	5802.47	3947.64	27.77	8.23	55.11	19.69
3.7 Hz	1	180.48	31.60	19.54	6.13	26.73	2.21
	2	508.26	179.52	20.10	6.29	27.66	7.43
	3	819.28	322.63	21.45	6.60	34.60	13.19
	4	1084.27	446.73	22.91	6.99	44.73	18.25
	5	1271.63	535.43	23.99	7.32	53.75	21.88

The bar charts shown in Figures 70-75 below compare the peak acceleration responses of passively isolated structure and MRE based isolated structures at harmonic excitation frequencies.

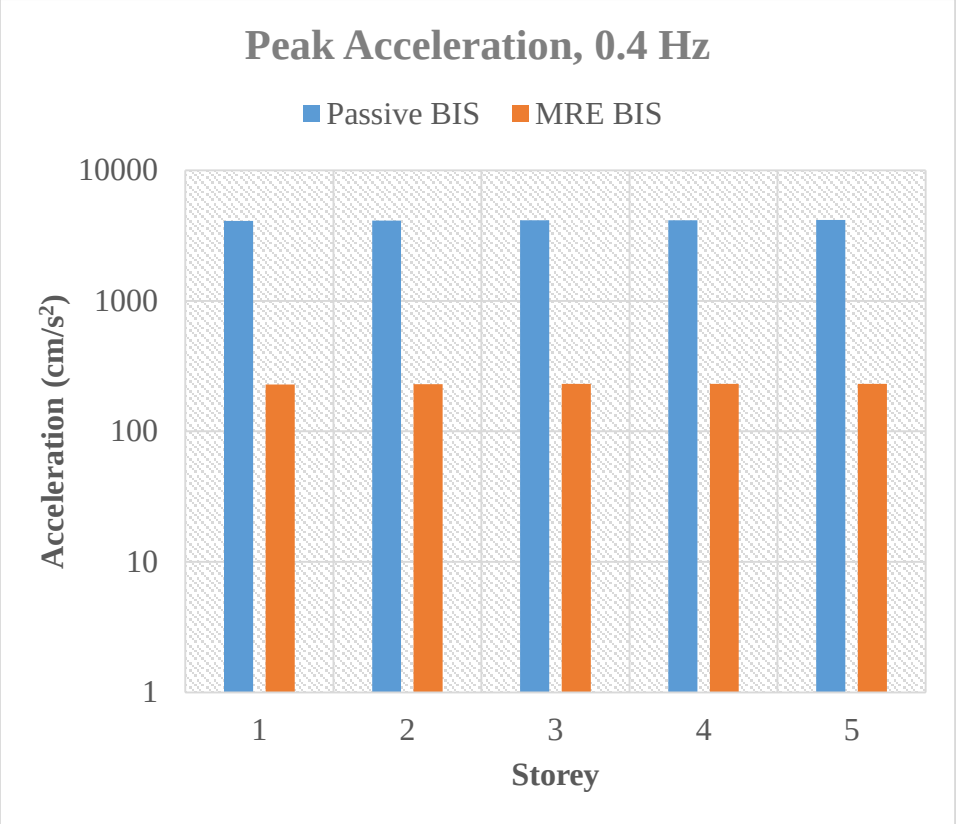

Figure 70: Peak accelerations at 0.4 Hz

The peak acceleration response show similar trends as that of storey drifts i.e. passive BIS outperforming MRE based isolated structure. This response is characteristic of hybrid base isolation systems where the supplementary force may forcefully confine the base displacement of the passive base isolation system [10, 11] at the expense of larger accelerations as well as increased inter-storey drifts in the superstructure [10, 12].

It is also evident that the accelerations increase as we move from lower storey to higher storey levels for both passively isolated and MRE isolated structures with minimum acceleration at first and maximum acceleration at the last storey. Moreover, like for the case of displacement and storey drifts, unrealistically large accelerations for passive base isolated structure have been observed at its fundamental frequency of 0.4 Hz and MRE based adjusTable isolation layer has managed to avoid the resonance in response.

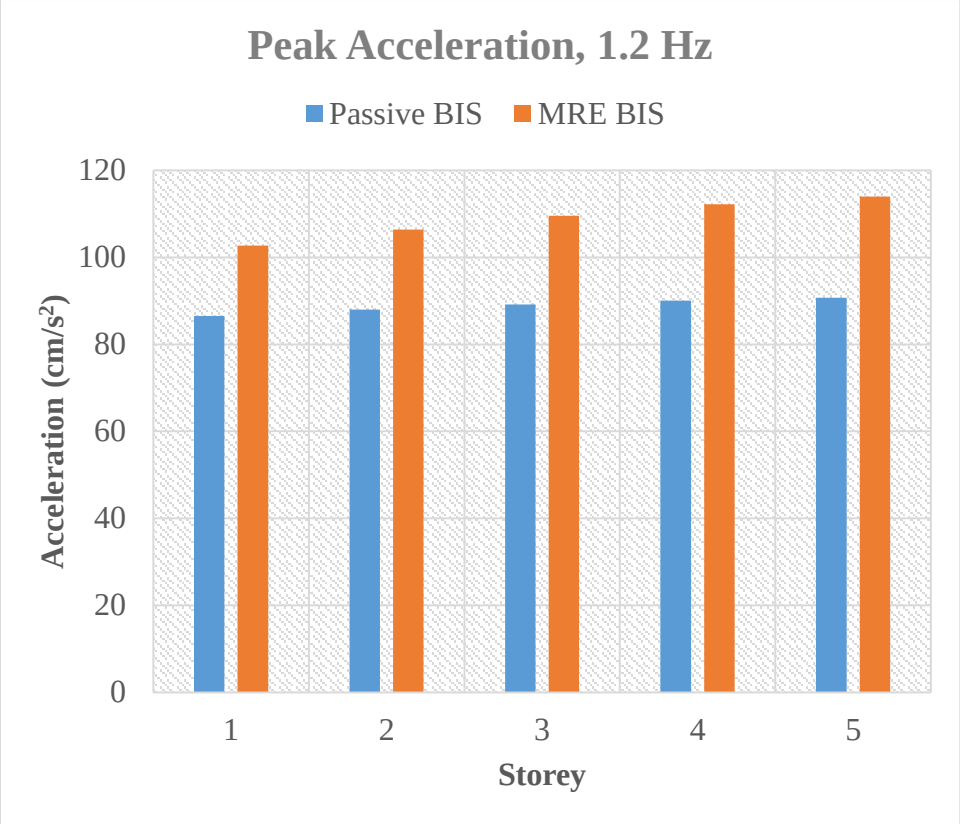

Figure 71: Peak accelerations at 1.2 Hz

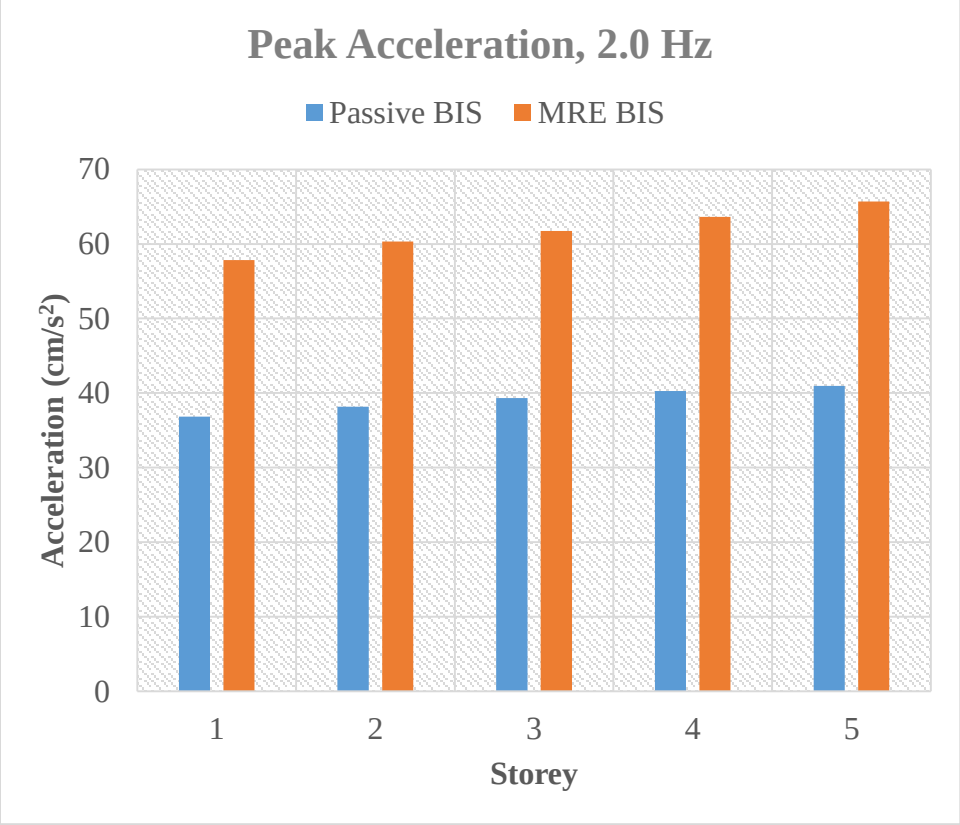

Figure 72: Peak accelerations at 2.0 Hz

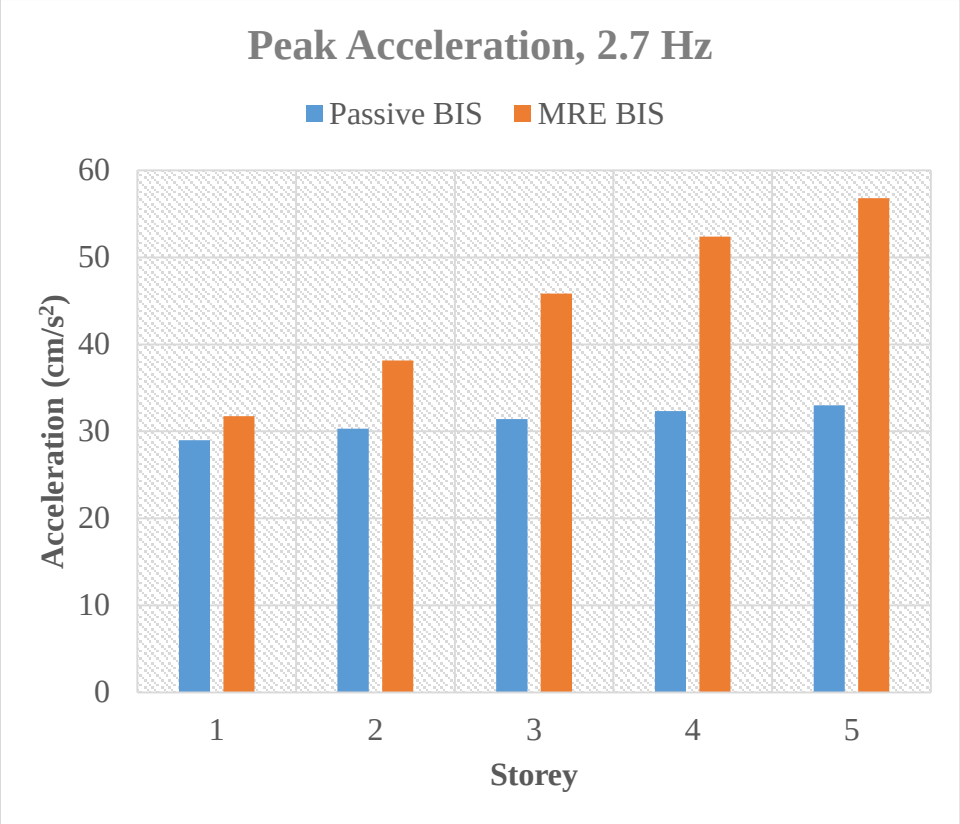

Figure 73: Peak accelerations at 2.7 Hz

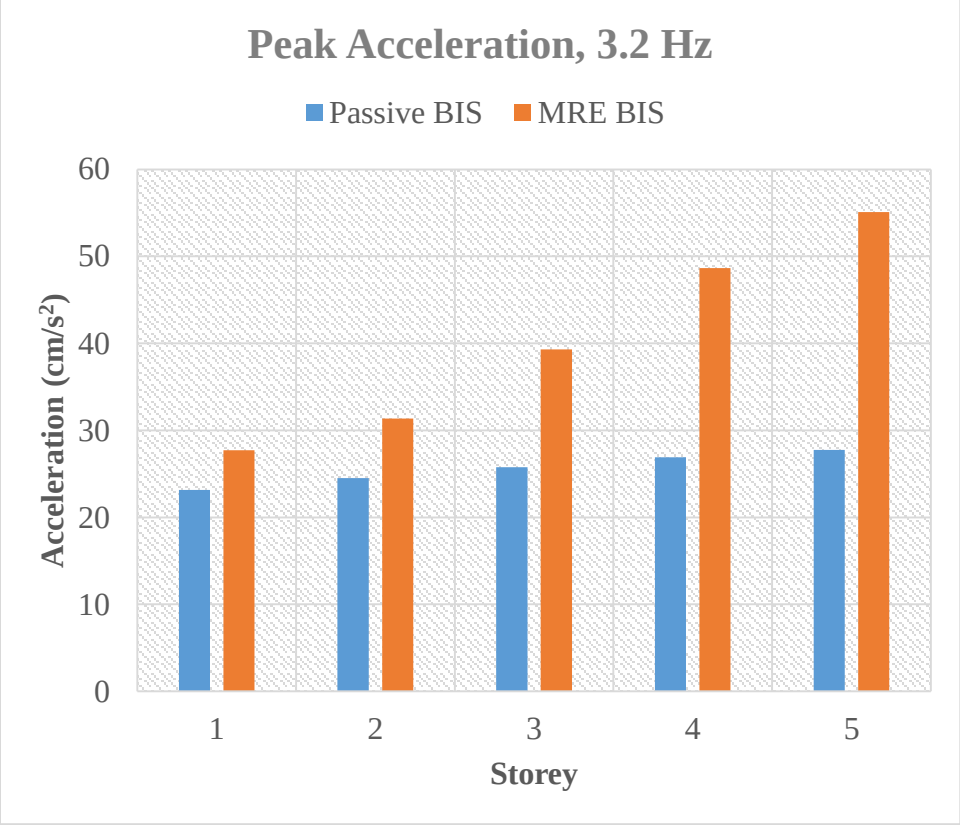

Figure 74: Peak accelerations at 3.2 Hz

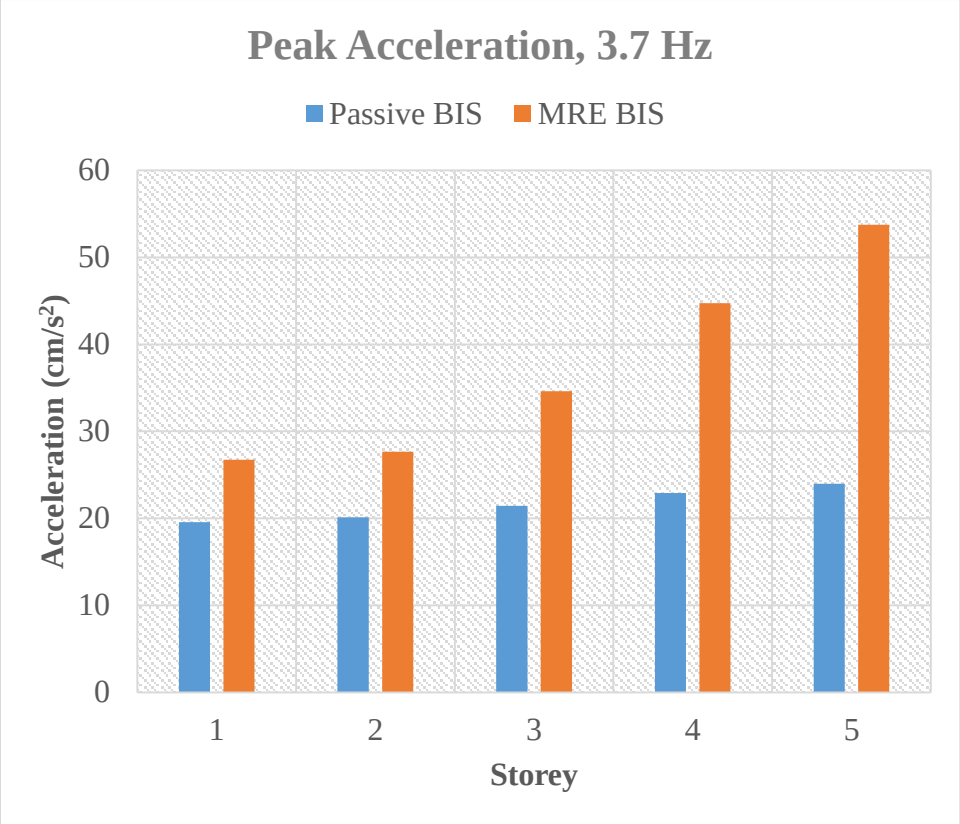

Figure 75: Peak accelerations at 3.7 Hz

Loading frequency vs. peak and RMS acceleration plots for the top stories of all the structures are compared in Figures 76 and 77 respectively.

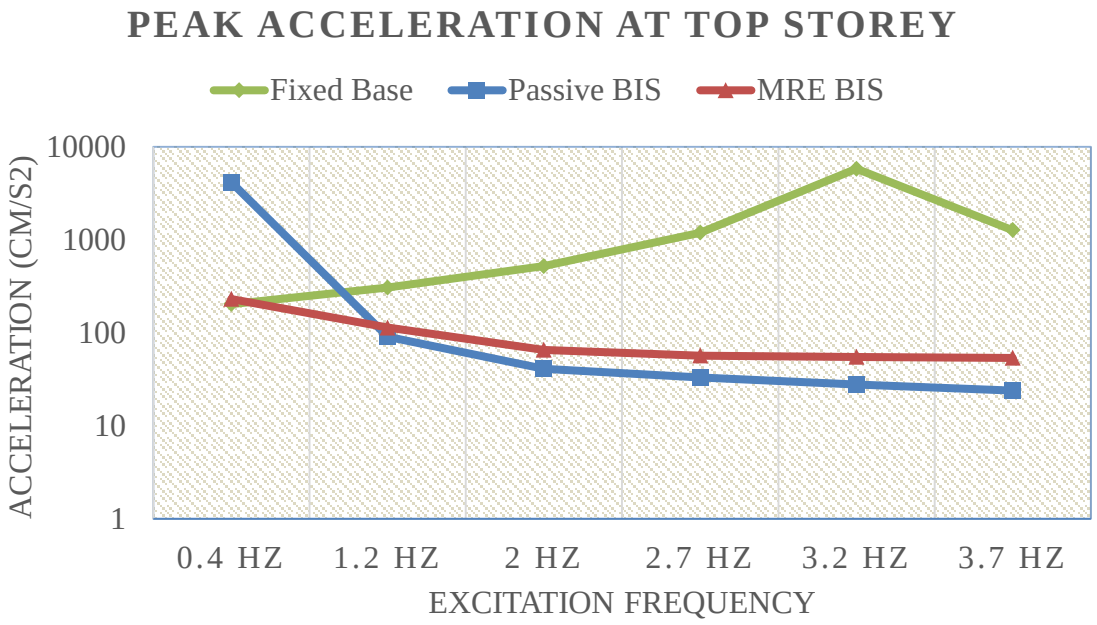

Figure 76: Loading frequency vs. peak acceleration plot

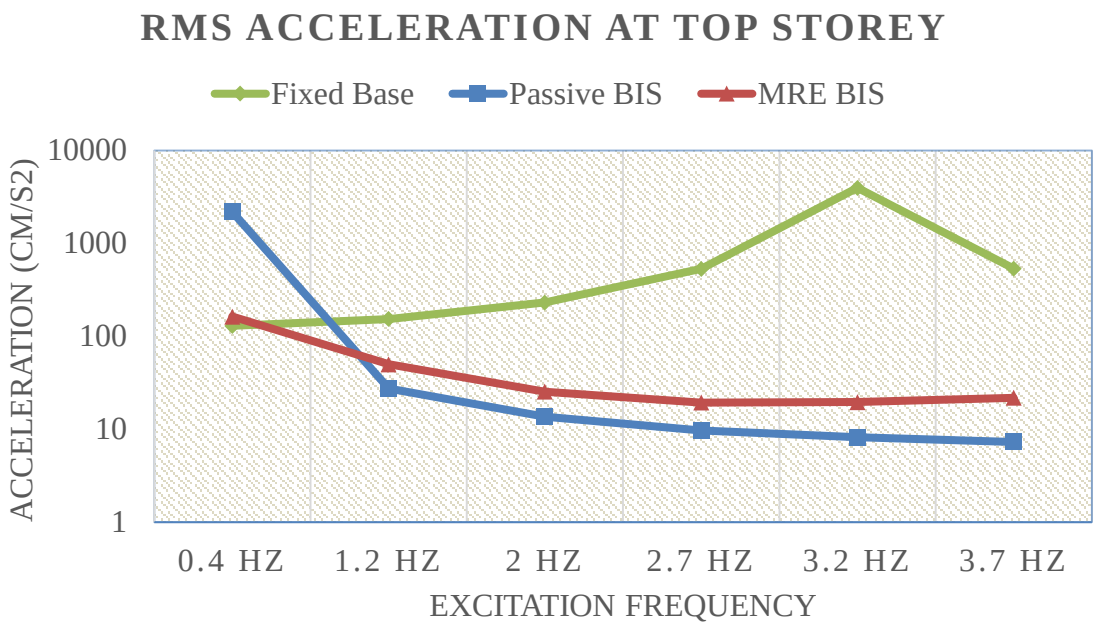

Figure 77: Loading frequency vs. RMS acceleration plot

The resonance of fixed base and passively isolated structures can be observed at their respective fundamental loading frequencies. It is evident from the Figures 76 and 77 that for isolated structures, the acceleration response decreases as the loading frequency increases. For fixed base structure, the acceleration response increases with the increasing loading frequency up to 3.2Hz and then the drop occurs as also observed in displacement responses. Moreover, the acceleration values show that the MRE based isolated structure does not possess any fundamental frequency rather the isolation layer adjusts its stiffness depending on loading frequency and thus changing the fundamental frequency of otherwise passively isolated structure.

5.2 Earthquake Excitation

Six loading cases (time histories) for earthquake excitation [78] have been selected for evaluating the response of structures out of which 3 are near field and 3 are far field [76, 77]. The details are given in Chapter 4. The responses against the earthquake excitation are discussed below.

5.2.1 Displacement Responses

Displacement response is the total displacement of the storey at the corresponding degree-of-freedom. The peak and RMS values of displacement responses against earthquake excitations

for fixed base, passively isolated and MR elastomer based isolated structures are tabulated in Table 12.

Table 12: Displacements peak and RMS values (earthquake excitations)

		Fixed Base		Passive BIS		MRE BIS	
	Storey	Peak (cm)	RMS (cm)	Peak (cm)	RMS (cm)	Peak (cm)	RMS (cm)
Chi-Chi (NF)	Base	0	0	24.4812	6.71451	5.03011	1.17488
	1	0.41546	0.0673	24.6184	6.75214	5.06036	1.18198
	2	0.85498	0.13922	24.746	6.78711	5.08803	1.18863
	3	1.22605	0.20049	24.8434	6.81381	5.10884	1.19374
	4	1.5332	0.2516	24.918	6.83425	5.12461	1.19768
	5	1.74621	0.28726	24.9669	6.84765	5.13494	1.20027
Chi-Chi (FF)	Base	0.0000	0.0000	9.1483	2.6868	2.5400	0.5443
	1	0.3660	0.0459	9.1995	2.7019	2.5545	0.5474
	2	0.7529	0.0946	9.2471	2.7159	2.5693	0.5504
	3	1.0781	0.1358	9.2834	2.7265	2.5809	0.5527
	4	1.3439	0.1703	9.3112	2.7347	2.5909	0.5544
	5	1.5248	0.1944	9.3294	2.7401	2.5974	0.5556
Imp. Valley (NF)	Base	0.0000	0.0000	30.0560	13.9880	7.8714	1.6331
	1	0.3527	0.0632	30.2243	14.0664	7.9227	1.6433
	2	0.7279	0.1313	30.3806	14.1393	7.9740	1.6528
	3	1.0470	0.1897	30.4999	14.1949	8.0155	1.6601
	4	1.3113	0.2387	30.5913	14.2375	8.0483	1.6657
	5	1.4973	0.2730	30.6512	14.2654	8.0699	1.6693
Imp. Valley (FF)	Base	0.0000	0.0000	8.1303	3.4807	1.8339	0.5056
	1	0.2690	0.0345	8.1759	3.5002	1.8446	0.5086
	2	0.5622	0.0717	8.2182	3.5184	1.8554	0.5113
	3	0.8176	0.1034	8.2506	3.5322	1.8640	0.5135
	4	1.0368	0.1301	8.2754	3.5428	1.8708	0.5151
	5	1.1950	0.1488	8.2916	3.5498	1.8753	0.5162
Kocaeli (NF)	Base	0.0000	0.0000	13.1110	2.9728	5.6498	1.4231
	1	0.3739	0.0897	13.1847	2.9895	5.6831	1.4315
	2	0.7815	0.1852	13.2534	3.0050	5.7137	1.4395
	3	1.1415	0.2663	13.3060	3.0168	5.7377	1.4456
	4	1.4473	0.3340	13.3462	3.0259	5.7558	1.4503
	5	1.6637	0.3812	13.3726	3.0319	5.7680	1.4534
Kocaeli (FF)	Base	0.0000	0.0000	3.5789	0.8547	2.0372	0.3822
	1	0.3999	0.0650	3.5990	0.8595	2.0483	0.3844
	2	0.8179	0.1344	3.6179	0.8640	2.0581	0.3865
	3	1.1704	0.1935	3.6323	0.8674	2.0657	0.3882
	4	1.4706	0.2429	3.6435	0.8700	2.0711	0.3894

	5	1.6797	0.2774	3.6508	0.8717	2.0746	0.3903

Representative displacement time histories for earthquake excitations are shown in Figures 78-79 below. It is clear from the Figures that passively isolated structures, subjected to earthquake loading time history vibrate at a lower frequency and higher amplitude whereas the fixed base structure vibrate at a much higher frequency. It can be observed from time history plots that MR elastomer based isolated structure does not vibrate at any single value of frequency rather it responds by vibrating at a range of frequencies. Higher amplitudes of both the isolated structures are due to larger displacements at base level.

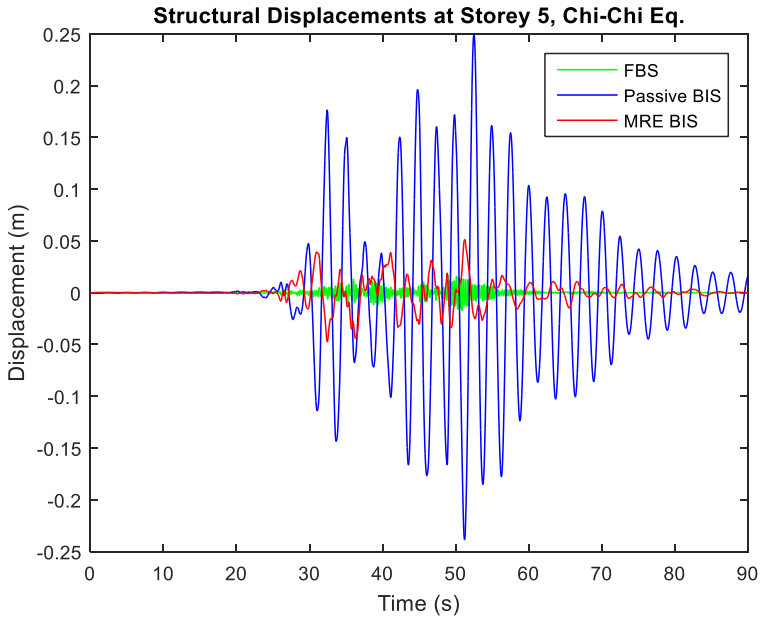

Figure 78: Displacement time history at storey 5 for Chi-Chi earthquake

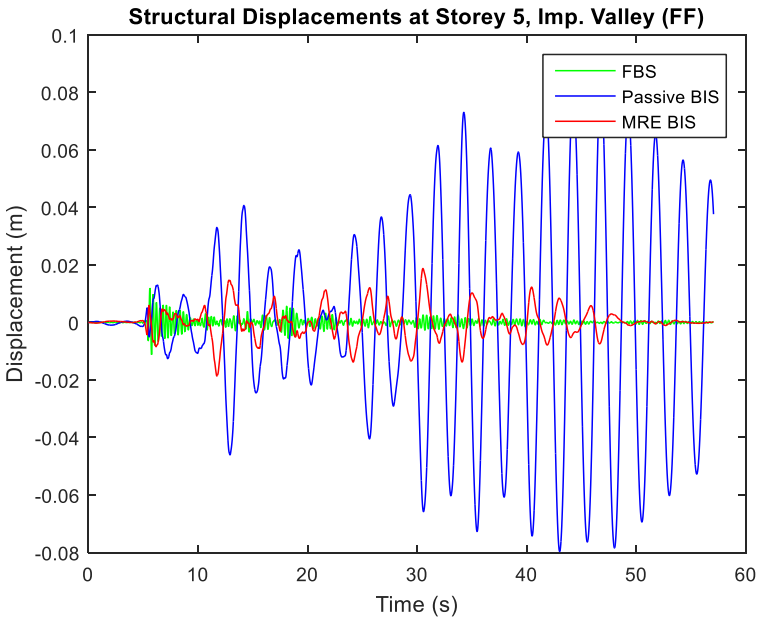

Figure 79: Displacement time history at storey 5 for Imperial Valley earthquake

Peak displacements relative to base for all 3 structures and both near and far field stations of Chi-Chi earthquake are presented in Figure 80. Description of the legend is that green is fixed base, blue is passively is and red is MRE BIS. Thicker lines with box markers show response against near field earthquake whereas thinner lines with star markers show response against far field time history.

From figure 80, it is clear that for both near field and far field time histories, MRE BIS has lowest response while fixed base structure shows highest displacement response. Furthermore, it can be observed that response against near field earthquake time history is higher than far field earthquake time history for all the 3 structures under consideration despite having the same peak ground acceleration values in their records.

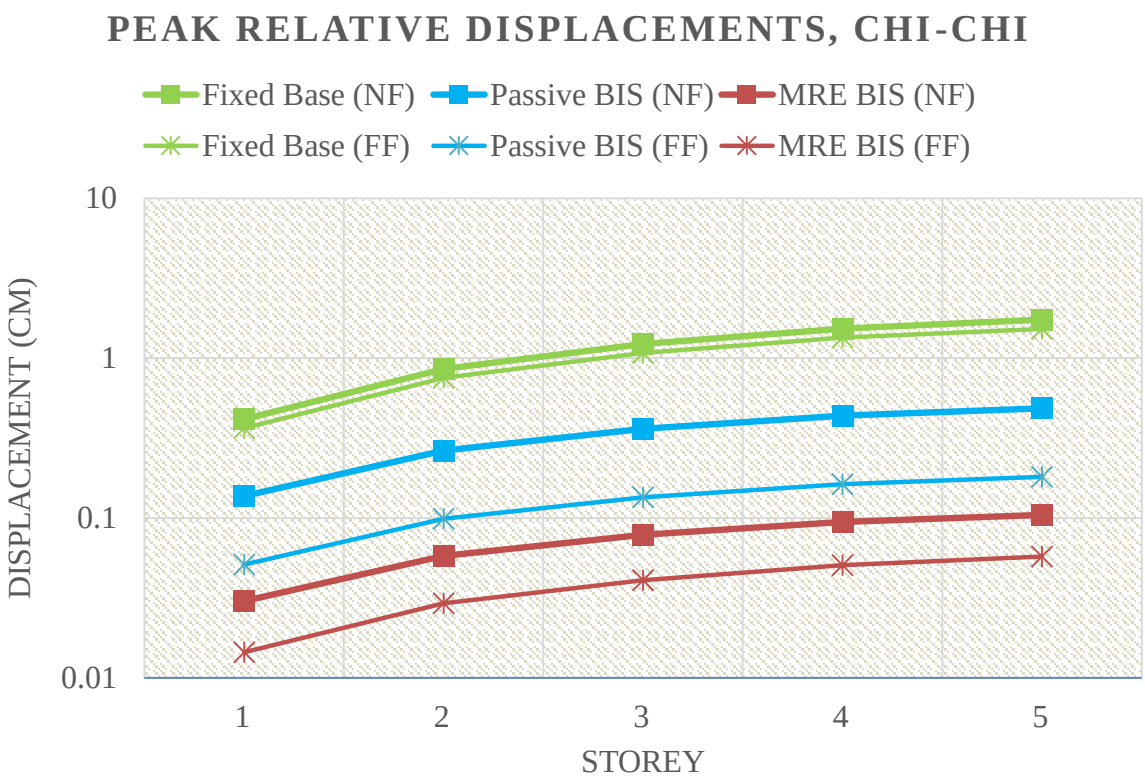

Figure 80: Peak Displacements, Chi-Chi Earthquake

Peak displacements relative to base for all 3 structures and both near and far field stations of Imperial Valley earthquake are presented in Figure 81.

From figure 81, it is evident that for both near field and far field time histories, MRE BIS has lowest response while fixed base structure shows highest displacement response. Furthermore, it can be observed that response against near field earthquake time history is higher than far field earthquake time history for all the 3 structures under consideration despite having the same peak ground acceleration values in their records.

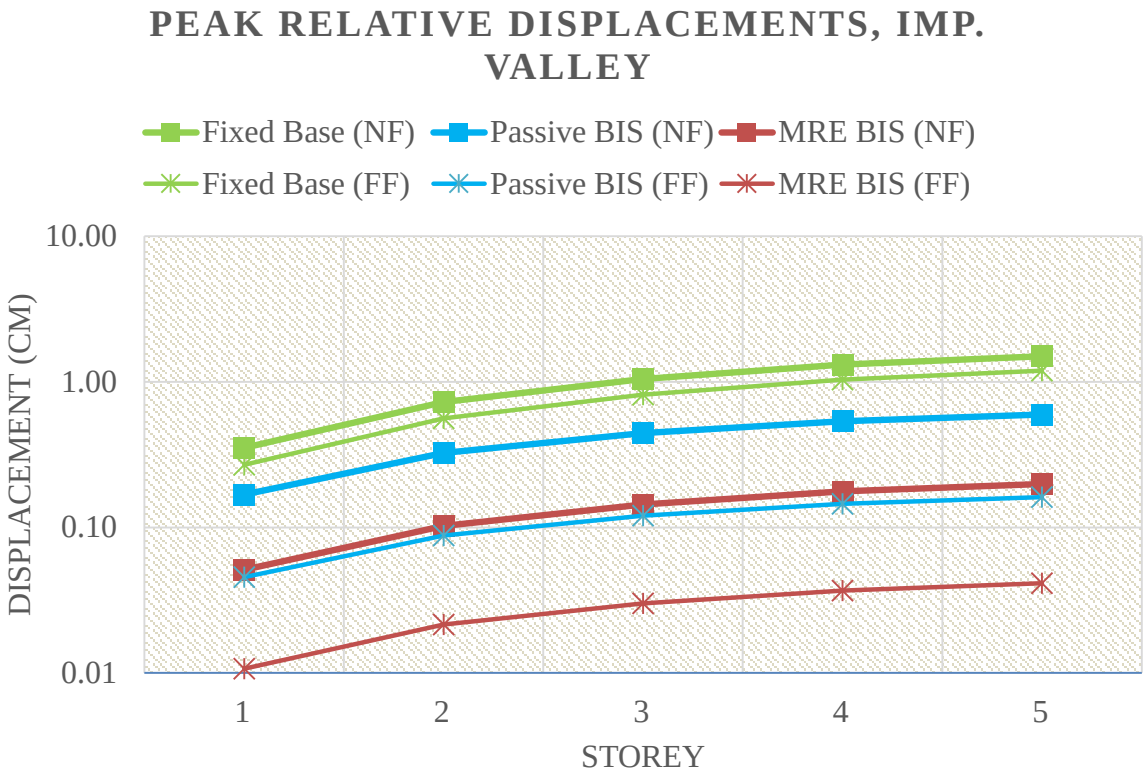

Figure 81: Peak Displacements rel. to base, Imperial Valley earthquake

Peak displacements relative to base for all 3 structures and both near and far field stations of Imperial Valley earthquake are presented in Figure 82.

From Figure 82, it is evident that for both near field and far field time histories, MRE BIS has lowest response while fixed base structure shows highest displacement response. Furthermore, it can be observed that response against near field earthquake time history is higher than far field earthquake time history for all the 3 structures under consideration despite having the same peak ground acceleration values in their records.

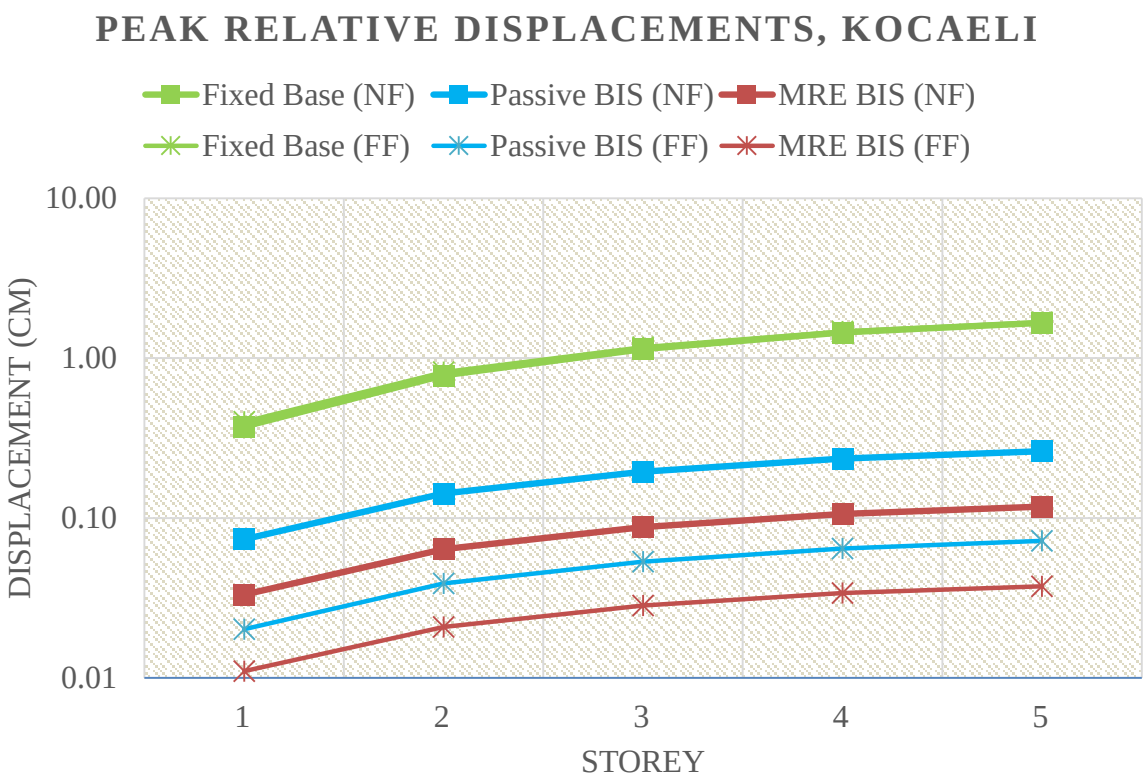

Figure 82: Peak Displacements rel. to base, Kocaeli earthquake

Storey wise line plots for peak displacements are presented in Figure 83. It can be seen from the figures that for the isolated structures, a major portion of total displacement (96-99%) in the structure is absorbed at the isolation level due to relatively soft isolation layer and very minimal displacement is being transferred to the superstructure. Whereas for the fixed base model, all the displacement is transferred rather uniformly to the superstructure.

Higher base drifts for near fault earthquake time histories compared to far fault earthquake time histories can be observed. A considerably lower response for Kocaeli earthquake far fault earthquake time histories can also be seen compared to other cases.

Storey wise line displacement plots for displacements relative to base for all the earthquake time histories are presented in Figure 84. It can be observed that isolated structures are successful in significantly reducing the transmission of displacements to superstructure compared to fixed base and MRE BIS showing the lowest response compared to other 2 structures for all earthquake excitations.

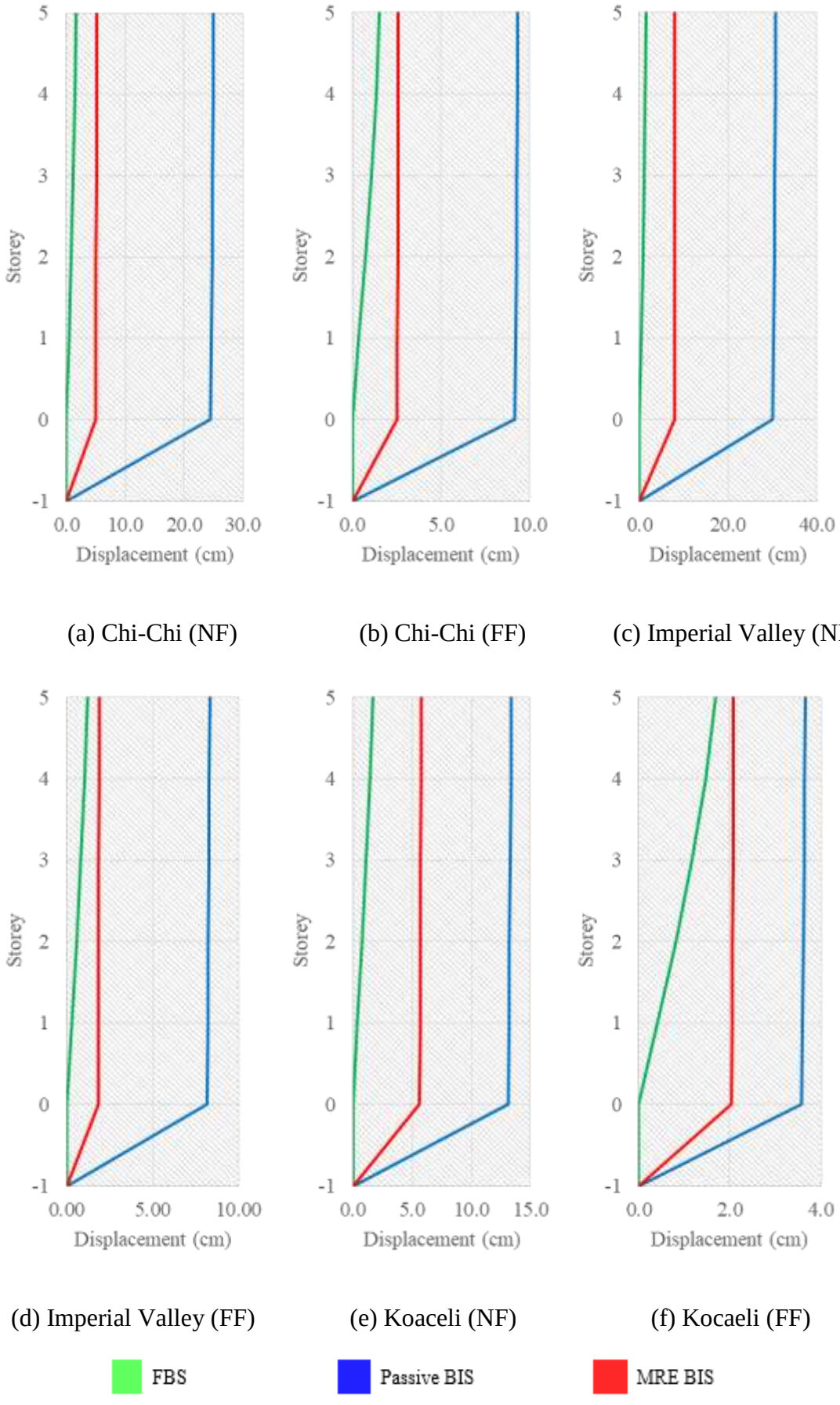

(a) Chi-Chi (NF) (b) Chi-Chi (FF) (c) Imperial Valley (NF)

(d) Imperial Valley (FF) (e) Koaceli (NF) (f) Kocaeli (FF)

Figure 83: Storey-wise total displacements

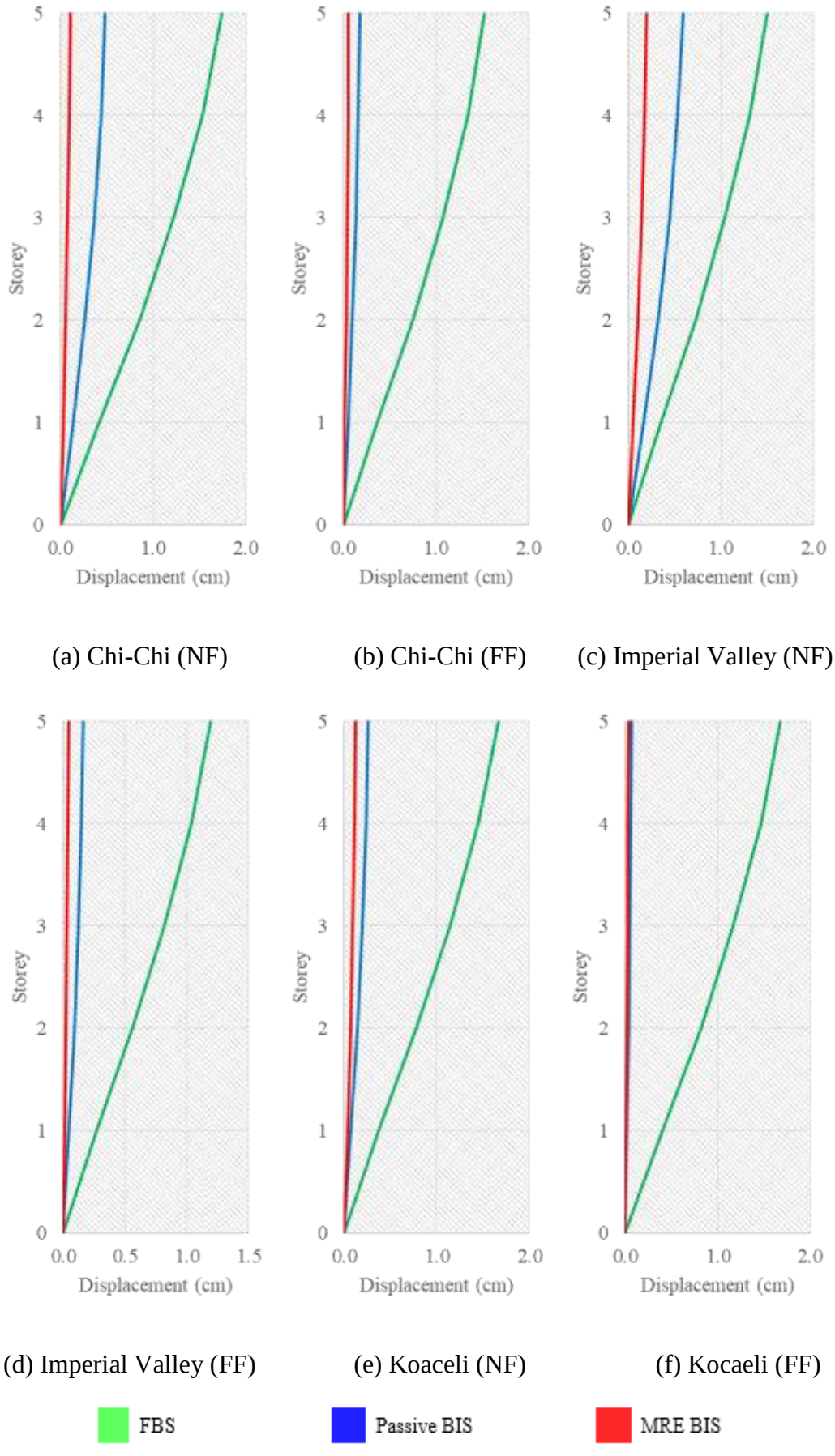

(a) Chi-Chi (NF) (b) Chi-Chi (FF) (c) Imperial Valley (NF)

(d) Imperial Valley (FF) (e) Koaceli (NF) (f) Kocaeli (FF)

Figure 84: Storey-wise displacements relative to base

A comparison of peak displacement response for all the adopted earthquake time histories is presented in Figure 85. Greater response for passively IS and greater subsequent reduction in response can be observed for near field earthquakes compared to far fault ones. It can also be observed that response of passively isolated structure against Kocaeli FF station is very low compared to that of other responses, thus its response reduction of MRE BIS compared to passively IS is also lower.

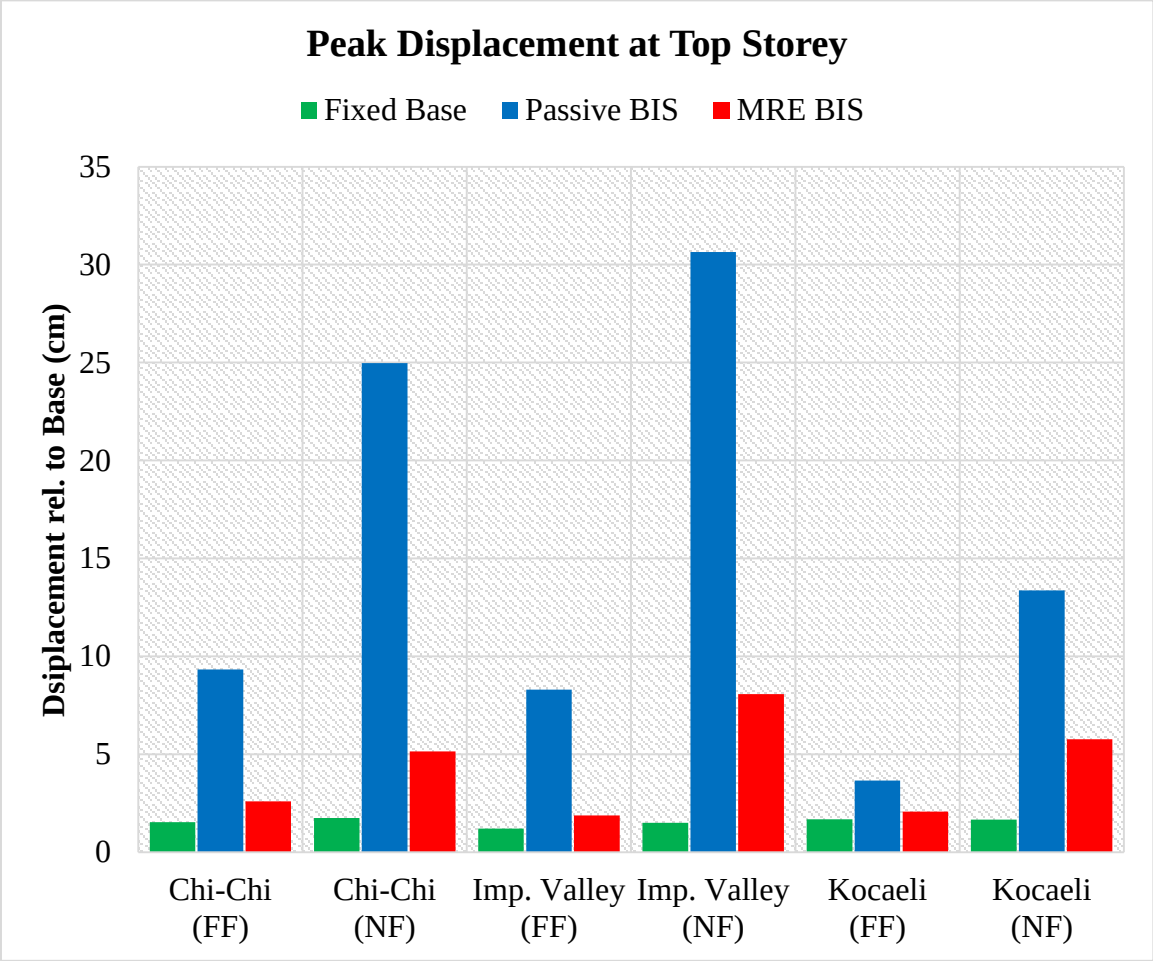

Figure 85: Peak displacement response at top storey vs. earthquake cases

The average displacement response improvement of MRE BIS compared to passively IS is presented in Figure 86. It is evident that response improvement is greater for near fault stations compared to far fault ones.

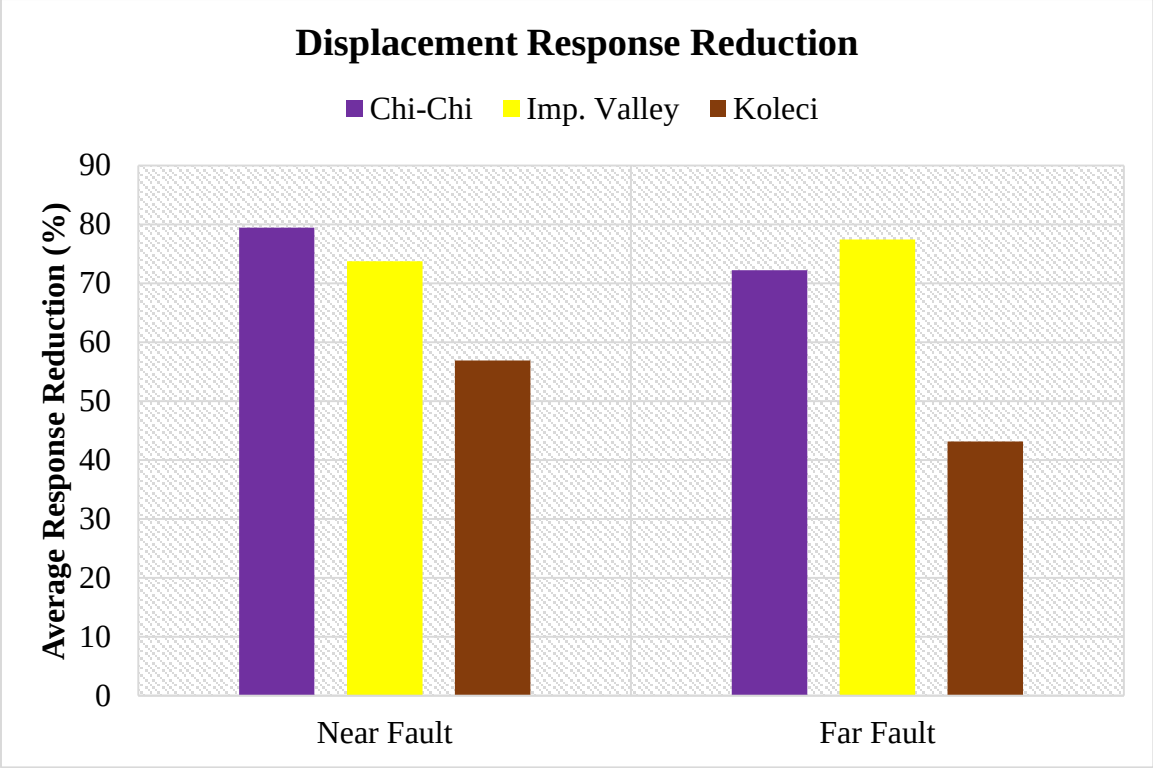

Figure 86: Average displacement response reduction

5.2.2 Storey Drift Responses

Storey drifts refer to difference of displacement of two consecutive stories. The peak and RMS values of storey drift responses against loading cases for fixed base, passively isolated and MR elastomer based isolated structures are tabulated below (Table 13).

Table 13: Storey Drift Peak and RMS Values (earthquake excitations)

		Fixed Base		Passive BIS		MRE BIS	
	Storey	Peak (mm)	RMS (mm)	Peak (mm)	RMS (mm)	Peak (mm)	RMS (mm)
Chi-Chi (NF)	1	4.15	0.67	1.37	0.38	0.50	0.10
	2	4.40	0.72	1.28	0.35	0.49	0.10
	3	3.71	0.61	0.98	0.27	0.40	0.08
	4	3.07	0.51	0.75	0.20	0.32	0.06
	5	2.13	0.36	0.49	0.13	0.22	0.04
Chi-Chi (FF)	1	3.66	0.46	0.51	0.15	0.24	0.04
	2	3.87	0.49	0.48	0.14	0.26	0.04
	3	3.25	0.41	0.36	0.11	0.22	0.04
	4	2.66	0.35	0.28	0.08	0.19	0.03
	5	1.81	0.25	0.18	0.05	0.15	0.02
Imp. Valley (NF)	1	3.53	0.63	1.68	0.78	0.79	0.15
	2	3.75	0.68	1.57	0.73	0.75	0.14
	3	3.21	0.59	1.19	0.56	0.59	0.11
	4	2.84	0.49	0.91	0.43	0.47	0.08
	5	2.11	0.35	0.60	0.28	0.31	0.06
Imp. Valley (FF)	1	2.69	0.35	0.46	0.20	0.19	0.04
	2	2.93	0.37	0.42	0.18	0.20	0.04
	3	2.55	0.32	0.32	0.14	0.18	0.03
	4	2.19	0.27	0.25	0.11	0.15	0.03
	5	1.58	0.19	0.16	0.07	0.10	0.02
Kocaeli (NF)	1	3.74	0.90	0.74	0.17	0.58	0.13
	2	4.11	0.96	0.69	0.16	0.58	0.13
	3	3.60	0.81	0.53	0.12	0.47	0.10
	4	3.06	0.68	0.40	0.09	0.39	0.08
	5	2.18	0.48	0.26	0.06	0.27	0.06
Kocaeli (FF)	1	4.00	0.65	0.20	0.05	0.20	0.04
	2	4.21	0.69	0.19	0.04	0.21	0.04
	3	3.60	0.59	0.15	0.03	0.22	0.03
	4	3.00	0.50	0.11	0.03	0.21	0.03
	5	2.09	0.35	0.07	0.02	0.16	0.02

Peak storey drift responses for both near and far field stations of Chi-Chi earthquake are presented in Figure 87. Same legends have been adopted as discussed previously with green blue and red representing fixed base, passively isolated and MRE BIS respectively and box marker against near fault and star marker against far field earthquakes is used. Firstly, it is evident that storey drift responses decrease as we move from bottom to top storeys. It can also

be observed that for both near field and far field time histories, MRE BIS has lowest response while FBS shows highest storey drift response. This validates the applicability of MRE BIS to earthquakes of both types i.e. near field and far field. Similarly, it is evident that response against near field earthquake time histories is higher than far field earthquake time histories for all the 3 structures under consideration.

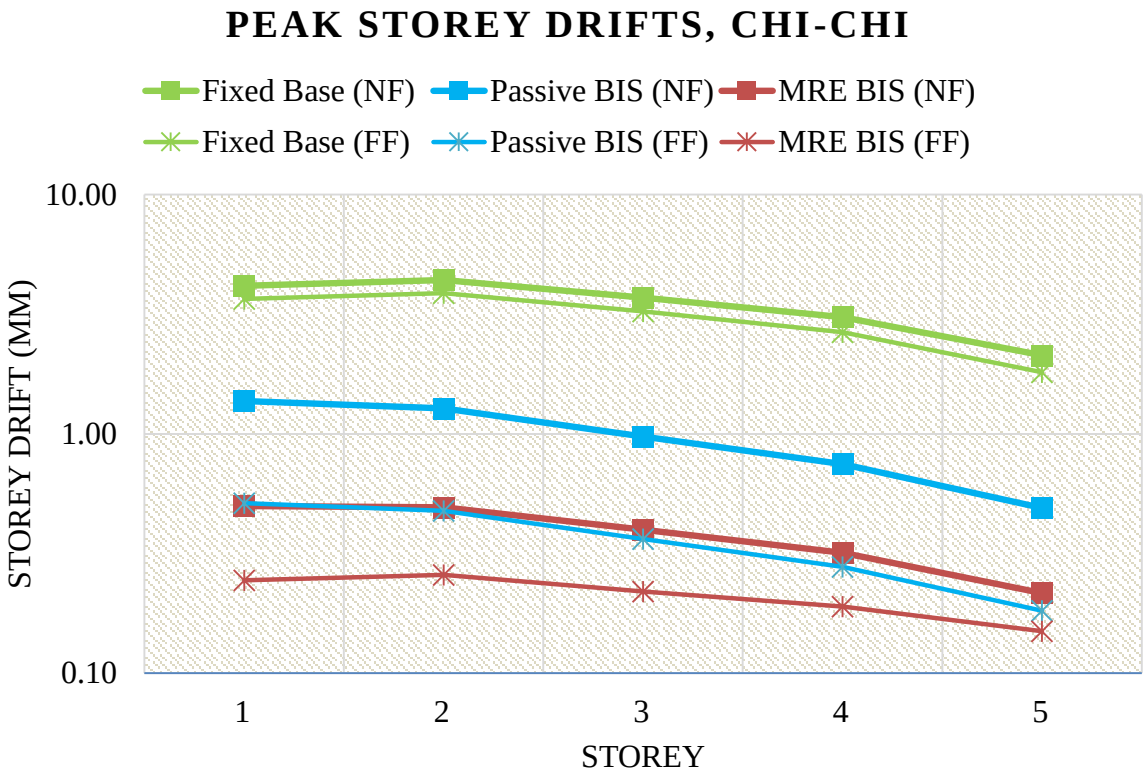

Figure 87: Peak Storey Drifts, Chi-Chi earthquake

Peak storey drift responses for both near and far field stations of Imperial Valley earthquake are presented in Figure 88. Same legends have been adopted as discussed previously. It is evident from the figure that storey drift responses decrease as we move from bottom to top storeys. It can also be observed that for both near field and far field time histories, MRE BIS has lowest response while FBS shows highest storey drift response. This validates the applicability of MRE BIS to earthquakes of both types i.e. near field and far field. Similarly, it is evident that response against near field earthquake time histories is higher than far field earthquake time histories for all the 3 structures under consideration.

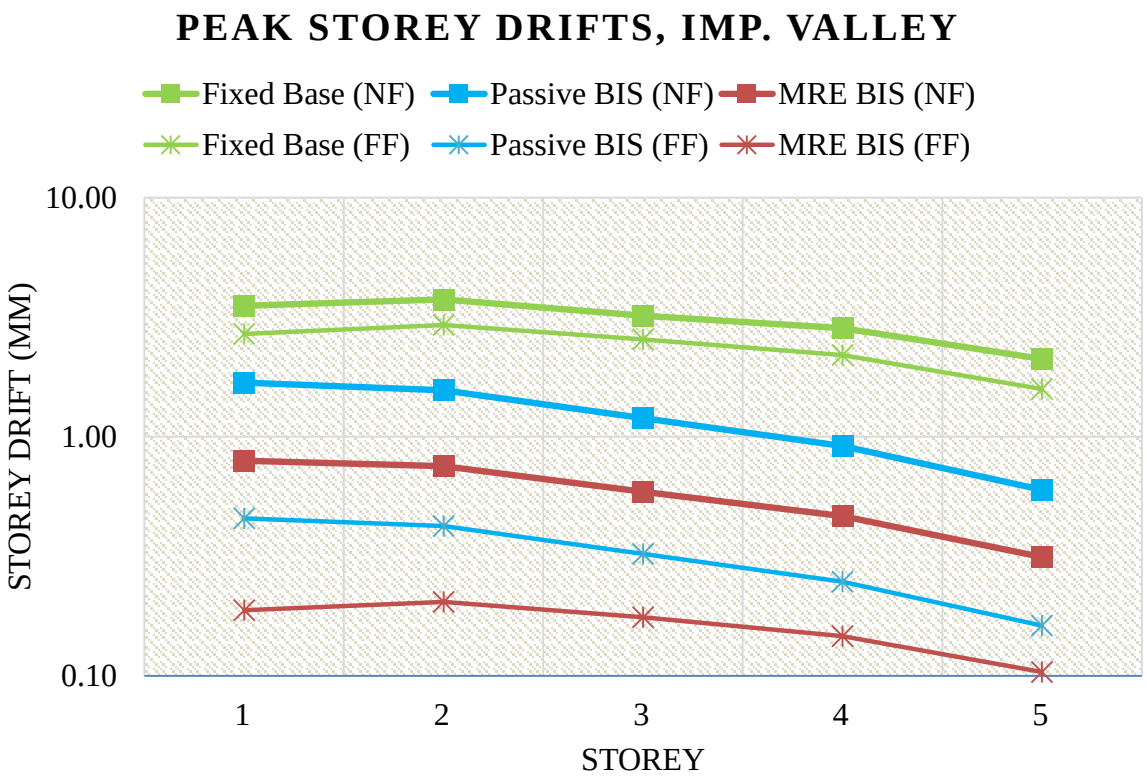

Figure 88: Peak Storey Drifts, Imperial Valley earthquake

Peak storey drift responses for near and far field stations of Kocaeli earthquake are presented in Figure 89. Same legends have been adopted as discussed previously. Somewhat different trends are observed for this earthquake compared to previous two earthquake events. For near field stations, FBS has the highest response while MRE BIS showing the lowest. For far field stations however, an observation of passively isolated structure possessing minimum response can be made. This might be due to the fact that response of passively isolated structure against far field time histories is already very small and MRE BIS cannot improve it any further. This phenomena can also be attributed to typical hybrid base isolation systems where the supplementary force forcefully confine the base displacement of the passive base isolation system for some cases[10, 11] at the expense of larger accelerations as well as increased inter-storey drifts in the superstructure [10, 12] as discussed for harmonic excitation responses.

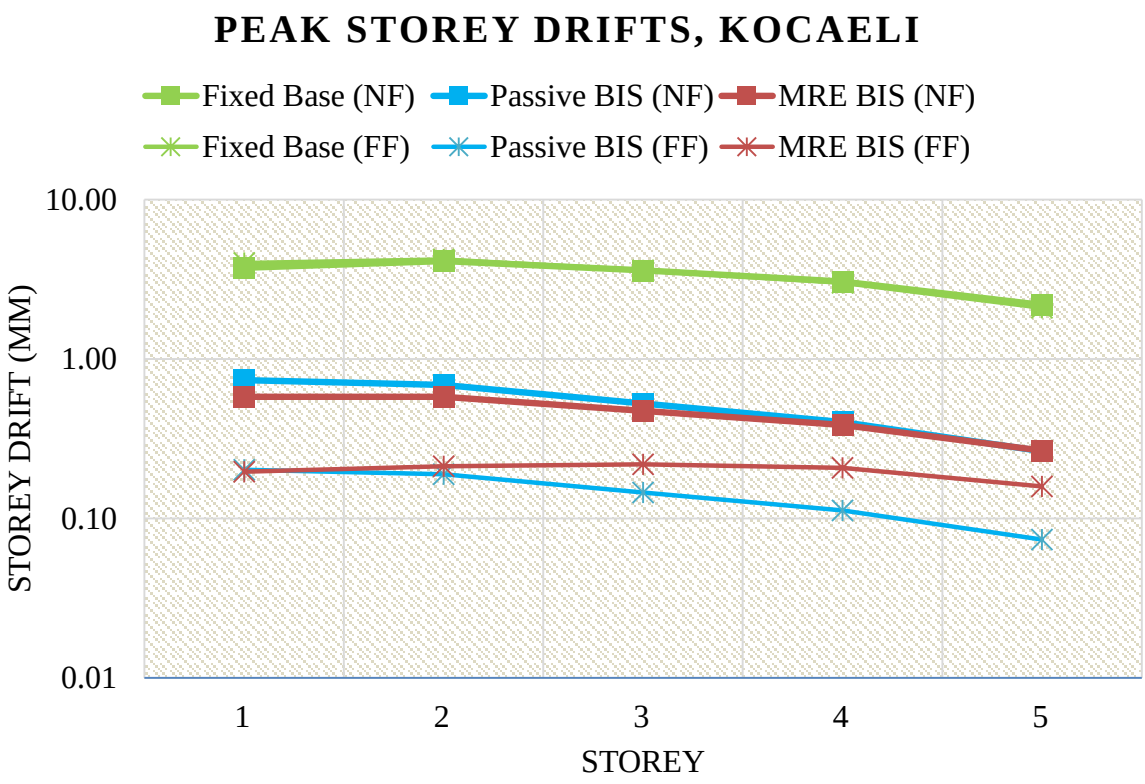

Figure 89: Peak Storey Drifts, Kocaeli earthquake

A comparison of peak storey drift response for all the adopted earthquake time histories is presented in Figure 90. Greater response for passively isolated structure and greater subsequent reduction in response can be observed for near field earthquakes compared to far field ones. It can also be observed that storey drift response of passively isolated structure against Kocaeli far field station is very low compared to that of other responses, thus its response reduction of MRE BIS compared to passively isolated structure is also lower.

The average storey drift response improvement of MRE BIS compared to passively IS is presented in Figure 91. It is evident that response improvement is greater for near fault stations compared to far field ones. Whereas no reduction in average response for Kocaeli far field station time histories can also be observed due to the discussed reasons in previous sections.

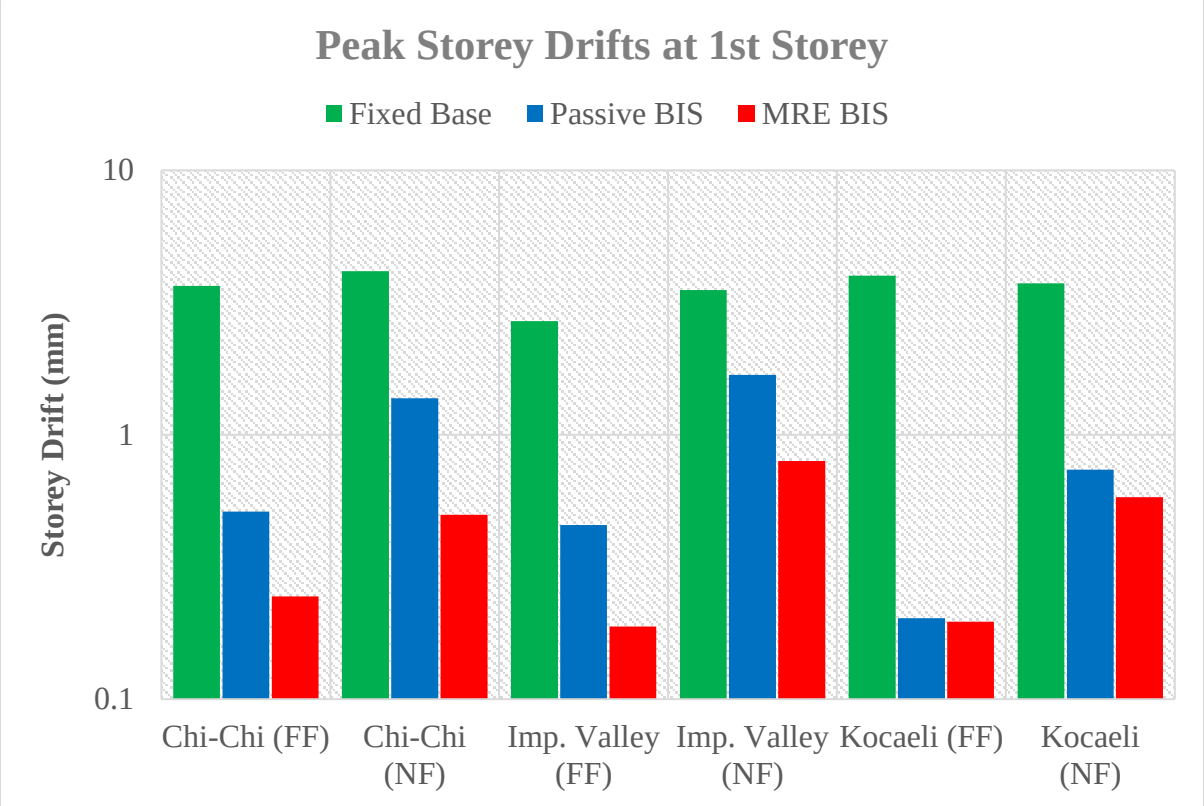

Figure 90: Peak SD response at storey 1 vs. earthquake cases

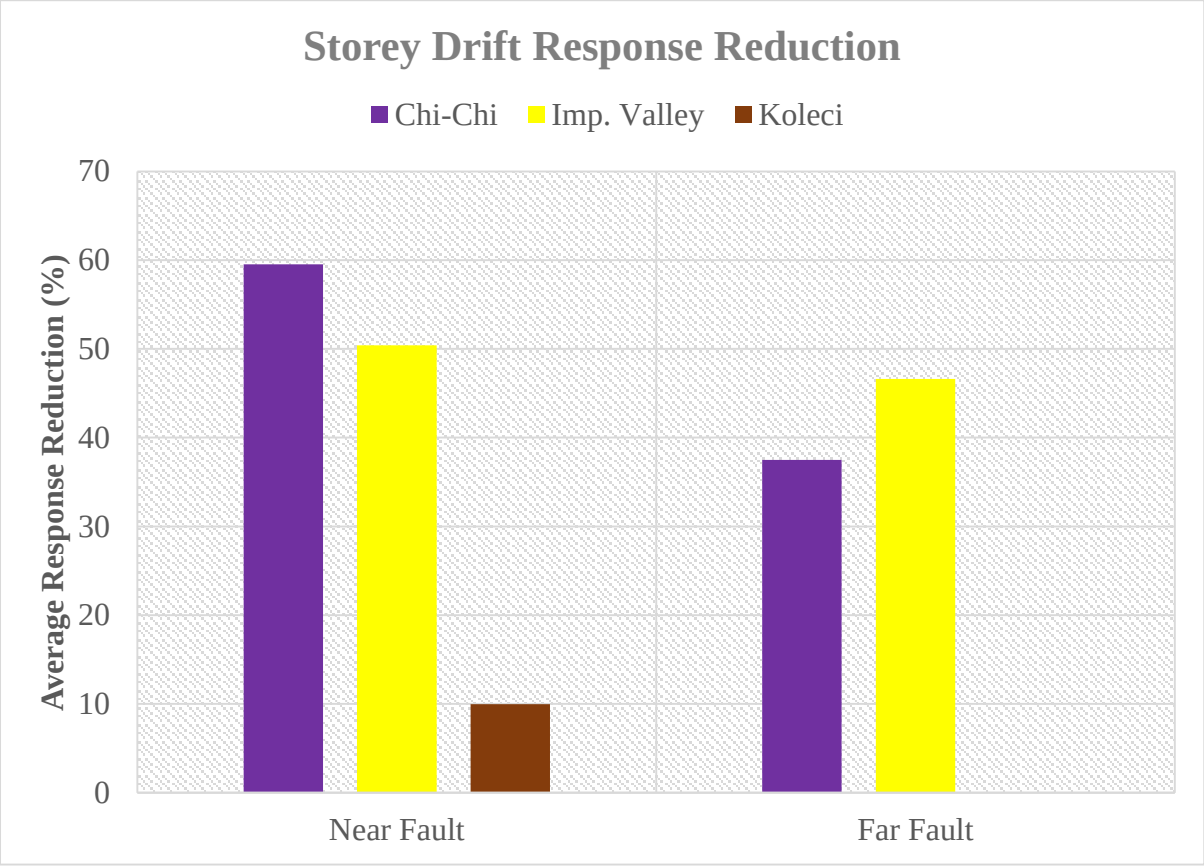

Figure 91: Average SD response reduction

5.2.3 Acceleration Responses

Acceleration response refer to the total acceleration occurring at corresponding degree-of-freedom/storey. The peak and RMS values of acceleration responses against earthquake time histories for fixed base, passively isolated and MR elastomer based isolated structures are tabulated below (Table 14).

Table 14: Acceleration Peak and RMS Values (earthquake excitations)

		Fixed Base		Passive BIS		MRE BIS	
	Storey	Peak (cm/s^2)	RMS (cm/s^2)	Peak (cm/s^2)	RMS (cm/s^2)	Peak (cm/s^2)	RMS (cm/s^2)
Chi-Chi (NF)	1	242.12	34.02	155.53	42.74	60.47	11.78
	2	367.34	58.61	156.41	42.95	61.02	11.85
	3	501.57	81.52	157.20	43.11	63.67	12.10
	4	611.55	101.34	157.90	43.24	65.13	12.56
	5	688.29	115.78	158.43	43.32	69.82	13.15
Chi-Chi (FF)	1	260.26	29.15	58.58	17.10	40.03	5.48
	2	332.01	43.67	58.68	17.19	42.67	5.24
	3	455.43	56.37	58.77	17.26	43.67	5.26
	4	542.28	68.47	58.84	17.32	45.77	5.79
	5	584.90	79.94	59.00	17.36	48.50	6.79
Imperial Valley (NF)	1	202.02	32.00	191.43	89.03	89.72	16.98
	2	328.53	55.34	192.29	89.48	91.21	16.92
	3	446.19	77.30	192.94	89.82	91.53	17.07
	4	539.51	96.88	193.40	90.09	95.50	17.53
	5	683.11	112.28	193.61	90.26	101.64	18.33
Imperial Valley (FF)	1	127.94	18.99	51.71	22.15	21.82	4.95
	2	213.86	31.07	52.00	22.27	22.74	4.71
	3	323.07	42.49	52.23	22.36	23.45	4.78
	4	420.68	52.82	52.42	22.43	29.39	5.25
	5	511.18	61.52	52.53	22.48	33.63	6.01
Kocaeli (NF)	1	209.34	48.95	83.43	18.90	66.82	15.47
	2	338.52	79.68	84.25	19.02	72.07	15.16
	3	462.98	108.86	84.73	19.12	77.32	15.50
	4	595.11	134.42	85.11	19.20	82.57	16.58
	5	707.05	153.90	85.41	19.26	86.41	18.12
Kocaeli (FF)	1	244.38	33.91	22.46	5.44	30.55	4.44
	2	395.43	57.03	22.83	5.47	35.80	4.11
	3	510.70	78.83	23.22	5.50	41.05	4.34
	4	595.52	97.95	23.61	5.55	46.30	5.22
	5	676.47	112.30	23.90	5.59	51.53	6.30

Peak acceleration responses for both near and far field stations of Chi-Chi earthquake are presented in Figure 92. Same legends have been adopted as discussed previously with green blue and red representing fixed base, passively isolated and MRE BIS respectively and box marker against near field and star marker against far field earthquakes is used. Firstly, it is evident that acceleration responses increase as we move from bottom to top storeys. It can also be observed that for both near field and far field time histories, MRE BIS has lowest response while FBS shows highest acceleration response. This validates the applicability of MRE BIS for acceleration response reduction for earthquakes of both types i.e. near field and far field. Similarly, it is evident that response against near field earthquake time histories is higher than far field earthquake time histories for all the 3 structures under consideration.

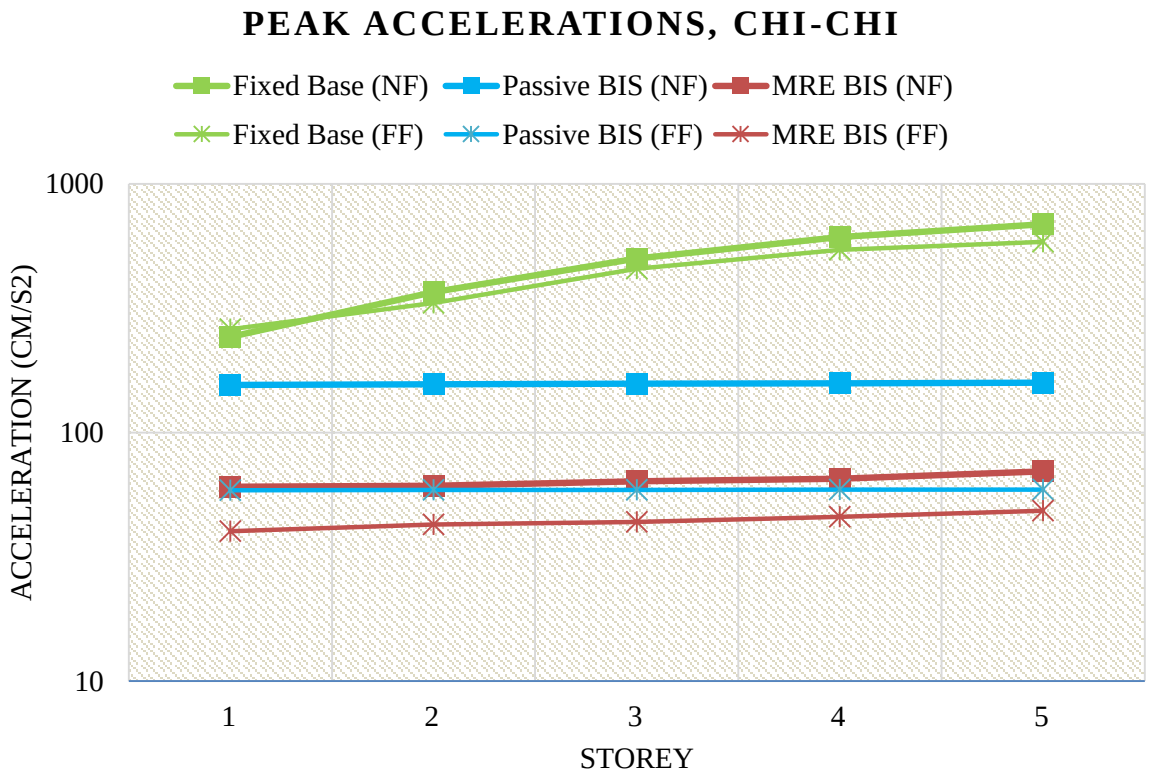

Figure 92: Peak Acceleration, Chi-Chi earthquake

Peak acceleration responses for both near and far field stations of Imperial Valley earthquake are presented in Figure 93. Same legends have been adopted as discussed previously. It can be observed that acceleration responses increase as we move from bottom to top storeys. It can also be observed that for both near field and far field time histories, MRE BIS has lowest response while FBS shows highest acceleration response. This validates the applicability of MRE BIS for acceleration response reduction for earthquakes of both types i.e. near field and

far field. Similarly, it is evident that response against near field earthquake time histories is higher than far field earthquake time histories for all the 3 structures under consideration.

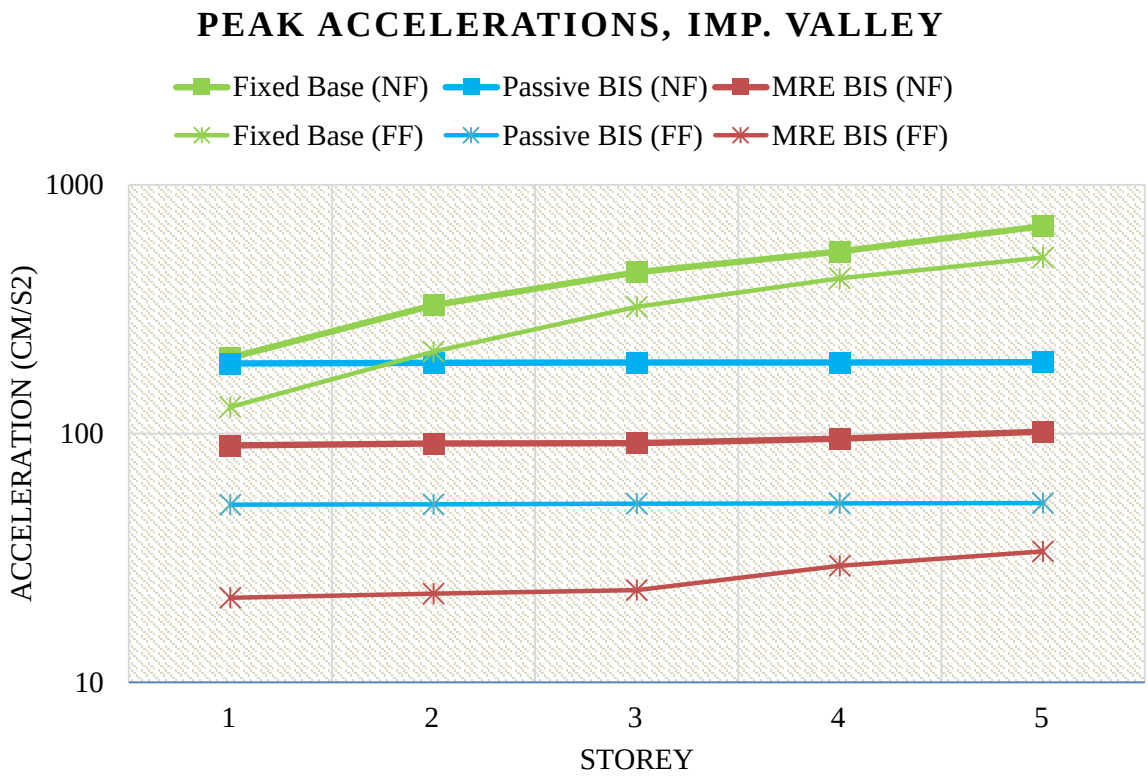

Figure 93: Peak acceleration, Imperial Valley earthquake

Peak acceleration responses for near and far field stations of Kocaeli earthquake are presented in Figure 94. Same legends have been adopted as discussed previously. Somewhat different trends are observed for this earthquake compared to previous two earthquake events. For near field stations, fixed base structure has the highest response while MRE BIS showing the lowest. For far field stations however, an observation of passively isolated structure possessing minimum acceleration response can be made. This might be due to the fact that response of passively isolated structure against far field time histories is already very small and MRE BIS cannot improve it any further. This phenomena can also be attributed to typical hybrid base isolation systems where the supplementary force forcefully confine the base displacement of the passive base isolation system for some cases[10, 11] at the expense of larger accelerations as well as increased inter-storey drifts in the superstructure [10, 12] as discussed for harmonic excitation responses.

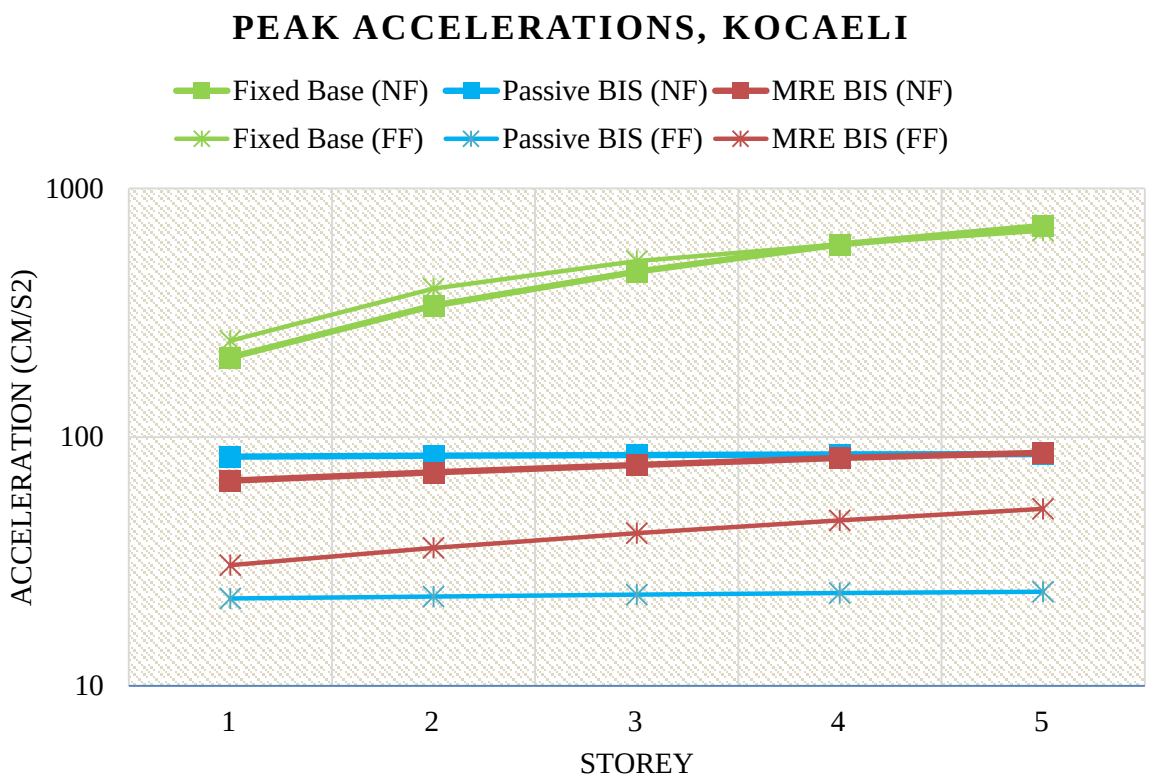

Figure 94: Peak acceleration, Kocaeli earthquake

A comparison of peak acceleration response for all the adopted earthquake time histories is presented in Figure 95. Greater response for passively isolated structure and greater subsequent reduction in acceleration response can be observed for near field earthquakes compared to far field ones. It can also be observed that acceleration response of passively isolated structure against Kocaeli far field station is very low compared to that of other responses, thus its response reduction of MRE BIS compared to passively isolated structure is also lower.

The average acceleration response improvement of MRE BIS compared to passively isolated structure is presented in Figure 96. It is evident that response improvement is greater for near fault stations compared to far field ones. Whereas no reduction in average acceleration response for Kocaeli far field station time histories can also be observed due to the discussed reasons in previous sections.

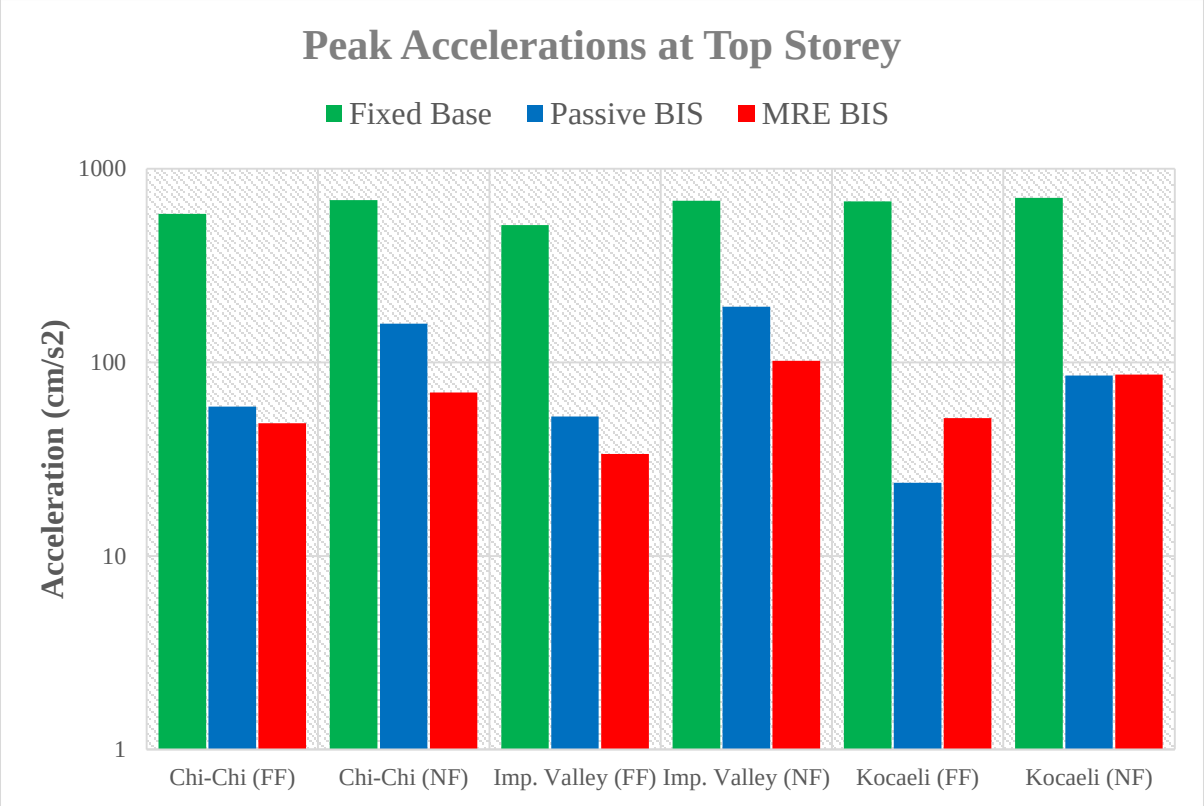

Figure 95: Peak acceleration response at top storey vs. earthquake cases

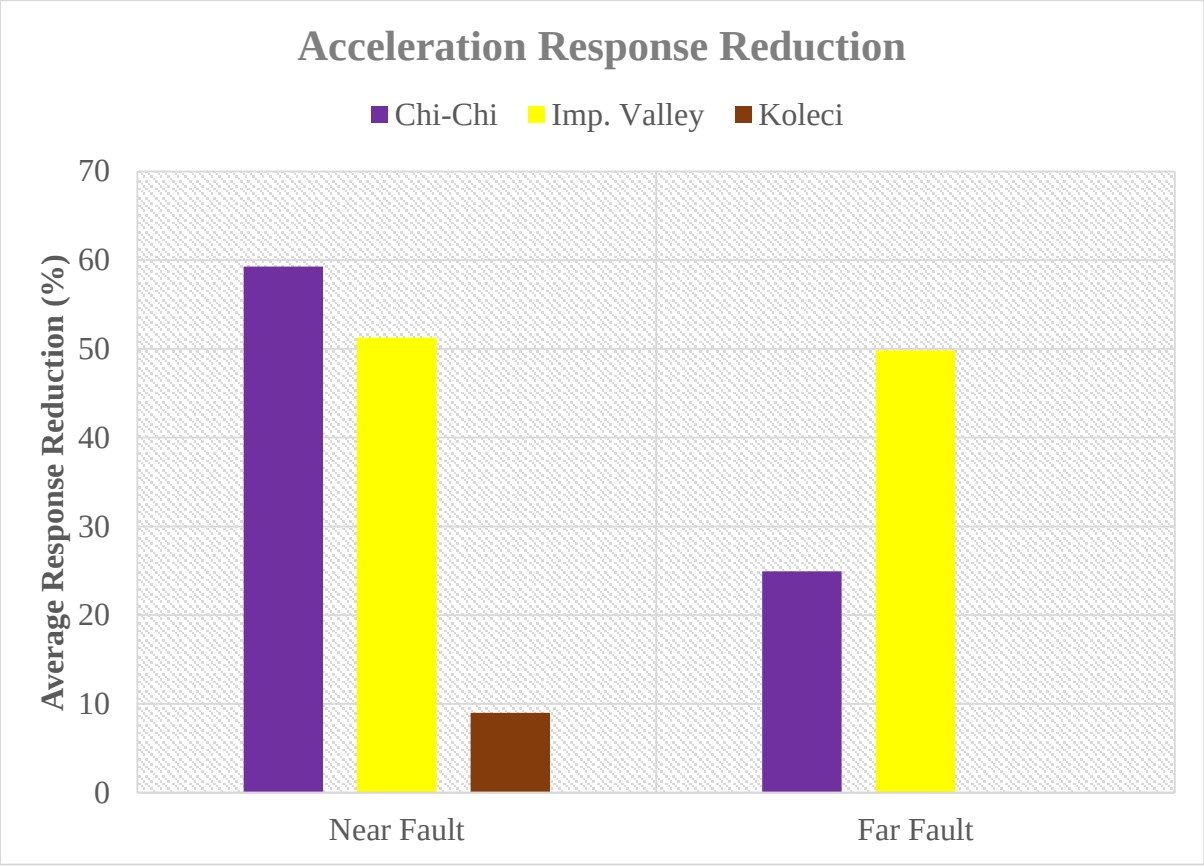

Figure 96: Average acceleration response reduction

Chapter 6: Conclusions and Recommendations

6.1 Conclusions

A Magneto-Rheological (MR) Elastomer based isolated structure has been modeled and the stiffness of isolation layer was controlled utilizing linear quadratic regulator (LQR) optimal control algorithm. Following conclusions can be drawn after analyzing the simulation results:

- MR elastomer based seismically isolated structure does not possess the characteristic fundamental frequency of vibration.
- MR elastomer based isolated structure with LQR control shows superior performance when excited at the fundamental frequencies of both passively isolated and fixed base structure which indicates the adaptability of MR elastomer based isolated structure (MRE BIS).
- On the input of sinusoidal acceleration, displacement response reduction for MR elastomer based isolated structure is better compared to its passive counterpart at all the input frequencies. However, the reduction in storey drifts and structural accelerations is more in passively isolated structure than MR elastomer based isolated structure.
- This behavior is typical for hybrid base isolation systems where the supplementary force may forcefully confine the base displacement of the passive base isolation system [10,11], larger accelerations as well as increase of inter-storey drifts may be introduced to the superstructure [10, 12]. A different control strategy may help in improving the response of MR elastomer based isolated structure under sinusoidal excitation.
- MRE BIS shows superior performance in reduction of all three responses evaluated for all the near field earthquakes compared to passively isolated structure. Similarly, displacements, storey drifts and structural accelerations have been reduced significantly compared to fixed base structure.
- MRE BIS shows superior performance in reduction of displacement response for all the far field earthquakes compared to Passive BIS. Similarly, relative displacements, storey drifts and structural accelerations have been reduced significantly compared to fixed base system.
- Apart from Kocaeli (FF) excitation time history, MRE BIS shows significantly better performance in reduction of storey drift and acceleration responses compared to Passive BIS for all far field earthquake excitations. The reasons have been discussed in detail

in Chapter 5. This response may improve on application of different control algorithm on the structure.

- The average response reduction of MRE BIS compared to Passive for all the earthquake cases is summarized in Table 15:

Table 15: Percentage response reduction, Earthquake excitations

Excitation Time History	**Displacement Reduction (%)**	**Storey Drift Reduction (%)**	**Acceleration Reduction (%)**
Chi-Chi (NF)	78.22	59.54	59.26
Imperial Valley (NF)	67.82	50.39	51.28
Kocaeli (NF)	54.93	9.98	8.98
Chi-Chi (FF)	69.77	37.51	24.93
Imperial Valley (FF)	75.20	46.61	49.82
Kocaeli (FF)	46.79	-51.71	-76.26

This improvement is in agreement with the trends outlined in previous studies. A comparison is presented in Table 16.

Table 16: Comparison with previous studies

Parameter Reported	**Usman et. al. (2009) [1]**	**Jung et. al. (2011) [13]**	**Ramallo et. al. (2014) [2]**	**This Study**
MR Effect	70%	Not Reported	30%	137%
Structure Type	5 DOF Benchmark	1 DOF Scaled	2 DOF Scaled	5 DOF Benchmark
Investigation Type	Numerical	Experimental	Experimental	Numerical
Control Algorithm	LQR	Fuzzy Logic	Lyapunov	LQR
Displacement Reduction	Up to 45%	Up to 41%	Up to 35%	Up to 78%
Acceleration Reduction	Up to 39%	Up to 39%	Up to 47%	Up to 60%

6.2 Future Recommendations

- Experimental evaluation of the base isolator developed in current study under harmonic loading and earthquake time histories using the shake Table.
- Understanding the complicated behavior of magneto rheological elastomer devices is critical for the future development and device applications. The behavior should be studied using standard characterization tests for both static and dynamic loading cases for all devices.
- As of now, efforts on the mathematical modelling of MRE devices are also limited. An MR elastomer based device that is well-understood, fairly simple and accurately modeled and capable of taking full advantage of adjustable dynamic properties in its applications is an area worth putting efforts into.
- Though numerous small-scale testing have been conducted, i.e. on a single degree-of-freedom building model with a total mass of 15 kg [13] and on a two degree-of-freedom building model with total building mass of 68 kg [14], the behavior of tall civil structures under severe earthquakes is a lot more complicated. Furthermore, experimental investigations on civil structures should involve testing on standardized building structures approved by international associations so that the results can be accepted by the community.
- Innovations employing MR elastomer based seismic isolator for structural response improvement is also a topic that should be explored, such as storey isolation system or segmental structures with smart isolations.
- Development of control algorithms exclusive for smart base isolation system employing MRE base isolator to optimize the structural response of the isolation system.

References

[1] Usman, M., Sung, S.H., Jang, D.D., Jung, H.J. and Koo, J.H., 2009, February. Numerical investigation of smart base isolation system employing MR elastomer. In Journal of Physics: Conference Series (Vol. 149, No. 1, p. 012099).

[2] Ramallo, J.C., Johnson, E.A. and Spencer Jr, B.F., 2002. "Smart" base isolation systems. *Journal of Engineering Mechanics*, *128*(10), pp.1088-1099.

[3] Khayam, S.U., Usman, M., Umer, M.A. and Rafique, A., 2020. Development and characterization of a novel hybrid magnetorheological elastomer incorporating micro and nano size iron fillers. *Materials & Design*, p.108748.

[4] Cheng, F.Y., 1988, August. Response control based on structural optimization and its combination with active protection. In *Proceeding of 9th World conference in Earthquake engineering, IAEE, Tokyo* (Vol. 3, p. 471).

[5] Cheng, F.Y., 1990. Application and assessment of structural optimization and active control for seismic structures.

[6] Cheng, F.Y., 1988, August. Response control based on structural optimization and its combination with active protection. In *Proceeding of 9th World conference in Earthquake engineering, IAEE, Tokyo* (Vol. 3, p. 471).

[7] Cheng, F. and Pantelides, C., 1998. Algorithm development for using optimal control in structural optimization subjected to seismic and wind forces. *NSF Report, US Department of Commerce, National Technical Information Service, NTIS No. PB90-1333471*.

[8] Cheng, F.Y., Jiang, H. and Lou, K., 2008. *Smart structures: innovative systems for seismic response control*. CRC press.

[9] Koo, J.H., Jang, D.D., Usman, M. and Jung, H.J., 2009. A feasibility study on smart base isolation systems using magneto-rheological elastomers. *Struct. Eng. Mech*, *32*(6), pp.755-770.

[10] Gu, X., 2017. *Investigation of adaptive base isolation system utilising magnetorheological elastomer* (Doctoral dissertation).

[11] Inaudi, J.A. and Kelly, J.M., 1993. Hybrid isolation systems for equipment protection. *Earthquake engineering & structural dynamics*, *22*(4), pp.297-313.

[12] Tsai, H.C. and Kelly, J.M., 1993. Seismic response of heavily damped base isolation systems. *Earthquake engineering & structural dynamics*, *22*(7), pp.633-645.

[13] Jung, H.J., Eem, S.H., Jang, D.D. and Koo, J.H., 2011. Seismic performance analysis of a smart base-isolation system considering dynamics of MR elastomers. *Journal of intelligent material systems and structures*, *22*(13), pp.1439-1450.

[14] Behrooz, M., Wang, X. and Gordaninejad, F., 2014. Modeling of a new semi-active/passive magnetorheological elastomer isolator. *Smart Materials and Structures*, *23*(4), p.045013.

[15] Castañeda, P.P. and Galipeau, E., 2011. Homogenization-based constitutive models for magnetorheological elastomers at finite strain. *Journal of the Mechanics and Physics of Solids*, *59*(2), pp.194-215.

[16] Galipeau, E. and Castañeda, P.P., 2013. A finite-strain constitutive model for magnetorheological elastomers: magnetic torques and fiber rotations. *Journal of the Mechanics and Physics of Solids*, *61*(4), pp.1065-1090.

[17] Rabinow, J., 1948. The magnetic fluid clutch. *Electrical Engineering*, *67*(12), pp.1167-1167.

[18] Anon, 1995. Brake Cuts Exercise-Equipment Cost. *Design News*, *39*, p.4.

[19] Carlson, J.D., Chrzan, M.J. and James, F.O., Lord Corp, 1994. *Magnetorheological fluid devices*. U.S. Patent 5,284,330.

[20] V.D. Chase, Cutting Edge, Appliance Manufacturer, 1996, pp. 6.

[21] Carlson, J.D., Catanzarite, D.M. and Clair, K.S., 1995, July. Magneto-rheological Suspensions and Associated Technology. In *5th Int Conf on Electrorheological*. Sheffield.

[22] Carlson, J.D. and Chrzan, M.J., Lord Corp, 1994. *Magnetorheological fluid dampers*. U.S. Patent 5,277,281.

[23] Carlson, J.D., Chrzan, M.J. and James, F.O., Lord Corp, 1994. *Magnetorheological fluid devices*. U.S. Patent 5,284,330.

[24] Böse, H. and Röder, R., 2009, February. Magnetorheological elastomers with high variability of their mechanical properties. In *Journal of physics: Conference series* (Vol. 149, No. 1, p. 012090).

[25] Farshad, M. and Benine, A., 2004. Magnetoactive elastomer composites. *Polymer testing*, *23*(3), pp.347-353.

[26] Feng, J., Xuan, S., Liu, T., Ge, L., Yan, L., Zhou, H. and Gong, X., 2015. The prestress-dependent mechanical response of magnetorheological elastomers. *Smart Materials and Structures*, *24*(8), p.085032.

[27] Chen, L., Gong, X.L., Jiang, W.Q., Yao, J.J., Deng, H.X. and Li, W.H., 2007. Investigation on magnetorheological elastomers based on natural rubber. *Journal of Materials Science*, *42*(14), pp.5483-5489.

[28] Wu, J., Gong, X., Fan, Y. and Xia, H., 2010. Anisotropic polyurethane magnetorheological elastomer prepared through in situ polycondensation under a magnetic field. *Smart materials and structures*, *19*(10), p.105007.

[29] Boczkowska, A. and Awietjan, S.F., 2009. Urethane magnetorheological elastomers-manufacturing, microstructure and properties. In *Solid State Phenomena* (Vol. 154, pp. 107-112). Trans Tech Publications Ltd.

[30] Li, Y., Li, J., Li, W. and Du, H., 2014. A state-of-the-art review on magnetorheological elastomer devices. *Smart materials and structures*, *23*(12), p.123001.

[31] Li, W.H., Zhang, X.Z. and Du, H., 2013. Magnetorheological elastomers and their applications. In *Advances in elastomers I* (pp. 357-374). Springer, Berlin, Heidelberg.

[32] Liu, T. and Xu, Y., 2019. Magnetorheological Elastomers: Materials and Applications. In *Smart and Functional Soft Materials*. IntechOpen.

[33] Chen, L., Gong, X.L. and Li, W.H., 2007. Microstructures and viscoelastic properties of anisotropic magnetorheological elastomers. *Smart Materials and Structures*, *16*(6), p.2645.

[34] Boczkowska, A. and Awietjan, S., 2012. Microstructure and properties of magnetorheological elastomers. *Advanced Elastomers-Technology, Properties and Applications*, *595*.

[35] Zhou, G.Y., 2003. Shear properties of a magnetorheological elastomer. *Smart materials and structures*, *12*(1), p.139.

[36] Chen, L., Gong, X.L. and Li, W.H., 2007. Microstructures and viscoelastic properties of anisotropic magnetorheological elastomers. *Smart Materials and Structures*, *16*(6), p.2645.

[37] Ju, B., Tang, R., Zhang, D., Yang, B., Yu, M. and Liao, C., 2015. Temperature-dependent dynamic mechanical properties of magnetorheological elastomers under magnetic field. *Journal of Magnetism and Magnetic Materials*, *374*, pp.283-288.

[38] Koo, J.H., Khan, F., Jang, D.D. and Jung, H.J., 2010. Dynamic characterization and modeling of magneto-rheological elastomers under compressive loadings. *Smart Materials and Structures*, *19*(11), p.117002.

[39] Demchuk, S.A. and Kuz'min, V.A., 2002. Viscoelastic properties of magnetorheological elastomers in the regime of dynamic deformation. *Journal of Engineering Physics and Thermophysics*, *75*(2), pp.396-400.

[40] Yu, M., Ju, B., Fu, J., Liu, X. and Yang, Q., 2012. Influence of composition of carbonyl iron particles on dynamic mechanical properties of magnetorheological elastomers. *Journal of Magnetism and Magnetic Materials*, *324*(13), pp.2147-2152.

[41] Li, Y., Li, J. and Samali, B., 2012, December. A novel adaptive base isolator utilising magnetorheological elastomer. In *22nd Australasian conference on the mechanics of structures and materials* (pp. 763-767).

[42] Ginder, J.M., Clark, S.M., Schlotter, W.F. and Nichols, M.E., 2002. Magnetostrictive phenomena in magnetorheological elastomers. *International Journal of Modern Physics B*, *16*(17n18), pp.2412-2418.

[43] Ge, L., Gong, X., Fan, Y. and Xuan, S., 2013. Preparation and mechanical properties of the magnetorheological elastomer based on natural rubber/rosin glycerin hybrid matrix. *Smart materials and structures*, *22*(11), p.115029.

[44] Lokander, M. and Stenberg, B., 2003. Improving the magnetorheological effect in isotropic magnetorheological rubber materials. *Polymer testing*, *22*(6), pp.677-680.

[45] Gong, X.L., Zhang, X.Z. and Zhang, P.Q., 2005. Fabrication and characterization of isotropic magnetorheological elastomers. *Polymer testing*, *24*(5), pp.669-676.

[46] Zając, P., Kaleta, J., Lewandowski, D. and Gasperowicz, A., 2010. Isotropic magnetorheological elastomers with thermoplastic matrices: structure, damping properties and testing. *Smart Materials and Structures*, *19*(4), p.045014.

[47] Hoang, N., Zhang, N. and Du, H., 2009. A dynamic absorber with a soft magnetorheological elastomer for powertrain vibration suppression. *Smart materials and structures*, *18*(7), p.074009.

[48] Deng, H.X. and Gong, X.L., 2008. Application of magnetorheological elastomer to vibration absorber. *Communications in nonlinear science and numerical simulation*, *13*(9), pp.1938-1947.

[49] Hitchcock, G.H., Gordaninejad, F. and Fuchs, A., Nevada System of Higher Education (University of Nevada), 2006. *Controllable magneto-rheological elastomer vibration isolator*. U.S. Patent 7,086,507.

[50] Yeh, J.Y., 2013. Vibration analysis of sandwich rectangular plates with magnetorheological elastomer damping treatment. *Smart Materials and Structures*, *22*(3), p.035010.

[51] Miedzińska, D., Gieleta, R. and Osiński, J., 2015. Experimental and analytical research on resonance phenomena of vibrating head with MRE regulating element. *International Journal of Applied Mechanics and Engineering*, *20*(1), pp.201-208.

[52] Liao, G., Gong, X. and Xuan, S., 2013. Phase based stiffness tuning algorithm for a magnetorheological elastomer dynamic vibration absorber. *Smart materials and structures*, *23*(1), p.015016.

[53] Sun, S., Deng, H., Yang, J., Li, W., Du, H. and Alici, G., 2015. Performance evaluation and comparison of magnetorheological elastomer absorbers working in shear and squeeze modes. *Journal of Intelligent Material Systems and Structures*, *26*(14), pp.1757-1763.

[54] Kallio, M., Lindroos, T., Aalto, S., Järvinen, E., Kärnä, T. and Meinander, T., 2007. Dynamic compression testing of a tunable spring element consisting of a magnetorheological elastomer. *Smart Materials and Structures*, *16*(2), p.506.

[55] Opie, S. and Yim, W., 2009, July. Design and control of a real-time variable stiffness vibration isolator. In *2009 IEEE/ASME international conference on advanced intelligent mechatronics* (pp. 380-385). IEEE.

[56] Zhu, S.S., Qu, L.J. and Zhou, Y.H., 2011. Experimental study of magnetorheological elastomer vibration isolator. In *Advanced Materials Research* (Vol. 335, pp. 1334-1339). Trans Tech Publications Ltd.

[57] Yang, C.Y., Fu, J., Yu, M., Zheng, X. and Ju, B.X., 2015. A new magnetorheological elastomer isolator in shear–compression mixed mode. *Journal of Intelligent Material Systems and Structures*, *26*(10), pp.1290-1300.

[58] Li, W., Zhang, X. and Du, H., 2012. Development and simulation evaluation of a magnetorheological elastomer isolator for seat vibration control. *Journal of Intelligent Material Systems and Structures*, *23*(9), pp.1041-1048.

[59] Liao, G.J., Gong, X.L., Xuan, S.H., Kang, C.J. and Zong, L.H., 2012. Development of a real-time tunable stiffness and damping vibration isolator based on magnetorheological elastomer. *Journal of Intelligent Material Systems and Structures*, *23*(1), pp.25-33.

[60] Yang, J., Sun, S.S., Du, H., Li, W.H., Alici, G. and Deng, H.X., 2014. A novel magnetorheological elastomer isolator with negative changing stiffness for vibration reduction. *Smart materials and structures*, *23*(10), p.105023.

[61] Li, Y. and Li, J., 2015. Finite element design and analysis of adaptive base isolator utilizing laminated multiple magnetorheological elastomer layers. *Journal of Intelligent Material Systems and Structures*, *26*(14), pp.1861-1870.

[62] Li, Y. and Li, J., 2015. A highly adjusTable base isolator utilizing magnetorheological elastomer: experimental testing and modeling. *Journal of vibration and acoustics*, *137*(1).

[63] Li, Y., Li, J., Tian, T. and Li, W., 2013. A highly adjusTable magnetorheological elastomer base isolator for applications of real-time adaptive control. *Smart Materials and Structures*, *22*(9), p.095020.

[64] Peng, G.R., Li, W.H., Du, H., Deng, H.X. and Alici, G., 2014. Modelling and identifying the parameters of a magneto-rheological damper with a force-lag phenomenon. *Applied Mathematical Modelling*, *38*(15-16), pp.3763-3773.

[65] Hwang, I.H., Lim, J.H. and Lee, J.S., 2006. A study on base isolation performance of magneto-sensitive rubbers. *Journal of the Earthquake Engineering Society of Korea*, *10*(4), pp.77-84.

[66] Li, Y., Li, J., Li, W. and Samali, B., 2013. Development and characterization of a magnetorheological elastomer based adaptive seismic isolator. *Smart Materials and Structures*, *22*(3), p.035005.

[67] Wahab, N.A.A., Mazlan, S.A., Sharif, A.H.R. and Kamaruddin, S., 2016, November. Steady compression characteristics of laminated MRE isolator. In *Journal of Physics: Conference Series* (Vol. 776, No. 1, p. 012036). IOP Publishing.

[68] Böse, H., Rabindranath, R. and Ehrlich, J., 2012. Soft magnetorheological elastomers as new actuators for valves. *Journal of Intelligent Material Systems and Structures*, *23*(9), pp.989-994.

[69] Zhou, G.Y. and Wang, Q., 2005. Design of a smart piezoelectric actuator based on a magnetorheological elastomer. *Smart materials and structures*, *14*(4), p.504.

[70] Zhou, G.Y. and Wang, Q., 2005. Study on the adjusTable rigidity of magnetorheological-elastomer-based sandwich beams. *Smart materials and structures*, *15*(1), p.59.

[71] Zhou, G.Y. and Wang, Q., 2006. Use of magnetorheological elastomer in an adaptive sandwich beam with conductive skins. Part II: Dynamic properties. *International Journal of Solids and Structures*, *43*(17), pp.5403-5420.

[72] Yalcintas, M. and Dai, H., 2003. Vibration suppression capabilities of magnetorheological materials based adaptive structures. *Smart Materials and Structures*, *13*(1), p.1.

[73] Du, H., Li, W. and Zhang, N., 2011. Semi-active variable stiffness vibration control of vehicle seat suspension using an MR elastomer isolator. *Smart materials and structures*, *20*(10), p.105003.

[74] Behrooz, M., Wang, X. and Gordaninejad, F., 2014. Performance of a new magnetorheological elastomer isolation system. *Smart Materials and Structures*, *23*(4), p.045014.

[75] Li, J., Li, Y., Li, W. and Samali, B., 2013, April. Development of adaptive seismic isolators for ultimate seismic protection of civil structures. In *Sensors and Smart Structures Technologies for Civil, Mechanical, and Aerospace Systems 2013* (Vol. 8692, p. 86920H). International Society for Optics and Photonics.

[76] Adanur, S., Altunişik, A.C., Bayraktar, A. and Akköse, M., 2012. Comparison of near-fault and far-fault ground motion effects on geometrically nonlinear earthquake behavior of suspension bridges. *Natural hazards*, *64*(1), pp.593-614.

[77] Akkar, S., Yazgan, U. and Gülkan, P., 2005. Drift estimates in frame buildings subjected to near-fault ground motions. *Journal of Structural Engineering*, *131*(7), pp.1014-1024.

[78] PEER (2020). https://ngawest2.berkeley.edu/. Accessed Aug 10, 2020.

[79] Mavroeidis, G.P. and Papageorgiou, A.S., 2003. A mathematical representation of near-fault ground motions. Bulletin of the seismological society of America, 93(3), pp.1099-1131.

[80] Koketsu, K. and Miyake, H., 2008. A seismological overview of long-period ground motion. *Journal of Seismology*, *12*(2), pp.133-143.

[81] Davoodi, M. and Sadjadi, M., 2015. Assessment of near-field and far-field strong ground motion effects on soil-structure SDOF system. *International Journal of Civil Engineering*, *13*(3), pp.153-166.

[82] Chopra, A.K. and Chintanapakdee, C., 2001. Comparing response of SDF systems to near-fault and far-fault earthquake motions in the context of spectral regions. *Earthquake engineering & structural dynamics*, *30*(12), pp.1769-1789.

[83] Moustafa, A. and Takewaki, I., 2010. Deterministic and probabilistic representation of near-field pulse-like ground motion. *Soil Dynamics and Earthquake Engineering*, *30*(5), pp.412-422.

[84] Davoodi, M., Sadjadi, M., Goljahani, P. and Kamalian, M., 2012, September. Effects of near-field and far-field earthquakes on seismic response of sdof system considering soil structure interaction. In *15th World Conference on Earthquake Engineering. Lisbon, Portugal*.

[85] Stewart, J.P., Chiou, S.J., Bray, J.D., Graves, R.W., Somerville, P.G. and Abrahamson, N.A., 2002. Ground motion evaluation procedures for performance-based design. *Soil dynamics and earthquake engineering*, *22*(9-12), pp.765-772.

[86] Maniatakis, C.A., Taflampas, I.M. and Spyrakos, C.C., 2008, October. Identification of near-fault earthquake record characteristics. In *The 14th World Conference on Earthquake Engineering*.

[87] Mavroeidis, G.P. and Papageorgiou, A.S., 2002, July. Near-source strong ground motion: characteristics and design issues. In *Proc. of the Seventh US National Conf. on Earthquake Engineering (7NCEE), Boston, Massachusetts* (Vol. 21, No. 2, p. 25).

[88] Hall, J.F., Heaton, T.H., Halling, M.W. and Wald, D.J., 1995. Near-source ground motion and its effects on flexible buildings. *Earthquake spectra*, *11*(4), pp.569-605.

[89] Bommer, J.J. and Martinez-Pereira, A., 2000. Strong-motion parameters: definition, usefulness and predictability. In *Proc. of the 12th World Conference on Earthquake Engineering, Auckland, New Zealand*.

[90] Bhandari, M., Bharti, S.D., Shrimali, M.K. and Datta, T.K., 2018. The numerical study of base-isolated buildings under near-field and far-field earthquakes. *Journal of Earthquake Engineering*, *22*(6), pp.989-1007.

[91] Mathworks.com. (2019). *MATLAB - MathWorks*. [online] Available at: https://www.mathworks.com/products/matlab.html.

Appendix A: MATLAB Code for Simulation under Earthquake Time History

```
clc; clear all; close all;
%% SYSTEM INPUTS
%Mass in kgs
mb=6800; %assumed mass of base isolation dof
m1=5897; m2=m1; m3=m1; m4=m1; m5=m1;

%Stiffness in N/m
kb=232e3;
k1=33732e3; k2=29093e3; k3=28621e3; k4=24954e3; k5=19059e3;

%Damping in N.s/m
cb=3.74e3;
c1=67e3; c2=58e3; c3=57e3; c4=50e3; c5=38e3;

%Importing Excitation Data
data=load('Chi NF.txt');
acc=data(:,2);acc=9.81.*acc';    %Scale Factor = 1.0g
t=data(:,1);
R=6.42e-10*eye(1);                %Weighting factor for Control Force
step=t(2)-t(1);
%% FBS SYSTEM

ki=[k1+k2 -k2 0 0 0;
    -k2 k2+k3 -k3 0 0;
    0 -k3 k3+k4 -k4 0;
    0 0 -k4 k4+k5 -k5;
    0 0 0 -k5 k5];

ci=[c1+c2 -c2 0 0 0;
    -c2 c2+c3 -c3 0 0;
    0 -c3 c3+c4 -c4 0;
    0 0 -c4 c4+c5 -c5;
    0 0 0 -c5 c5];

mi=[m1 0 0 0 0;
    0 m2 0 0 0;
    0 0 m3 0 0;
    0 0 0 m4 0;
    0 0 0 0 m5];

% Frequencies and modes FBS
[modes,freq]=eig(ki,mi);
wnu=diag(sqrt(freq));       %natural frequencies in rad/sec
tu=(2*pi)./wnu;             %time periods in sec.
%% BI SYSTEM

kc=[kb+k1 -k1 0 0 0 0;
    -k1 k1+k2 -k2 0 0 0;
    0 -k2 k2+k3 -k3 0 0;
    0 0 -k3 k3+k4 -k4 0;
    0 0 0 -k4 k4+k5 -k5;
    0 0 0 0 -k5 k5];
```

```
cc=[cb+c1 -c1 0 0 0 0;
    -c1 c1+c2 -c2 0 0 0;
    0 -c2 c2+c3 -c3 0 0;
    0 0 -c3 c3+c4 -c4 0;
    0 0 0 -c4 c4+c5 -c5;
    0 0 0 0 -c5 c5];

mc=[mb 0 0 0 0 0;
    0 m1 0 0 0 0;
    0 0 m2 0 0 0;
    0 0 0 m3 0 0;
    0 0 0 0 m4 0;
    0 0 0 0 0 m5];

% Frequencies and modes BI system
[modescs,freqcs]=eig(kc,mc);
wnc=diag(sqrt(freqcs));       %natural frequencies in rad/sec
tc=(2*pi)./wnc;               %time periods in sec.
%% FBS Response

figure
uA=[zeros(5) eye(5);
    -inv(mi)*ki -inv(mi)*ci];
uB=[zeros(5); eye(5)];
uC=[eye(5) zeros(5);
    zeros(5) eye(5);
    -inv(mi)*ki -inv(mi)*ci];
uD=[zeros(15,5)];
ucs=ss(uA,uB,uC,uD);
initial(ucs,zeros(10,1),t);
uf=[-acc; -acc; -acc; -acc; -acc];
[yunc]=lsim(ucs,uf,t);

close all
%% Passive BIS Response

figure
uA=[zeros(6) eye(6);
    -inv(mc)*kc -inv(mc)*cc];

uB=[zeros(6); eye(6)];

uC=[eye(6) zeros(6);
    zeros(6) eye(6);
    -inv(mc)*kc -inv(mc)*cc];

uD=[zeros(18,6)];

bis=ss(uA,uB,uC,uD);

fbis=[-acc; -acc; -acc; -acc; -acc; -acc];
[ybis]=lsim(bis,fbis,t);

close all

%% MRE BIS Response
gb=[-1 1 zeros(1,4);
    zeros(1,1) -1 1 zeros(1,3);
```

```
    zeros(1,2) -1 1 zeros(1,2);
    zeros(1,3) -1 1 zeros(1,1);
    zeros(1,4) -1 1;
    zeros(1,5) -1];      %6x6 Matrix (n x n)

ta=[1;
    zeros(5,1)];         %6x1 Matrix (n x r)
g=gb*ta;

%LQR parameters
cA=[zeros(6) eye(6);
    -inv(mc)*kc -inv(mc)*cc];            %FBS plant matrix
Bu=[zeros(6,1);inv(mc)*g];               %Bu for LQR control
Q=eye(12);                               %Weighting factor for System
Response
[K,S,E]=lqr(cA,Bu,Q,R);

As=Bu*K;
Ac=cA-As;
Br=[zeros(6); -1*eye(6)];
C=[eye(6) zeros(6);
    zeros(6) eye(6);
    -inv(mc)*kc -inv(mc)*cc];
D=[zeros(18,6)];
css=ss(Ac,Br,C,D);
initial(css,zeros(12,1),t);
fcs=[-acc; -acc; -acc; -acc; -acc; -acc];
[yct]=lsim(css,fcs,t);

c=1;
for i=0:step:max(t)
    u{c}=K*yct(c,1:12)';
    umax(c,1)=u{c}(1);
    c=c+1;
end
u=u';
umax(:,2)=(1.375*kb).*yct(:,1);
fck=max(abs(umax));
%% Response Data Processing

%BIS Storey Displacements relative to Base
rbis(:,1)=ybis(:,2)-ybis(:,1);
rbis(:,2)=ybis(:,3)-ybis(:,1);
rbis(:,3)=ybis(:,4)-ybis(:,1);
rbis(:,4)=ybis(:,5)-ybis(:,1);
rbis(:,5)=ybis(:,6)-ybis(:,1);
%BIS Storey Velocities relative to Base
rbis(:,6)=ybis(:,8)-ybis(:,7);
rbis(:,7)=ybis(:,9)-ybis(:,7);
rbis(:,8)=ybis(:,10)-ybis(:,7);
rbis(:,9)=ybis(:,11)-ybis(:,7);
rbis(:,10)=ybis(:,12)-ybis(:,7);
%BIS Storey Accelerations relative to Base
rbis(:,11)=ybis(:,14)-ybis(:,13);
rbis(:,12)=ybis(:,15)-ybis(:,13);
rbis(:,13)=ybis(:,16)-ybis(:,13);
rbis(:,14)=ybis(:,17)-ybis(:,13);
rbis(:,15)=ybis(:,18)-ybis(:,13);

%LQR Storey Displacements relative to Base
```

```
rct(:,1)=yct(:,2)-yct(:,1);
rct(:,2)=yct(:,3)-yct(:,1);
rct(:,3)=yct(:,4)-yct(:,1);
rct(:,4)=yct(:,5)-yct(:,1);
rct(:,5)=yct(:,6)-yct(:,1);
%LQR Storey Velocities relative to Base
rct(:,6)=yct(:,8)-yct(:,7);
rct(:,7)=yct(:,9)-yct(:,7);
rct(:,8)=yct(:,10)-yct(:,7);
rct(:,9)=yct(:,11)-yct(:,7);
rct(:,10)=yct(:,12)-yct(:,7);
%LQR Storey Accelerations relative to Base
rct(:,11)=yct(:,14)-yct(:,13);
rct(:,12)=yct(:,15)-yct(:,13);
rct(:,13)=yct(:,16)-yct(:,13);
rct(:,14)=yct(:,17)-yct(:,13);
rct(:,15)=yct(:,18)-yct(:,13);

%US Storey Drifts
sdu(:,1)=yunc(:,1);
sdu(:,2)=yunc(:,2)-yunc(:,1);
sdu(:,3)=yunc(:,3)-yunc(:,2);
sdu(:,4)=yunc(:,4)-yunc(:,3);
sdu(:,5)=yunc(:,5)-yunc(:,4);
%BIS Storey Drifts
sdbis(:,1)=rbis(:,1);
sdbis(:,2)=rbis(:,2)-rbis(:,1);
sdbis(:,3)=rbis(:,3)-rbis(:,2);
sdbis(:,4)=rbis(:,4)-rbis(:,3);
sdbis(:,5)=rbis(:,5)-rbis(:,4);
%LQR Storey Drifts
sdct(:,1)=rct(:,1);
sdct(:,2)=rct(:,2)-rct(:,1);
sdct(:,3)=rct(:,3)-rct(:,2);
sdct(:,4)=rct(:,4)-rct(:,3);
sdct(:,5)=rct(:,5)-rct(:,4);

%% Plotting

%Plot 1: Base Drift, Base Velocity and Base Acceleration
figure('Name','Base Response')
subplot(3,1,1)
plot(t,ybis(:,1),t,yct(:,1))
title(sprintf('Base Displacement/Drift'))
xlabel('Time'), ylabel('Drift (m)')
legend('Passive BIS','MRE BIS')

subplot(3,1,2)
plot(t,ybis(:,7),t,yct(:,7))
title(sprintf('Base Velocity'))
xlabel('Time'), ylabel('Velocity (m/s)')
legend('Passive BIS','MRE BIS')

subplot(3,1,3)
plot(t,ybis(:,13),t,yct(:,13))
title(sprintf('Base Acceleration'))
xlabel('Time'), ylabel('Acceleration (m/s2)')
legend('Passive BIS','MRE BIS')

% Plot 2: Storey Drifts
```

```
figure('Name','Storey Drifts')
for i=1:5
    subplot(2,3,i)
    plot(t,sdu(:,i))
    title(sprintf('Storey %d',i))
    hold on
    plot(t,sdbis(:,i))
    plot(t,sdct(:,i))
    legend('FBS','Passive BIS','MRE BIS')
    xlabel('Time (s)'), ylabel('Storey Drift (m)')
end

% Plot 3: Structural Displacements
figure('Name','Structure Displacements')
for i=1:5
    subplot(2,3,i)
    plot(t,yunc(:,i))
    title(sprintf('Storey %d',i))
    hold on
    plot(t,ybis(:,i+1))
    plot(t,yct(:,i+1))
    legend('FBS','Passive BIS','MRE BIS')
    xlabel('Time (s)'), ylabel('Displacement (m)')
end


% Plot 5: Structural Acceleration
figure('Name','Structural Acceleration')
for i=1:5
    subplot(3,2,i)
    plot(t,yunc(:,i+10))
    title(sprintf('Storey %d',i))
    hold on
    plot(t,ybis(:,i+13))
    plot(t,yct(:,i+13))
    legend('FBS','Passive BIS','MRE BIS')
    xlabel('Time (s)'), ylabel('Acceleration (m/s2)')
end
%% MAX TIME HISTORIES


for i=1:5
    max_uu(i)=max(abs(yunc(:,i)));
    max_uv(i)=max(abs(yunc(:,i+5)));
    max_ua(i)=max(abs(yunc(:,i+10)));
    max_usd(i)=max(abs(sdu(:,i)));
    max_mu(i)=max(abs(ybis(:,i+1)));
    max_mv(i)=max(abs(ybis(:,i+7)));
    max_ma(i)=max(abs(ybis(:,i+13)));
    max_msd(i)=max(abs(sdbis(:,i)));
    max_cu(i)=max(abs(yct(:,i+1)));
    max_cv(i)=max(abs(yct(:,i+7)));
    max_ca(i)=max(abs(yct(:,i+13)));
    max_csd(i)=max(abs(sdct(:,i)));
end
max_comp_u=[max_cu' max_mu' max_uu'];
max_comp_v=[max_cv' max_mv' max_uv'];
max_comp_a=[max_ca' max_ma' max_ua'];
max_comp_sd=[max_csd' max_msd' max_usd'];
```

```
figure('Name','Maximum Responses')
subplot(2,2,1)
bar(max_comp_u)
title(sprintf('Maximum Displacements'))
xlabel('Storey'), ylabel('Displacements (m)')
legend('MRE BIS','Passive BIS','FBS','Location','northwest')
subplot(2,2,2)
bar(max_comp_v)
title(sprintf('Maximum Velocities'))
xlabel('Storey'), ylabel('Velocity (m/s)')
legend('MRE BIS','Passive BIS','FBS','Location','northwest')
subplot(2,2,3)
bar(max_comp_a)
title(sprintf('Maximum Accelerations'))
xlabel('Storey'), ylabel('Acceleration (m/s2)')
legend('MRE BIS','Passive BIS','FBS','Location','northwest')
subplot(2,2,4)
bar(max_comp_sd)
title(sprintf('Maximum Storey Drifts'))
xlabel('Storey'), ylabel('Storey Drift (m)')
legend('MRE BIS','Passive BIS','FBS')
%% RMS Plots
for i=1:5
    rms_uu(i)=rms(yunc(:,i));
    rms_uv(i)=rms(yunc(:,i+5));
    rms_ua(i)=rms(yunc(:,i+10));
    rms_usd(i)=rms(sdu(:,i));
    rms_mu(i)=rms(ybis(:,i+1));
    rms_mv(i)=rms(ybis(:,i+7));
    rms_ma(i)=rms(ybis(:,i+13));
    rms_msd(i)=rms(sdbis(:,i));
    rms_cu(i)=rms(yct(:,i+1));
    rms_cv(i)=rms(yct(:,i+7));
    rms_ca(i)=rms(yct(:,i+13));
    rms_csd(i)=rms(sdct(:,i));
end
rms_comp_u=[rms_cu' rms_mu' rms_uu'];
rms_comp_v=[rms_cv' rms_mv' rms_uv'];
rms_comp_a=[rms_ca' rms_ma' rms_ua'];
rms_comp_sd=[rms_csd' rms_msd' rms_usd'];

figure('Name','RMS Responses')
subplot(2,2,1)
bar(rms_comp_u)
title(sprintf('Displacements RMS Values'))
xlabel('Storey'), ylabel('Displacements (m)')
legend('MRE BIS','Passive BIS','FBS','Location','northwest')
subplot(2,2,2)
bar(rms_comp_v)
title(sprintf('Velocities RMS Values'))
xlabel('Storey'), ylabel('Velocity (m/s)')
legend('MRE BIS','Passive BIS','FBS','Location','northwest')
subplot(2,2,3)
bar(rms_comp_a)
title(sprintf('Accelerations RMS Values'))
xlabel('Storey'), ylabel('Acceleration (m/s2)')
legend('MRE BIS','Passive BIS','FBS','Location','northwest')
subplot(2,2,4)
bar(rms_comp_sd)
title(sprintf('Storey Drift RMS Values'))
```

```
xlabel('Storey'), ylabel('Storey Drift (m)')
legend('MRE BIS','Passive BIS','FBS')

% Maximum displacements for line plots
maxd(3:7,1)=max(abs(yunc(:,1:5)))';
maxd(2:7,2)=max(abs(ybis(:,1:6)))';
maxd(2:7,3)=max(abs(yct(:,1:6)))';
dof=[-1 0 1 2 3 4 5]';
figure('Name','Displacements Line Plot');
subplot(1,2,1)
title(sprintf('Total Displacements'))
plot(maxd(:,1),dof,maxd(:,2),dof,maxd(:,3),dof);
set(gca,'YLim',[-1 5])
set(gca,'YTick',(-1:1:5))
xlabel('Total Disp.'), ylabel('Storey')
legend('FBS','Passive BIS','MRE BIS')
grid on
% Relative Displacements for line plot
subplot(1,2,2)
title(sprintf('Displacements Relative to Base'))
plot([0; max_comp_u(:,3)],[0 1 2 3 4 5]')
hold on
plot([0; max_comp_u(:,2)],[0 1 2 3 4 5]')
plot([0; max_comp_u(:,1)],[0 1 2 3 4 5]')
set(gca,'YLim',[0 5])
set(gca,'YTick',(0:1:5))
xlabel('Disp. rel to Base')
legend('FBS','Passive BIS','MRE BIS')
grid on

% Displacements relative to base
xlu=[0 0 max(abs(ybis(:,1))) rms(abs(ybis(:,1))) max(abs(yct(:,1)))
rms(abs(yct(:,1))); max_uu' rms_uu' max_mu' rms_mu' max_cu' rms_cu'];

%Storey Drifts
xlsd=[max_usd' rms_usd' max_msd' rms_msd' max_csd' rms_csd'];

%Accelerations
xla=[max_ua' rms_ua' max_ma' rms_ma' max_ca' rms_ca'];
```

Appendix B: MATLAB Code for Simulation under Sinusoidal Excitation

```
clc; clear all; close all;
%% SYSTEM INPUTS
%Mass in kgs
mb=6800;
m1=5897; m2=m1; m3=m1; m4=m1; m5=m1;

%Stiffness in N/m
kb=232e3;
k1=33732e3; k2=29093e3; k3=28621e3; k4=24954e3; k5=19059e3;

%Damping in N.s/m
cb=3.74e3;
c1=67e3; c2=58e3; c3=57e3; c4=50e3; c5=38e3;

t=0:0.01:50;
f=1.2*2*pi;                              %Excitation frequency definition
acc=18*sin(f*t);
R=9e-10*eye(1);                          %Weighting factor for Control Force
%% UNCONTROLLED SYSTEM

ki=[k1+k2 -k2 0 0 0;
    -k2 k2+k3 -k3 0 0;
    0 -k3 k3+k4 -k4 0;
    0 0 -k4 k4+k5 -k5;
    0 0 0 -k5 k5];

ci=[c1+c2 -c2 0 0 0;
    -c2 c2+c3 -c3 0 0;
    0 -c3 c3+c4 -c4 0;
    0 0 -c4 c4+c5 -c5;
    0 0 0 -c5 c5];

mi=[m1 0 0 0 0;
    0 m2 0 0 0;
    0 0 m3 0 0;
    0 0 0 m4 0;
    0 0 0 0 m5];

% Frequencies and modes uncontrolled
[modes,freq]=eig(ki,mi);
wnu=diag(sqrt(freq));       %natural frequencies in rad/sec
tu=(2*pi)./wnu;             %time periods in sec.
%% BI SYSTEM

kc=[kb+k1 -k1 0 0 0 0;
    -k1 k1+k2 -k2 0 0 0;
    0 -k2 k2+k3 -k3 0 0;
    0 0 -k3 k3+k4 -k4 0;
    0 0 0 -k4 k4+k5 -k5;
    0 0 0 0 -k5 k5];

cc=[cb+c1 -c1 0 0 0 0;
    -c1 c1+c2 -c2 0 0 0;
    0 -c2 c2+c3 -c3 0 0;
```

```
    0 0 -c3 c3+c4 -c4 0;
    0 0 0 -c4 c4+c5 -c5;
    0 0 0 0 -c5 c5];

mc=[mb 0 0 0 0 0;
    0 m1 0 0 0 0;
    0 0 m2 0 0 0;
    0 0 0 m3 0 0;
    0 0 0 0 m4 0;
    0 0 0 0 0 m5];

% Frequencies and modes BI system
[modescs,freqcs]=eig(kc,mc);
wnc=diag(sqrt(freqcs));       %natural frequencies in rad/sec
tc=(2*pi)./wnc;               %time periods in sec.
%% Uncontrolled Response

figure
uA=[zeros(5) eye(5);
    -inv(mi)*ki -inv(mi)*ci];
uB=[zeros(5); eye(5)];
uC=[eye(5) zeros(5);
    zeros(5) eye(5);
    -inv(mi)*ki -inv(mi)*ci];
uD=[zeros(15,5)];
ucs=ss(uA,uB,uC,uD);
initial(ucs,zeros(10,1),t);

uf=[acc; acc; acc; acc; acc];
[yunc]=lsim(ucs,uf,t);

close all
%% Passive Response

figure
uA=[zeros(6) eye(6);
    -inv(mc)*kc -inv(mc)*cc];

uB=[zeros(6); eye(6)];

uC=[eye(6) zeros(6);
    zeros(6) eye(6);
    -inv(mc)*kc -inv(mc)*cc];

uD=[zeros(18,6)];

bis=ss(uA,uB,uC,uD);

fbis=[acc; acc; acc; acc; acc; acc];
[ybis]=lsim(bis,fbis,t);

close all
%% Controlled Response
gb=[-1 1 zeros(1,4);
    zeros(1,1) -1 1 zeros(1,3);
    zeros(1,2) -1 1 zeros(1,2);
    zeros(1,3) -1 1 zeros(1,1);
    zeros(1,4) -1 1;
    zeros(1,5) -1];      %6x6 Matrix (n x n)
```

```
ta=[1;
    zeros(5,1)];          %6x1 Matrix (n x r)
g=gb*ta;

%LQR parameters
cA=[zeros(6) eye(6);
    -inv(mc)*kc -inv(mc)*cc];            %uncontrolled plant matrix
Bu=[zeros(6,1);inv(mc)*g];               %Bu for LQR control
Q=eye(12);                               %Weighting factor for System
Response
[K,S,E]=lqr(cA,Bu,Q,R);

As=Bu*K;
Ac=cA-As;
Br=[zeros(6); -1*eye(6)];
C=[eye(6) zeros(6);
    zeros(6) eye(6);
    -inv(mc)*kc -inv(mc)*cc];
D=[zeros(18,6)];
css=ss(Ac,Br,C,D);
initial(css,zeros(12,1),t);
fcs=fbis;
[yct]=lsim(css,fcs,t);

c=1;
for i=0:0.01:max(t)
    u{c}=K*yct(c,1:12)';
    umax(c,1)=u{c}(1);
    c=c+1;
end
u=u';
umax(:,2)=(1.375*kb).*yct(:,1);
fck=max(abs(umax));
%% Response Data Processing

%BIS Storey Displacements relative to Base
rbis(:,1)=ybis(:,2)-ybis(:,1);
rbis(:,2)=ybis(:,3)-ybis(:,1);
rbis(:,3)=ybis(:,4)-ybis(:,1);
rbis(:,4)=ybis(:,5)-ybis(:,1);
rbis(:,5)=ybis(:,6)-ybis(:,1);
%BIS Storey Velocities relative to Base
rbis(:,6)=ybis(:,8)-ybis(:,7);
rbis(:,7)=ybis(:,9)-ybis(:,7);
rbis(:,8)=ybis(:,10)-ybis(:,7);
rbis(:,9)=ybis(:,11)-ybis(:,7);
rbis(:,10)=ybis(:,12)-ybis(:,7);
%BIS Storey Accelerations relative to Base
rbis(:,11)=ybis(:,14)-ybis(:,13);
rbis(:,12)=ybis(:,15)-ybis(:,13);
rbis(:,13)=ybis(:,16)-ybis(:,13);
rbis(:,14)=ybis(:,17)-ybis(:,13);
rbis(:,15)=ybis(:,18)-ybis(:,13);

%LQR Storey Displacements relative to Base
rct(:,1)=yct(:,2)-yct(:,1);
rct(:,2)=yct(:,3)-yct(:,1);
rct(:,3)=yct(:,4)-yct(:,1);
rct(:,4)=yct(:,5)-yct(:,1);
```

```
rct(:,5)=yct(:,6)-yct(:,1);
%LQR Storey Velocities relative to Base
rct(:,6)=yct(:,8)-yct(:,7);
rct(:,7)=yct(:,9)-yct(:,7);
rct(:,8)=yct(:,10)-yct(:,7);
rct(:,9)=yct(:,11)-yct(:,7);
rct(:,10)=yct(:,12)-yct(:,7);
%LQR Storey Accelerations relative to Base
rct(:,11)=yct(:,14)-yct(:,13);
rct(:,12)=yct(:,15)-yct(:,13);
rct(:,13)=yct(:,16)-yct(:,13);
rct(:,14)=yct(:,17)-yct(:,13);
rct(:,15)=yct(:,18)-yct(:,13);

%US Storey Drifts
sdu(:,1)=yunc(:,1);
sdu(:,2)=yunc(:,2)-yunc(:,1);
sdu(:,3)=yunc(:,3)-yunc(:,2);
sdu(:,4)=yunc(:,4)-yunc(:,3);
sdu(:,5)=yunc(:,5)-yunc(:,4);
%BIS Storey Drifts
sdbis(:,1)=rbis(:,1);
sdbis(:,2)=rbis(:,2)-rbis(:,1);
sdbis(:,3)=rbis(:,3)-rbis(:,2);
sdbis(:,4)=rbis(:,4)-rbis(:,3);
sdbis(:,5)=rbis(:,5)-rbis(:,4);
%LQR Storey Drifts
sdct(:,1)=rct(:,1);
sdct(:,2)=rct(:,2)-rct(:,1);
sdct(:,3)=rct(:,3)-rct(:,2);
sdct(:,4)=rct(:,4)-rct(:,3);
sdct(:,5)=rct(:,5)-rct(:,4);

%% Plotting

%Plot 1: Base Drift, Base Velocity and Base Acceleration
figure('Name','Base Response')
subplot(3,1,1)
plot(t,ybis(:,1),t,yct(:,1))
title(sprintf('Base Displacement/Drift'))
xlabel('Time'), ylabel('Drift (m)')
legend('Passive','Controlled')

subplot(3,1,2)
plot(t,ybis(:,7),t,yct(:,7))
title(sprintf('Base Velocity'))
xlabel('Time'), ylabel('Velocity (m/s)')
legend('Passive','Controlled')

subplot(3,1,3)
plot(t,ybis(:,13),t,yct(:,13))
title(sprintf('Base Acceleration'))
xlabel('Time'), ylabel('Acceleration (m/s2)')
legend('Passive','Controlled')

% Plot 2: Storey Drifts
figure('Name','Storey Drifts')
for i=1:5
    subplot(2,3,i)
    plot(t,sdu(:,i))
```

```
    title(sprintf('Storey %d',i))
    hold on
    plot(t,sdbis(:,i))
    plot(t,sdct(:,i))
    legend('Uncontrolled','Passive','Controlled')
    xlabel('Time (s)'), ylabel('Storey Drift (m)')
end

% Plot 3: Structural Displacements
figure('Name','Structure Displacements')
for i=1:5
    subplot(2,3,i)
    plot(t,yunc(:,i))
    title(sprintf('Storey %d',i))
    hold on
    plot(t,ybis(:,i+1))
    plot(t,yct(:,i+1))
    legend('Uncontrolled','Passive','Controlled')
    xlabel('Time (s)'), ylabel('Displacement (m)')
end

% Plot 5: Structural Acceleration
figure('Name','Structural Acceleration')
for i=1:5
    subplot(3,2,i)
    plot(t,yunc(:,i+10))
    title(sprintf('Storey %d',i))
    hold on
    plot(t,ybis(:,i+13))
    plot(t,yct(:,i+13))
    legend('Uncontrolled','Passive','Controlled')
    xlabel('Time (s)'), ylabel('Acceleration (m/s2)')
end
%% MAX TIME HISTORIES
for i=1:5
    max_uu(i)=max(abs(yunc(:,i)));
%     max_uv(i)=max(abs(yunc(:,i+5)));
    max_ua(i)=max(abs(yunc(:,i+10)));
    max_usd(i)=max(abs(sdu(:,i)));
    max_mu(i)=max(abs(ybis(:,i+1)));
%     max_mv(i)=max(abs(ybis(:,i+7)));
    max_ma(i)=max(abs(ybis(:,i+13)));
    max_msd(i)=max(abs(sdbis(:,i)));
    max_cu(i)=max(abs(yct(:,i+1)));
%     max_cv(i)=max(abs(yct(:,i+7)));
    max_ca(i)=max(abs(yct(:,i+13)));
    max_csd(i)=max(abs(sdct(:,i)));
end
max_comp_u=[max_cu' max_mu' max_uu'];
% max_comp_v=[max_cv' max_mv' max_uv'];
max_comp_a=[max_ca' max_ma' max_ua'];
max_comp_sd=[max_csd' max_msd' max_usd'];


figure('Name','Maximum Responses')
subplot(2,2,1)
bar(max_comp_u)
title(sprintf('Maximum Displacements'))
xlabel('Storey'), ylabel('Displacements (m)')
legend('Controlled','Passive','Uncontrolled','Location','northwest')
```

```
subplot(2,2,2)
subplot(2,2,3)
bar(max_comp_a)
title(sprintf('Maximum Accelerations'))
xlabel('Storey'), ylabel('Acceleration (m/s2)')
legend('Controlled','Passive','Uncontrolled','Location','northwest')
subplot(2,2,4)
bar(max_comp_sd)
title(sprintf('Maximum Storey Drifts'))
xlabel('Storey'), ylabel('Storey Drift (m)')
legend('Controlled','Passive','Uncontrolled')
%% RMS Plots
for i=1:5
    rms_uu(i)=rms(yunc(:,i));
%    rms_uv(i)=rms(yunc(:,i+5));
    rms_ua(i)=rms(yunc(:,i+10));
    rms_usd(i)=rms(sdu(:,i));
    rms_mu(i)=rms(ybis(:,i+1));
%    rms_mv(i)=rms(ybis(:,i+7));
    rms_ma(i)=rms(ybis(:,i+13));
    rms_msd(i)=rms(sdbis(:,i));
    rms_cu(i)=rms(yct(:,i+1));
%    rms_cv(i)=rms(yct(:,i+7));
    rms_ca(i)=rms(yct(:,i+13));
    rms_csd(i)=rms(sdct(:,i));
end
rms_comp_u=[rms_cu' rms_mu' rms_uu'];
% rms_comp_v=[rms_cv' rms_mv' rms_uv'];
rms_comp_a=[rms_ca' rms_ma' rms_ua'];
rms_comp_sd=[rms_csd' rms_msd' rms_usd'];

figure('Name','RMS Responses')
subplot(2,2,1)
bar(rms_comp_u)
title(sprintf('Rel. Displacements RMS Values'))
xlabel('Storey'), ylabel('Displacements (m)')
legend('Controlled','Passive','Uncontrolled','Location','northwest')

subplot(2,2,3)
bar(rms_comp_a)
title(sprintf('Accelerations RMS Values'))
xlabel('Storey'), ylabel('Acceleration (m/s2)')
legend('Controlled','Passive','Uncontrolled','Location','northwest')
subplot(2,2,4)
bar(rms_comp_sd)
title(sprintf('Storey Drift RMS Values'))
xlabel('Storey'), ylabel('Storey Drift (m)')
legend('Controlled','Passive','Uncontrolled')

% Maximum displacements for line plots
maxd(3:7,1)=max(abs(yunc(:,1:5)))';
maxd(2:7,2)=max(abs(ybis(:,1:6)))';
maxd(2:7,3)=max(abs(yct(:,1:6)))';
dof=[-1 0 1 2 3 4 5]';
figure('Name','Displacements Line Plot');
subplot(1,3,1)
title('Total Displacements')
plot(maxd(:,1),dof,'g',maxd(:,2),dof,'b',maxd(:,3),dof,'r');
set(gca,'YLim',[-1 5])
set(gca,'YTick',(-1:1:5))
xlabel('Total Disp (m)'), ylabel('Storey')
```

```
% legend('Uncontrolled','Passive','Controlled')
grid on

% Displacements relative to base
xlu=[0 0 max(abs(ybis(:,1))) rms(abs(ybis(:,1))) max(abs(yct(:,1)))
rms(abs(yct(:,1))); max_uu' rms_uu' max_mu' rms_mu' max_cu' rms_cu'];
%Storey Drifts
xlsd=[max_usd' rms_usd' max_msd' rms_msd' max_csd' rms_csd'];
%Accelerations
xla=[0 0 max(abs(ybis(:,13))) rms(abs(ybis(:,13))) max(abs(yct(:,13)))
rms(abs(yct(:,13))); max_ua' rms_ua' max_ma' rms_ma' max_ca' rms_ca'];
```

Appendix C: Earthquake Ground Motion Parameters and Frequency Content

Parameter	CHI-CHI (NF)	Imperial Valley (NF)	Kocaeli (NF)	CHI-CHI (FF)	Imperial Valley (FF)	Kocaeli (FF)
Velocity RMS: (cm/sec)	7.14	7.77	5.37	2.24	1.65	2.38
Displacement RMS: (cm)	12.58	6.64	3.57	2.08	0.89	4.65
Arias Intensity: (m/sec)	0.67	0.31	0.56	0.60	0.18	0.67
Specific Energy Density (cm^2/sec)	4593.10	2288.74	866.27	453.37	154.40	453.75
Housner Intensity (cm)	77.40	89.06	89.56	54.34	27.48	33.95
Predominant Period (sec)	0.30	0.26	0.28	0.14	0.26	0.38
Bracketed Duration ($0.05a_g$) 's'	20.76	11.63	15.90	15.70	13.74	34.27
Significant Duration (5-95% Arias) 's'	22.11	14.92	15.07	17.16	28.73	33.81

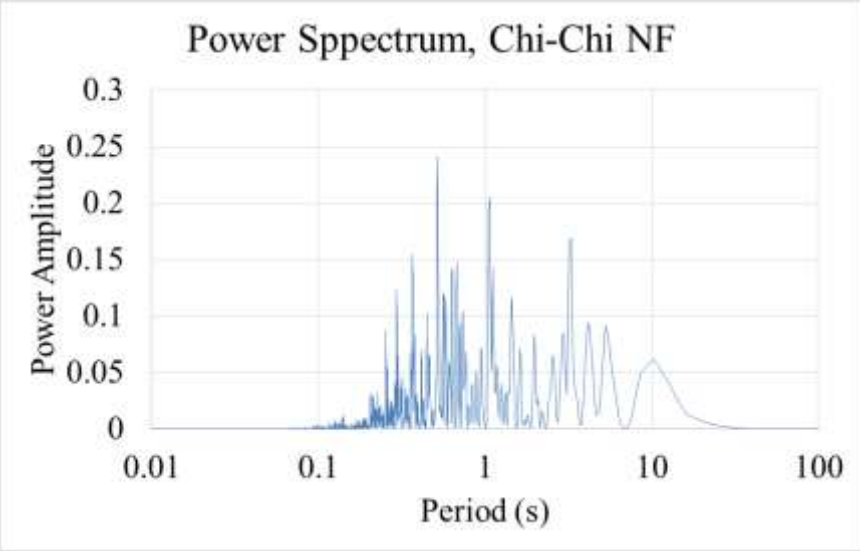
Power Sppectrum, Chi-Chi NF
Power Amplitude
0.3
0.25
0.2
0.15
0.1
0.05
0
0.01
0.1
1
10
100
Period (s)

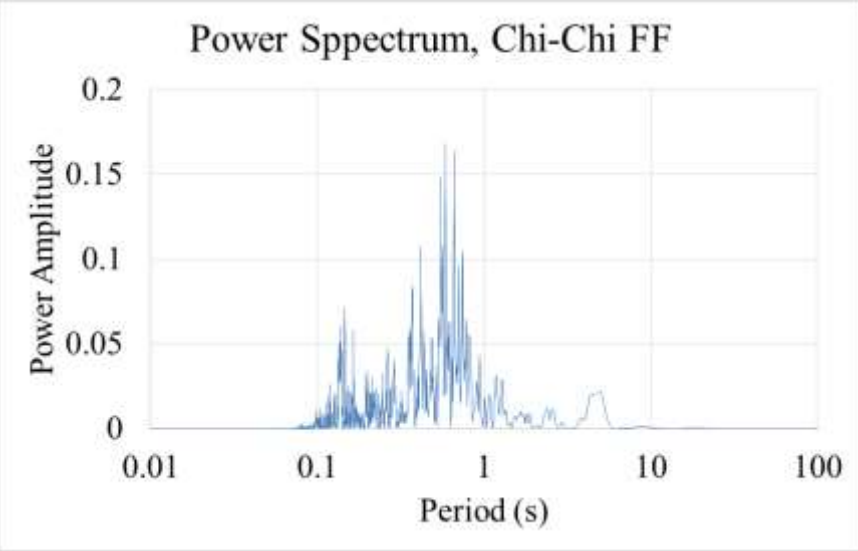
Power Sppectrum, Chi-Chi FF
Power Amplitude
0.2
0.15
0.1
0.05
0
0.01
0.1
1
10
100
Period (s)

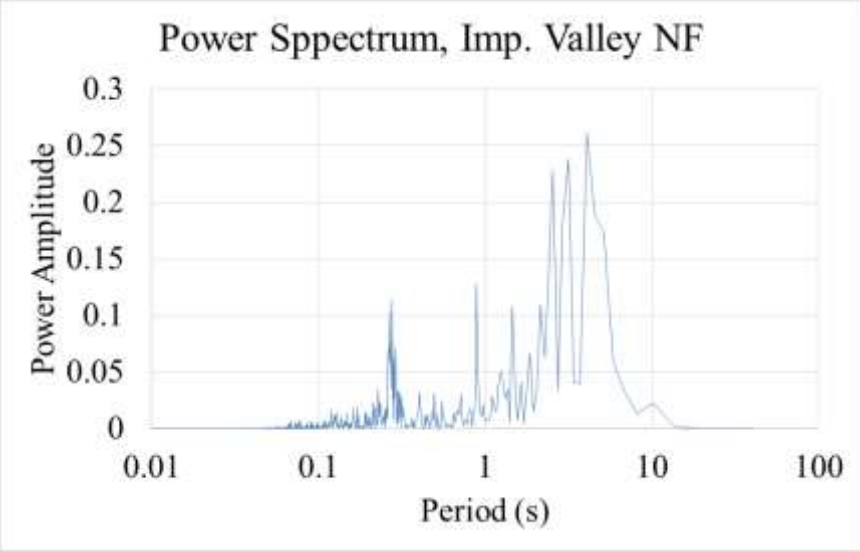
Power Sppectrum, Imp. Valley NF
Power Amplitude
0.3
0.25
0.2
0.15
0.1
0.05
0
0.01
0.1
1
10
100
Period (s)

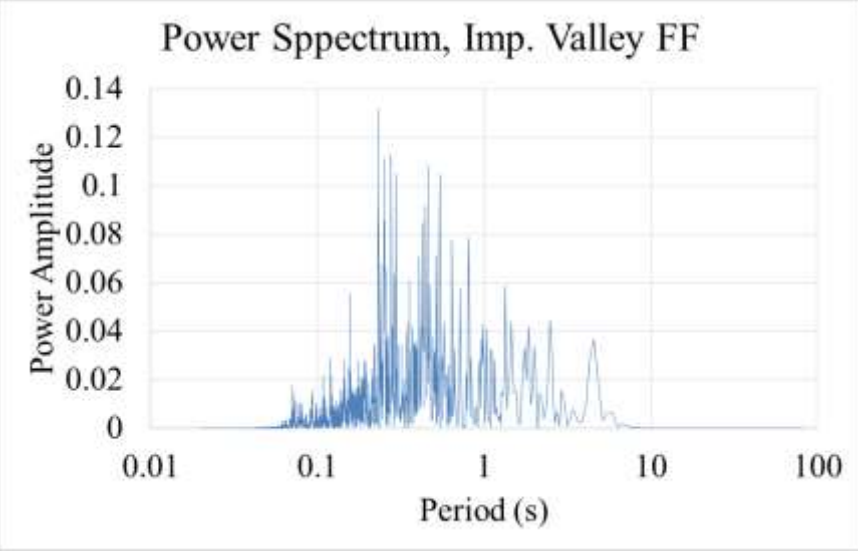
Power Sppectrum, Imp. Valley FF
Power Amplitude
0.14
0.12
0.1
0.08
0.06
0.04
0.02
0
0.01
0.1
1
10
100
Period (s)

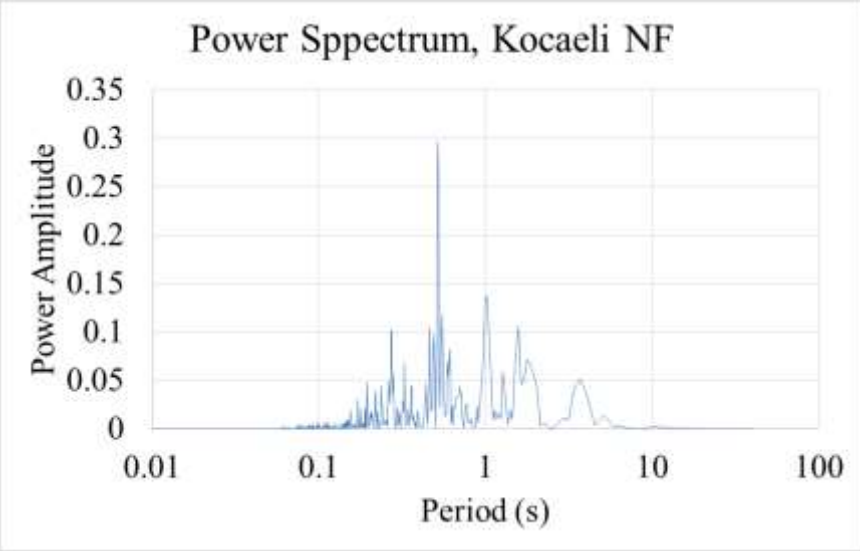
Power Sppectrum, Kocaeli NF
Power Amplitude
0.35
0.3
0.25
0.2
0.15
0.1
0.05
0
0.01
0.1
1
10
100
Period (s)

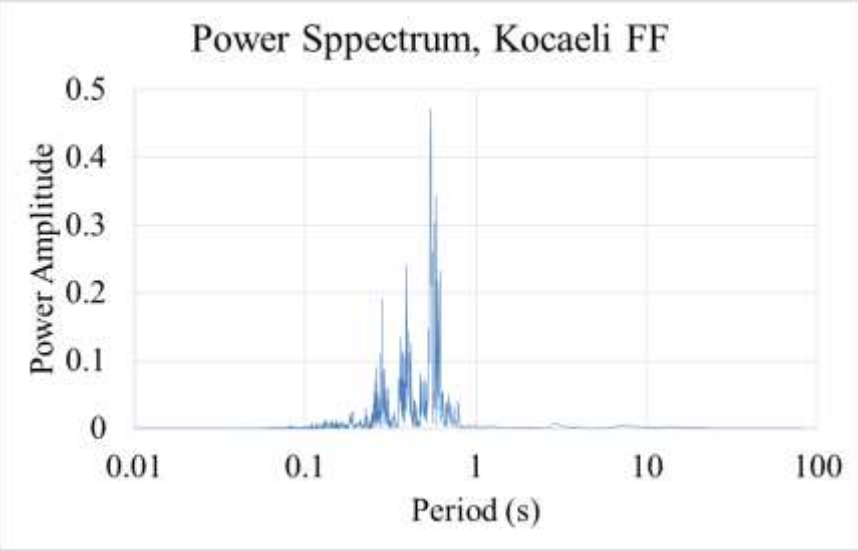
Power Sppectrum, Kocaeli FF
Power Amplitude
0.5
0.4
0.3
0.2
0.1
0
0.01
0.1
1
10
100
Period (s)